PROGRAMA DE DOCTORADO EN

Ingeniería Termodinámica de Fluidos

TESIS DOCTORAL:

Lignin valorization using supercritical water technology

Presentada por Tijana Adamovic para optar al grado de Doctora por la Universidad de Valladolid

Dirigida por:

Dr. María José Cocero Alonso

The presented thesis has been realized in the research group Press Tech in the University of Valladolid, Spain. This group is part of the Bioeconomy Institute, economically supported by different research projects from different official institutions: Ministry of Science and Innovation and European Regional Development Fund (CTQ2016-79777R and PID2019-105975GB-100) and Junta de Castilla y Leon (CLU-2019-04). This thesis was supported by the research fellowship from the University of Valladolid. Part of the thesis has been conducted at the Institute of Thermal-, Environmental- and Resources' Process Engineering in Freiberg, Germany.

"Nothing in life is to be feared, it is only to be understood.

Now is the time to understand more, so that we may fear less."

Marie Curie

List of content

List of symbols and abbreviations

[P]	Parachor
2D-NMR	Two-Dimensional Nuclear Magnetic Resonance
AAD	Average absolute deviation
AIL	Acid insoluble lignin
ASL	Acid soluble lignin
c	Concentration
DMSO-d6	Deuterated dimethyl sulfoxide
DSC	Differential Scanning Calorimetry
FT-IR	Fourier-Transform Infrared Spectroscopy
g	Gravitational force
GPC	Gel Permeation Chromatography
GS	Grape seeds
HPLC	High-Performance Liquid Chromatography
HPVC	High-pressure visual cell
LAP	Laboratory Analytical Procedure
LCC	Lignin-Carbohydrate Complex
m	Segment number
MC	Model compounds
MC	Model compounds
MWL	Milled Wood Lignin
NREL	National Renewable Energy Laboratory
PC-SAFT	Perturbed Chain-Statistical Associating Fluid Theory
R	Radius for La Place equation
SBP	Sugar beet pulp
SCW	Supercritical Water
SCWH	Supercritical Water Hydrolysis
SCWL	Supercritical water lignin
SEM	Scanning Electron Microscopy
SEMR	Sudden Expansion Micro Reactor

SKL	Sulphonated Kraft Lignin
st. dev.	Standard deviation
Tg	Class Transition Temperature
TOC	Total Organic Carbon
UV-VIS Spectroscopy	Ultraviolet-visible spectroscopy
WB	Wheat bran
X	Conversion rate
x	Mole fraction in the liquid phase
Y	Yield
y	Mole fraction in the vapor phase
Z	Compressibility factor
γ	Interfacial tension
λ_{ij}	Interaction coefficient (Macleod-Sugdan)
ρ	Density
σ	Segment diameter

Abstract

Lignin valorisation using supercritical water technology

Limited resources of fossil fuels and environmental concerns arose from their exhaustive use make us move to a new sustainable approach for energy production and use. The Development of Biorefineries that use biomass for the production of fuels and chemicals, unlike common crude oil-based refineries, is a key transformation process on which our society relies on. Lignocellulosic biomass is the most abundant and easiest grown kind of biomass. This biomass, composed of the three main fractions cellulose, hemicellulose and lignin, could be a good source for fuel and a wide range of chemicals. However, to use biomass effectively and make biorefinery feasible and competitive, different challenges need to be faced. One of the technologies that can face these challenges is the technology that uses supercritical water (SCW) as solvent and reaction medium.

A key challenge hereby is biomass recalcitrance due to its very complex and rigid structure. The Lignin fraction contributes significantly to biomass recalcitrance. **Chapter 1** of this thesis discusses therefore the supercritical water hydrolysis of defatted grape seeds, as high lignin content biomass. Hereby conditions of 380 °C and 260 bar were investigated with reaction times ranging from 0.18 s to 1 s. The focus of the analysis lay on the potential recovery of sugars and the detailed characterization of the remaining solid phase enriched in polyaromatics. After the longest reaction time of 1 s, 56 % of carbohydrates could be recovered in the liquid phase, as a result of carbohydrate hydrolysis. Total extraction of carbohydrates from biomass could not be obtained as after the longest reaction time still 10 % of the solid phase was composed of carbohydrates.

Milled wood lignin was extracted from the original biomass and compared to dioxane extract of the solid phase, to understand the main structural changes during

the SCW hydrolysis process. The analysis showed that dioxane extract of the solid phase can be regarded as a complex mixture, consisting of lipophilic extractives, flavonoids and lignin with a certain amount of chemically linked carbohydrates. 2D-NMR analysis of compared extracts indicates very subtle changes in the amounts of main lignin moieties (β-O-4', β-β' (resinol) and β-5 (phenylcoumaran)) after the SCW process. This subtle change of the main lignin structures is an important feature in the further valorization of this sulfur-free lignin residue.

Lignin is a by-product of different biorefineries and its valorization is an important contribution to their economic development. The production of aromatic compounds is hereby the most attractive way for lignin valorization. However, the repolymerization reaction of depolymerization products was reported to be the main challenge for a better recovery of aromatic compounds from lignin using different technologies.

In **Chapter 2** of the thesis, this repolymerization reaction is studied following the reactivity of lignin depolymerization products among each other and with lignin. Sulfonated kraft lignin (SKL) was used together with four model compounds: vanillin, vanillic acid, vanillyl alcohol and acetovanillone. As the structure of SKL is less known, Indulin as kraft lignin with a well-known structure was also employed as the reference for a better understanding of the repolymerization reaction. 2D-NMR analysis of the solid residue from different samples showed the presence of diarylmethane structures. Those structures could be responsible for the repolymerization reaction. However, the study shows that the formation of diarylmethene structures from lignin and model compounds follows a different mechanism, including lignin released fragments with free phenolic β-O-4 structures

and monomeric product vanillyl alcohol. Understanding of repolymerization process is crucial for the development of strategies for better recovery of aromatic compounds from lignin.

The properties of water vary significantly over a wide temperature and pressure range. When crossing its critical point fluids exist in a unique supercritical state, where no boundary between liquid and vapor phase exists. **Chapter 3** of the thesis follows the fading of this boundary. The interfacial tension of water was measured in two systems: liquid water in its saturated vapor (water/water system) and liquid water in a pressurized nitrogen atmosphere (water/nitrogen system). The measurements were performed by using the pendant drop method. In the water/water system the measurements follow the saturation line of water up to the temperature of 350 °C, while in the water/nitrogen system measurements were performed under the pressure of 10 MPa, 15 MPa and 18 MPa and a temperature of up to 325 °C. The experimental data were correlated using the Macleod-Sugden equation. Good agreement of equation with measurement results was found, showing low absolute average deviations (AADs of 4.97 % for water/nitrogen and 3.02 % for the water/water system).

Introduction

Biorefineries and the potential of supercritical water to contribute to their development

The supply of resources has been one of the key human needs ever since. Since mankind discovered the ignition of flammable materials, that brought along heat, preparation of food and light, a vast majority of time was spent to access these resources.

The search for ways for using and transforming natural resources to fulfil these human needs has been of great importance. Regarding the transformation of resources into the following products, refineries were developed to enable the supply of energy in different manners and at different times.

The extensive need and ineffective usage of wooden resources resulted in a crisis in many European countries, letting become large parts of former woodlands entirely deforested (John U, 1977). The progress in mining enabled humanity in the early industrialized countries to switch from wood as the main resource to coal and later on to oil and gas (Fernihough and O'Rourke, 2014).

The complex structure of fossil fuels created the necessity of refineries as we know them nowadays. Although supporting our needs for heat, power, transportation and chemicals, the disadvantages of those refineries such as price volatility of the final product, supply security, growing competition for a limited resource and environmental concerns, started to become evident (de Jong et al., 2011). Warning predictions about global future demand and natural resources consumption with the direct impact on the environment are raising global awareness that something has to be changed. This change is based on sustainability, through the environmental, social and economic spheres. The need to build a sustainable society is the main driver for establishing biorefineries.

Biomass – the crude oil of the future

Every step towards the transition to renewable resources is a significant contributor to a sustainable future. Renewable energy resources such as wind, solar and hydropower plants have an important role in current and future energy supply. However, those resources cannot provide transportation fuels and chemicals. For this reason, the development of biorefinery is of particular importance. There are different definitions of what is a biorefinery and some of them are listed in the text below:

"Biorefining is the sustainable processing of biomass into a spectrum of marketable products and energy" (de Jong et al., 2011);

"A biorefinery is a facility where biofuels, bioenergy, biochemical, biomaterials, food and feed are coproduced from biomass" (Cherubini et al., 2009);

"Biorefinery is optimized use of biomass for materials, chemicals, fuels and energy applications, where use relates to costs, economics, markets, yield, environment, impact, carbon balance and social aspects" (Bridgwater, 2013).

Although the discussion on the biorefinery scope is presented in the literature, from the above listed definitions the main goal is clear and that is refining the renewable resources through sustainable ways to the sustainable products.

The input of biorefinery or its 'crude oil' is biomass. Biomass is a renewable feedstock that is widely available, has relatively low cost and can be sustainably grown. One of the proposed definitions of biomass is: "The term biomass means any organic matter that is available on a renewable or recurring basis, including agricultural crops and trees, wood and wood wastes and residues, plants (including aquatic plants), grasses, residues, fibers, and animal wastes, municipal wastes, and

other waste materials" (Bracmort and Gorte, 2010). The term biomass thus covers a wide range of different feedstock. 1st generation biorefinery has been developed using sugars, starch, vegetable oil, or animal fats, where the basic feedstock often are seeds and grains, such as wheat, corn and rapeseeds (Cherubini, 2010). High sugar or oil content in raw materials used in 1st generation biorefinery is an important advantage as it facilitates biomass conversion to biofuel (Cherubini, 2010). Nevertheless, the use of this feedstock raises questions, such as the impact it might have on biodiversity, as well as land use and competitiveness with food and feed crops (Naik et al., 2010). De facto the production of these crops occupies fertile land, intended for food production, as it might be more profitable to harvest crops for energy than for food or animal feed (De Buck et al., 2020). Additionally, the availability of these crops is potentially limited by soil fertility, while also high energy inputs required for crops cultivation and conversion must be considered (Cherubini, 2010).

Ethical concerns that arose from the 1st generation biorefineries, brought the necessity for the development of 2nd generation biorefineries. The 2nd generation biomass feedstock includes lignocellulosic materials, green fertilizers and farm residues, waste from kitchen, industry and forestry (De Buck et al., 2020). As this thesis is part of a project that gives a contribution to the valorization of lignocellulosic biomass using supercritical water technology to the development of biorefineries, more attention will be dedicated to lignocellulosic biomass as a feedstock. Only to mention, the 3rd generation of biorefineries are coming and are still in the early stage of development. Those are the marine biorefineries whose feedstock are algae (De Buck et al., 2020).

Lignocellulosic biomass as a feedstock

Lignocellulosic biomass is one of the most abundant organic resources worldwide with the contribution to more than 70 % of the total biomass (Kumar et al., 2020). Lignocellulosic biomass is generally composed of three main constituents: cellulose (40-50%), hemicellulose (25-30%), lignin (15-20%) and in addition, other extractable components. Cellulose is a linear polymer made out of glucose units linked together by β-(l/4)-glycosidic bonds. Hemicellulose is mainly an amorphous polymer, that consists of a mixture of C5 and C6 sugars (D-xylose, L-arabinose, D- mannose, D-glucose, D-galactose and D-glucuronic acid). Lignin is composed of the three major phenolic components p-coumaryl alcohol, coniferyl alcohol and sinapyl alcohol and is synthesized by polymerization of these units. The structures of the lignocellulosic biomass and its main fractions cellulose, hemicellulose and lignin are presented in Figure 1. The main fractions of lignocellulosic biomass are very different by their structure and building blocks. This diversity opens a door for a very wide spectrum of possible chemicals and products.

Widely distributed, easily grown, not competitive with food and feed, with a chemical composition that has the potential to be used for further conversion to fuels and chemicals, lignocellulosic biomass presents an interesting candidate for input for advanced biorefineries. What are then the challenges on the way to its conversion? The highly complex and heterogeneous multi-scale structure of plant cell wall that makes the rigid and recalcitrant structure, presents the major limitation for lignocellulosic biomass valorization (Himmel et al., 2007).

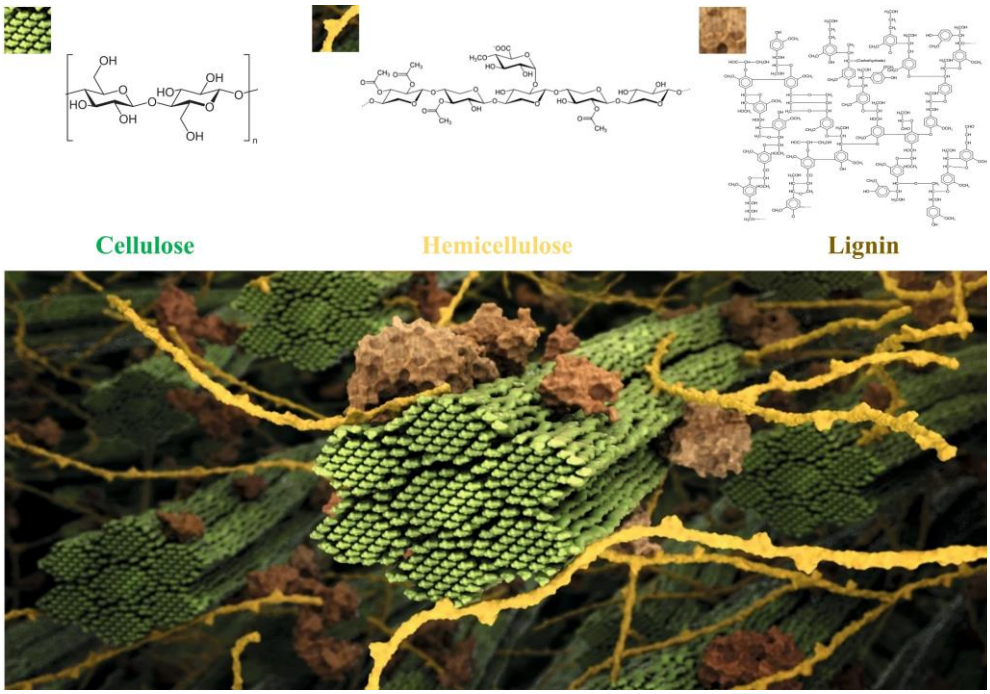

Figure 1. Structure of biomass and its fractions: cellulose, hemicellulose and lignin

Factors that are affecting lignocellulosic biomass recalcitrance are chemical (lignin composition and content, hemicelluloses, acetyl groups) and structural (cellulose crystallinity, degree of polymerization, cellulose specific surface area, pore size and volume) (Zoghlami and Paës, 2019). The number of glucose units in the cellulose determines the degree of polymerization. By default, long cellulose chains contain more hydrogen bonds and are thus more difficult to hydrolyze, while the hydrogen-bonding system is weaker in shorter cellulose chains so that hydrolysis is facilitated (Zoghlami and Paës, 2019). Cellulose crystallinity is another important contributor to recalcitrance as crystalline cellulose fibres are closely related to each other by non-covalent hydrogen bonds. This result in a slower hydrolysis rate of crystalline cellulose portion compared to amorphous (Yu and Wu, 2010).

Lignin provides transport of water and solutes through the vascular system of the plant and further protects the plant against pathogens. It also provides stiffness and strength of the plant (Boerjan et al., 2003). Lignin together with hemicellulose act as a physical barrier for cellulose accessibility (Zoghlami and Paës, 2019).

Lignin-Carbohydrate Complex

An important factor that contributes to biomass recalcitrance is the interaction between cellulose, hemicellulose and lignin. While carbohydrate polymers are connected through hydrogen bonding, they are also connected with lignin through covalent bonds, forming Lignin-Carbohydrate Complex (LCC) (Tarasov et al., 2018). Different studies reported the existence of LCC as an additional obstacle for carbohydrates separation from lignin in the biorefining processes (Zhao et al., 2020). LCC strengthens the integrity and rigidity of the plant cell wall and the stability of LCC bonds plays an important role in biomass recalcitrance (Giummarella and Lawoko, 2017; Li et al., 2016a). Lignin is covalently bonded mainly with hemicellulose, whereas some studies demonstrate lignin bonding with cellulose polymer (Jin et al., 2006). Main LCC linkages are: benzyl ether, benzyl ester, phenyl glycosidic, ferulate and diferulate esters (Tarasov et al., 2018) and they are presented in Figure 2.

Studies focused on valorisation of LCC showed that such complex possesses high anti-UV effect (Vinardell and Mitjans, 2017), antibacterial and antiviral activity (Lee et al., 2011; Sakagami et al., 2010), antioxidant activity (Dong et al., 2020) and anti-protein aggregation activity (Pei et al., 2020).

Despite the LCC contribution to biomass recalcitrance and the just small amount that is present in biomass, this complex could play from another side important role in the valorization of biomass due to its biological activity suitable for the pharmaceutical and cosmetic industry.

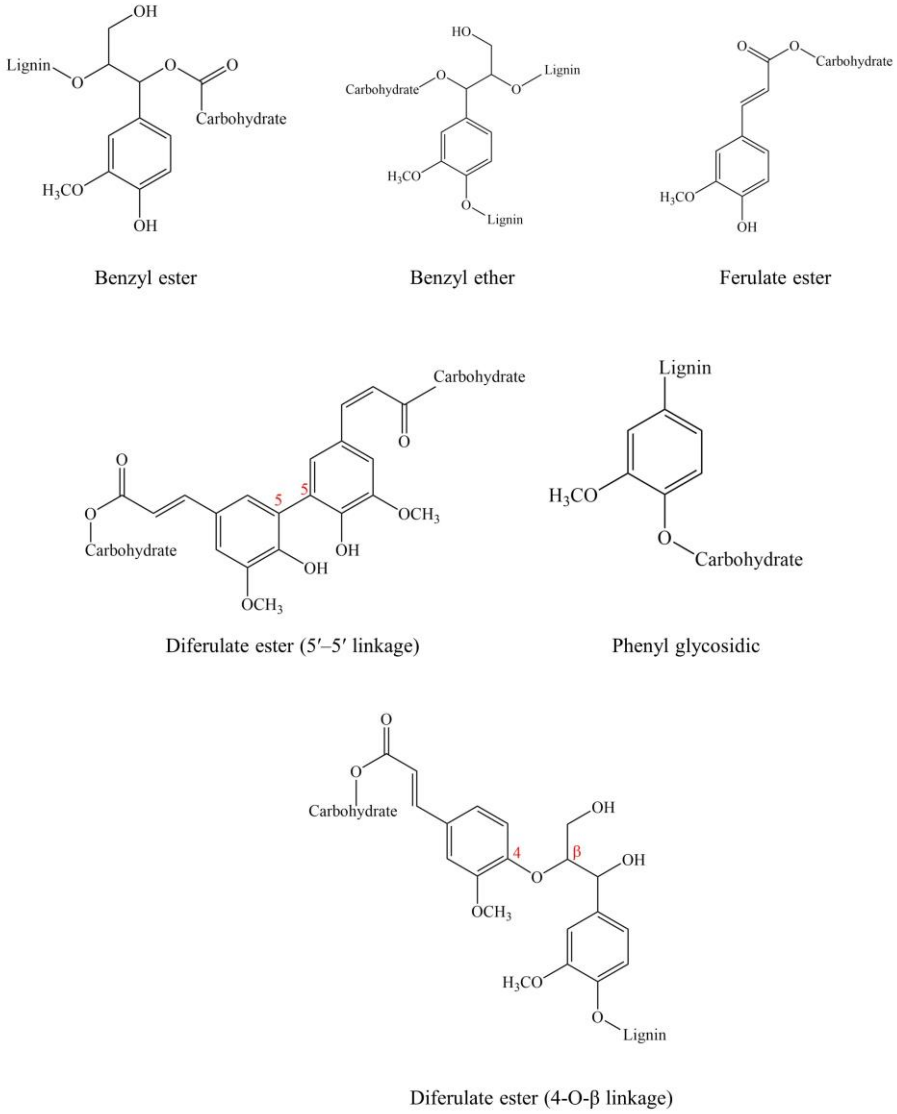

Figure 2. Main linkages in lignin carbohydrate complex

Lignin

The emphasis of current biorefineries is on the carbohydrate's fractions and their conversion to sugars and further to bioethanol as a biofuel or potential precursor for chemicals. In order to build competitive and economically stable biorefineries, the potential of each fraction needs to be utilized to a maximum. Difficulties in efficient lignin utilization lay in its complex structure, inefficient fractionization, poor processibility and low yield of target products (Liu et al., 2021). Biorefineries that concentrate on carbohydrate conversion accumulate a high amount of lignin enriched residue while lignin is also produced as a by-product in Pulp and Paper industry where different technologies are used to isolate cellulosic fibres (Nguyen et al., 2021). Although being a by-product of different processes, the aromatic and polymeric nature suggests that lignin could be converted to numerous products. Lignin valorization is essential to economically support the development of biorefineries and to reduce the residue accumulated in the biorefineries processes thus contributing to zero-waste requests.

Lignin's complex nature presents the main challenge for its valorization. Significant effort has been made in the last years, even decades to firstly understand lignin structure. A good understanding of lignin structure is a base for finding the solution for cost-effective lignin conversion and application. A very basic overview of lignin structure is given in the following text, written based on the book Lignin and Lignans (Heitner et al., 2016) and First Chapter in the book Lignin Valorisation (Katahira et al., 2018), so that no references are presented further in the text and for

advanced and detailed discussion on the lignin structure the reader is directed to those books.

Overview on lignin structure

The lignin structure is based on the three main monomeric units: coniferyl alcohol, p-coumaryl alcohol and sinapyl alcohol, presented in Figure 3.

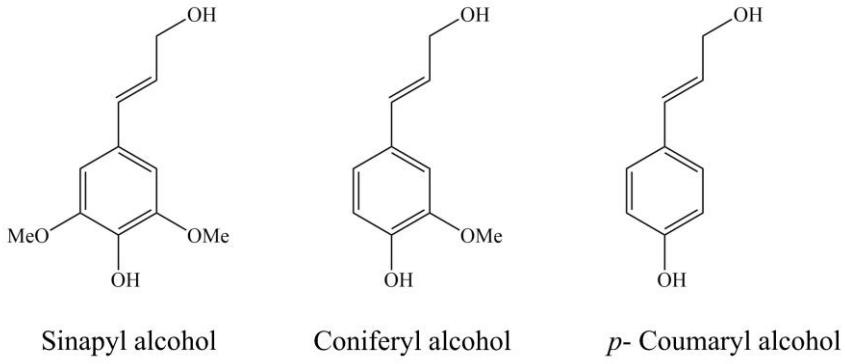

Figure 3. Lignin monomers: sinapyl, coniferyl and p-coumaryl alcohol

Their structures differ by the substitute on the positions three and five of the aromatic ring. The aromatic rings of monomers correspond to guaiacyl unit – **G** unit (derived from coniferyl alcohol), syringyl unit – **S** unit (derived from sinapyl alcohol) and *p*-hydroxyphenyl unit – **H** unit (derived from *p*-coumaryl alcohol). Oxidative coupling of lignin monomers among each other and with the growing polymer result in the formation of three-dimensional lignin polymer. The distribution of lignin monomers varies depending on the lignin origin. Coniferyl alcohol is the main monomer presented in softwood lignins, coniferyl alcohol and sinapyl alcohol are the

main monomers of hardwood lignin, while all three monomers, coniferyl, sinapyl and *p*-coumarin alcohol are presented in lignins from grasses.

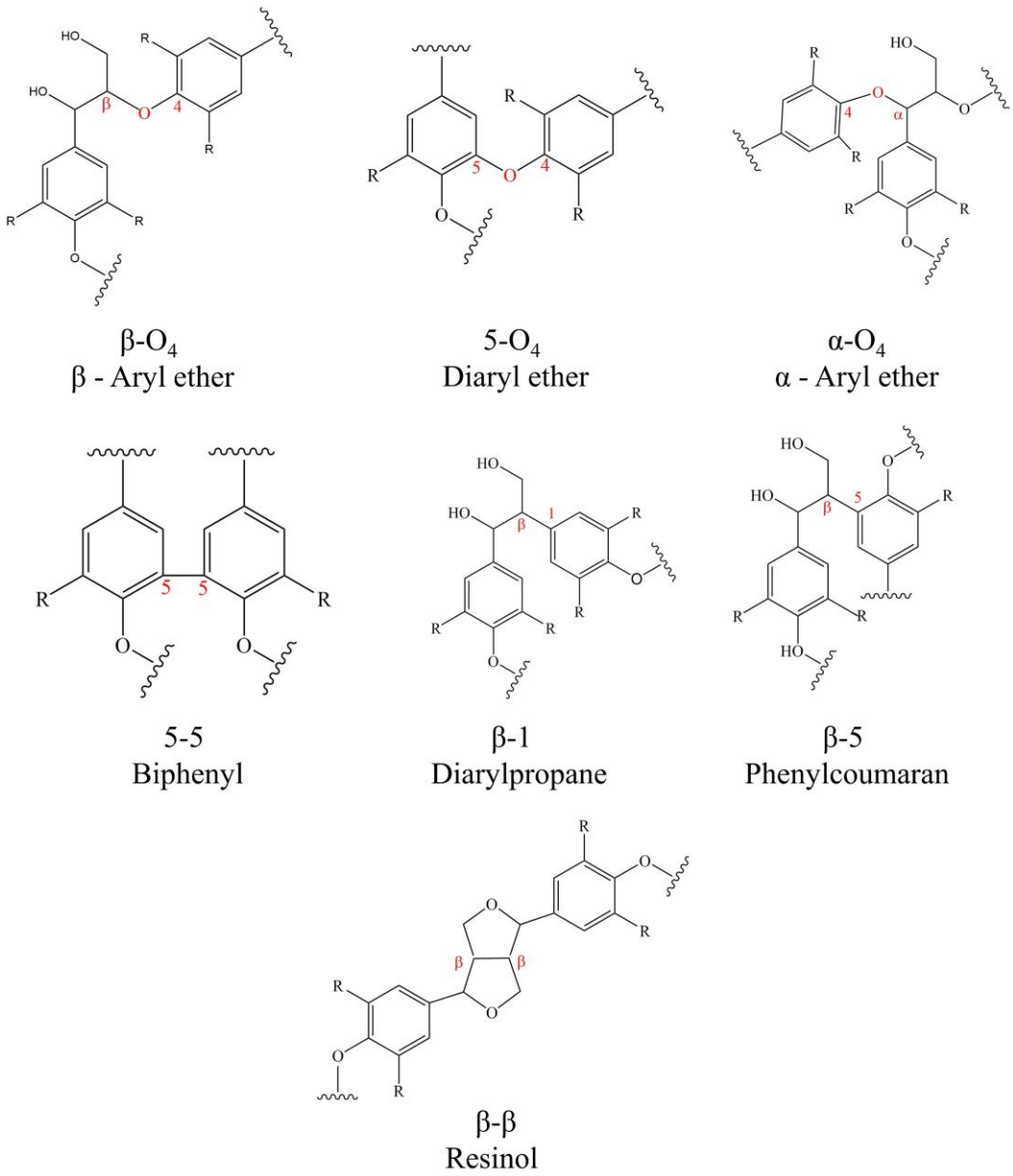

Figure 4. Main linkages in lignin

Lignin units are connected by C-O (ether) linkages or C-C linkages. β-O-4 (β-aryl ether) ether linkage is the most dominant one, with the contribution of 40-60% in softwood and hardwood. This bond is crucial for lignin depolymerization and its predominance arises from the reactivity of phenoxy C-β position. Other important ether bonds in lignin are β-β (resinol unit), α-O-4 (α-Aryl ether), 5-O-4 (diaryl ether). Examples of condense C-C bonds are β-5 (phenylcoumaran unit), 5-5 (biphenyl unit), β-1 (1,2-Diarylpropane).The distribution of different linkages, as in the case of the three main building blocks, depends on lignin origin. C-C linkages are much less reactive than ether linkages, thus their proportion in lignin determines its reactivity. Main interunit linkages are presented in Figure 4.

The amount of different functional groups in lignin also affects lignin reactivity. Functional groups presented in lignin are: phenolic hydroxyl, aliphatic hydroxyl, benzyl alcohol, noncyclic benzyl ether, carbonyl groups and methoxyl groups. The high reactivity of various functional groups in lignin is a key factor for the production of chemical pulps used in high-quality paper production.

Lignin phenolic and aliphatic hydroxyl groups are important in lignin biosynthesis and degradation reaction. Phenolic hydroxyl groups are related to the degree of pulp brightness and stability while ring conjugated carbonyl groups are related to a darker pulp color. The degradation reaction in lignin normally starts from the benzyl position, thus benzyl ether and benzyl alcohol groups are important in lignin chemical reactions. The structural model of softwood lignin is presented in Figure 5. This model is proposed by Balakshin et al. (Balakshin et al., 2020b). for spruce milled wood lignin.

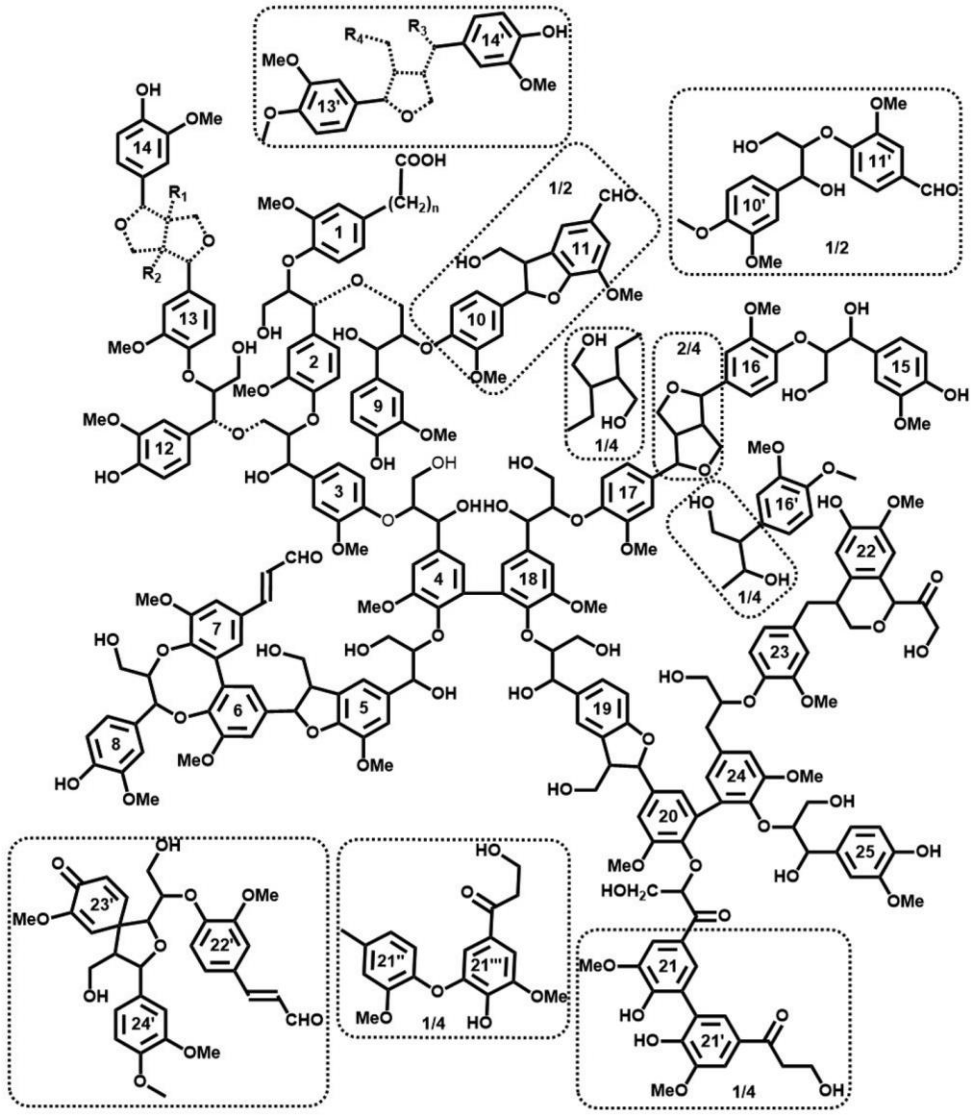

Figure 5. Structural model for softwood lignin (spruce milled wood lignin)(Balakshin et al., 2020b)

Supercritical water technology

Based on the idea of a sustainable future through an environmental perspective, biorefineries should be based on environmentally benign technologies, not involving potentially harmful reagents. There is no more benign technology for the environment than one that uses just water as the major chemical. Different technologies that use the benefit of water properties at elevated pressure and temperature have been investigated for decades. Supercritical water-based technologies are used in many fields, from conduction of reaction to the treatment of wastewater or even treatment of human metabolic wastes in space (Tester and Cline, 1999).

Supercritical water

Hydrogen bonds in water are responsible for its unique properties. These properties and the "green chemical profile" make water be applied in numerous industrial processes. The properties of water change significantly with the change of temperature and pressure, which opens even more possibilities for application. Once the water reaches the critical pressure and temperature (22 MPa and 374 °C), it becomes supercritical, as presented in the p-T diagram of water in Figure 6.

From a solvent for ionic species as it is at ambient conditions, water changes its character to a solvent for non-ionic species at and above critical conditions (Brunner, 2014). This is due to the change of properties that govern dissolving power. Water properties from the liquid phase to the supercritical state are a function of hydrogen bonding, which is affected by temperature and pressure.

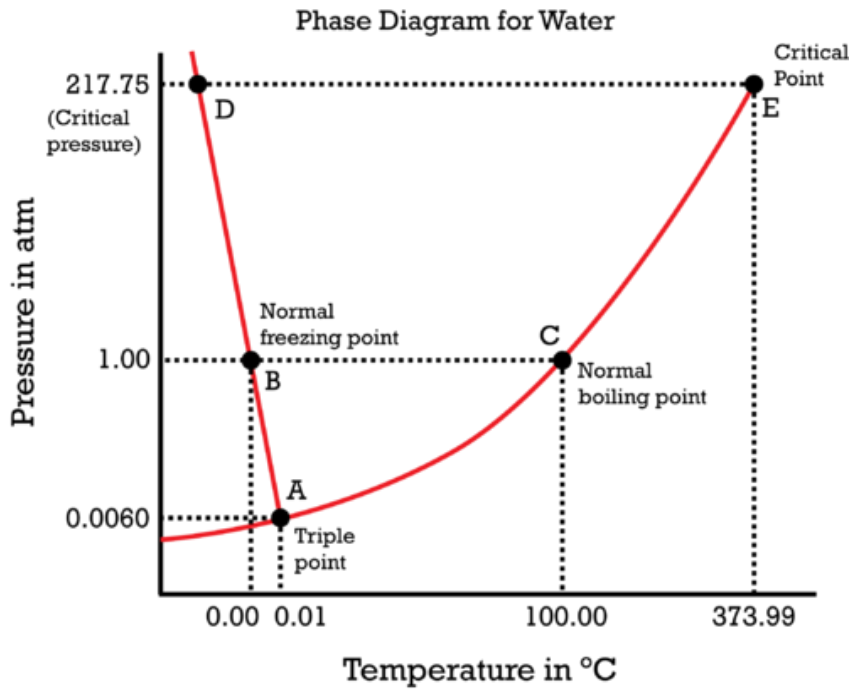

Figure 6. p-T diagram of water

The density, ionic product and dielectric constant of water as a function of temperature are presented in Figure 7. As it can be seen when approaching the critical point, small changes in P and T cause a significant change in density, influencing strongly in this way the properties of water. Due to corresponding density change and level of hydrogen bonding, the dielectric constant also decreases significantly, from about 80 as it is in ambient condition to close to 5 at supercritical conditions. Water dissociation is simulated at higher temperatures, up to 250 °C, thus the increased ions concentration is favorable for acid-catalyzed reactions. However, when approaching the critical point, ionic product changes strongly, as dissociation is strongly reduced. In this region, water becomes favorable for radical reactions (Brunner, 2014).

Transportation properties of water, viscosity and diffusivity are also important properties of SCW. At supercritical conditions, viscosity decreases as a function of density and temperature, while the diffusivity increase. This is important especially when complex material such as biomass is processed in SCW as those properties facilitate penetration of water into biomass structures (Cocero et al., 2018).

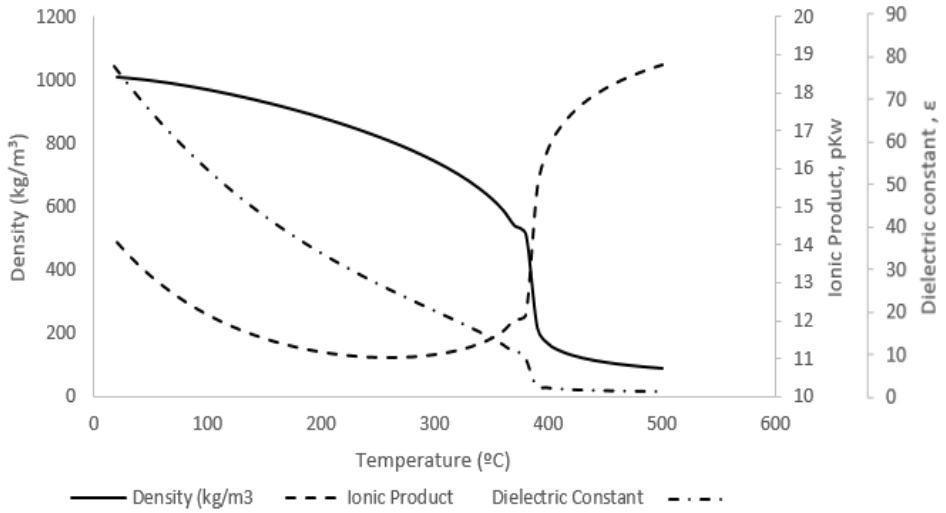

Figure 7. Water properties as a function of temperature

Because water in the supercritical state does not have phase boundaries, mass transfer limitation can be avoided which causes faster reaction rates. Reaction speed can be an important advantage for process intensification. To enable modular units to deal with a large volume of biomass, the processes need to be intensified (Cocero et al., 2018).

Biomass fractionization

Three main constituents of lignocellulosic biomass are potential feedstock for different products. Sugars obtained from cellulose and hemicellulose can be further used for bioethanol production, but also as building blocks for chemicals production (Werpy and Petersen, 2004). Isolated hemicellulose can be used for packaging, food, cosmetical or pharmaceutical applications (Arzami et al., 2022; Chen et al., 2016). A wide assortment of products could be obtained from lignin ether considering its aromatic nature for the production of chemicals or its polymeric nature for the production of macromolecules (Holladay et al., 2007). In order to convert biomass into the desired products, the main biomass building blocks cellulose, hemicellulose and lignin firstly need to be separated (Cocero et al., 2018). Acid and enzymatic hydrolysis are classical methods used to fractionate biomass. Enzymatic hydrolysis of biomass requires the implementation of pretreatment steps so that recalcitrance barriers are removed and enzymatic digestibility increased (Hendriks and Zeeman, 2009). This is a crucial step to enhance enzymatic efficiency, but it is the costliest part of the process (Capolupo and Faraco, 2016). Pre-treatment includes physical, chemical, physicochemical or biological methods, or their combination (Łukajtis et al., 2018). The price of enzymes makes enzymatic hydrolysis a cost-intensive step as well (Capolupo and Faraco, 2016). Concentrated acid hydrolysis uses high acid concentration (over 30%) at ambient and moderate temperatures (<100 °C) to obtain high sugar yield without additional enzymatic hydrolysis (Jung and Kim, 2015). Avoiding enzymatic hydrolysis is an advantage of this process, but the highly corrosive nature of used acids is the main disadvantage. The use of concentrated acids

needs expensive equipment and necessary steps of acid recovery because of the economic and environmental concerns (Solarte-Toro et al., 2019). In order to avoid drawbacks of conventional technologies used to fractionate biomass, hydrothermal and supercritical water processes were introduced as a green alternative.

Biomass fractions processed under hydrothermal and supercritical water conditions

The absence of a phase boundary (between vapor and liquid phase) is an important advantage for reaction kinetics in SCW processes. In order to understand the potential of SCW for biomass processing, the hydrolysis of its separate fractions has been intensively studied. Cellulose hydrolysis was performed in batch and continuous reactors. It was found that the main parameters of hydrolysis are temperature and reaction time (Cocero et al., 2018). As reactions in batch reactors normally take longer reaction times, the degradation of hydrolyzed sugars further occurs, yielding the undesired degradation products (Ehara and Saka, 2002; Zhao et al., 2009). Continuous reactors on the other hand allow shorter reaction times and better time control. Hydrolyzing cellulose in a continuous reactor with a reaction time in the range of milliseconds, a high yield of 96 % was obtained and further degradation was avoided (Cantero et al., 2013). While the rigid structure makes cellulose insoluble in ambient, partially soluble in subcritical water and completely soluble at temperatures above 330 °C (Kumar and Gupta, 2008), hemicellulose can be easily dissolved in water at temperatures above 160 °C (Gallina et al., 2016a; Kim et al., 2014). Mild temperatures of 160 °C to 210 °C are normally used to extract

hemicellulose from biomass (Cocero et al., 2018). Using a temperature of 180 °C 60 % of hemicellulose could be extracted from biomass (Gallina et al., 2016; Yedro et al., 2017). The higher temperature allows higher extraction yield but leads from the other side to a higher yield of degradation products as well. Lignin depolymerization has been studied intensively to prove its potential as a source of aromatic compounds. Temperature and time also were found as main parameters for process optimization, while time was found to be the more determining one. 10 % w/w aromatic compound could be obtained in SCW hydrolysis of lignin for the optimal time of 0.3 s (Abad-Fernández et al., 2019). The main problem reported in lignin depolymerization is char production that limits the yield of desired products (Jiang et al., 2016; Yong and Matsumura, 2012; Yong and Yukihiko, 2013). Actually, in supercritical water lignin is depolymerized to smaller fractions (monomeric, dimeric compounds …), but those compounds show the tendency to further react and upgrade to molecules of higher molecular mass in already mentioned repolymerization reactions. As reaction time has a crucial role in the depolymerization of lignin, its control is essential for governing the reaction.

Biomass processed under hydrothermal and supercritical water conditions

Three main constituents of biomass show different kinetics and behavior under hydrothermal and SCW conditions. While SCW conditions are too severe for amorphous hemicellulose polymer, cellulose can be easily hydrolyzed with a high yield for a very short time around 0.01 s (Cantero et al., 2013). A longer reaction time,

of 0.3 s, is however needed to obtain the maximum yield of phenolic compounds from lignin (Abad-Fernández et al., 2019), but an even longer reaction time will favor undesired repolymerization reaction. As discussed in the previous sections, those fractions are in biomass connected through chemical bonding that strengthens the rigidity of the whole structure. This contributes significantly to mass transfer limitation when the whole biomass is processed in SCW. Transportation properties of SCW, such as high diffusivity and low viscosity can help to face biomass recalcitrant structure. The dialectic constant of SCW is similar to non-polar organic solvents, thus solubility of organic compounds is enhanced (Cocero et al., 2018), making SCW a good solvent for hydrolysis products.

On the other hand, the composition of biomass does differ between different types. The biomass that has a higher amount of carbohydrate fraction will be easier fractionated in SCW compared to biomass with high content of lignin. The influence of biomass composition in the processes that use SCW will be later discussed in Chapter 1.

Press Tech Biorefinery approach

The development of biorefinery requires technology that will be able to deal with a high amount of biomass. On the other side reaction time is a crucial parameter for biomass hydrolysis in SCW. Press Tech group has developed a Supercritical water hydrolysis plant that operates in continues mode. Operation in continuous mode gives the opportunity of intensifying process but also to have precise control of reaction time. The mentioned group possesses a pilot, as well as a lab scale of the plant, each

of them will be in detail discussed in Chapter 1 and Chapter 2. Herein, the principle of the design will be demonstrated.

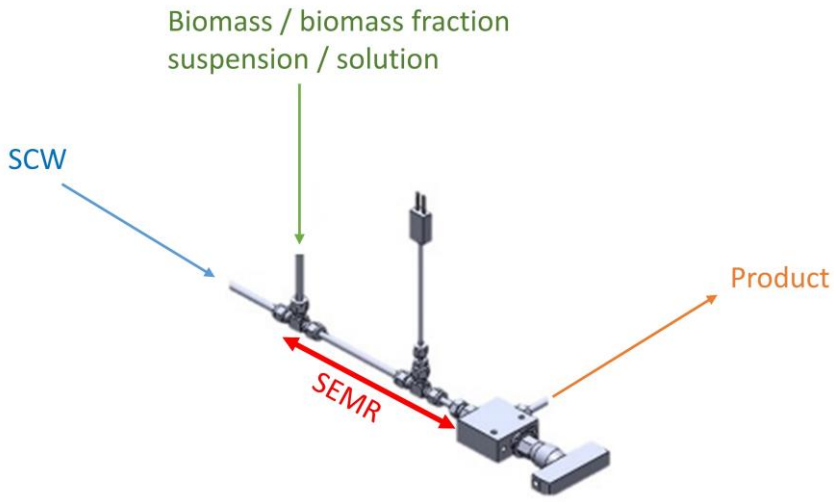

Figure 8. Sudden Expansion Micro Reactor for Supercritical water hydrolysis plant

The so-called Sudden Expansion Micro Reactor (SEMR) can be seen in Figure 8). SEMR is composed of a T-junction which is also the mixing point for SCW and the biomass suspension. After the T-junction stainless steel tube is installed, that is actually a variable part of the reactor as the length of this tube can be changed depending on the desired reaction time. Another T-junction with a thermocouple is installed after the tube, which provides the temperature measurement from inside the reactor. A high pressure and temperature valve is installed at the end of the SEMR. By passing through this valve, the product is cooled down due to the Joules-Tomson effect, so that sudden termination of the reaction is provided.

This simple design of the reactor provides instant start and termination of reaction and further the possibility to avoid degradation reaction due to the cooling

and heating slopes. Furthermore, the easy adjustment of the reaction time is provided by changing only the length of the tube or the flow through the reactor. Continuous mode from the other side gives the possibility to deal with a high amount of biomass. Although the reactor describes just the principle, the design of the plant also provides in-line separation of the product by installed filters and flash separators, as well as heat integration.

Application of green technologies such as SCW hydrolysis to valorize second generation biomass, help us to take further steps towards new environmentally compatible and sustainable chemicals and materials. Anastas and Zimmerman established 12 principles of green engineering and herein the discussion of how the use of supercritical water technology in lignocellulosic biomass valorization meet the requirements of green engineering is discussed (Anastas and Zimmerman, 2007):

Inherent rather than circumstantial. Second generation biomass is not competitive with food or feed. Furthermore, this thesis discussed the valorization of defatted grape seeds that are a by-product of grape seed oil production. The SCWH process requires thermal and electrical energy. The use of a gas turbine can lead to zero-energy consumption in the process, where the detailed explanation of heat integration with calculations can be found in the previous work (Cantero et al., 2015b).

Prevention Instead of Treatment. This process opens the possibility to valorize a by-product.

Design for Separation. Filters and flash separators are installed and can be used in line. Sample eluent can be sent to the filters for liquid and solids separation. The liquid eluent can be further sent to the flash separator for further concentration. The separation steps require no extra energy.

Maximize Efficiency. Mass transfer is the limiting step in the biomass fractionation process (Cocero et al., 2018). SCW improve the mass transfer as there is no boundary between the liquid and gas phase and the reaction is conducted in one, supercritical water state. This is the key point for process intensification, as reaction time is very short, in the range of ms and s. This results in the low required reaction volume.

Output-pulled versus Input-pushed. Zero-petroleum-based society is getting closer. Future legislation is going in that direction. Soon, a great demand for nature-based products will require processes like this one. After the hydrolysis of lignocellulosic biomass in SCW water liquid and solid effluents are obtained. The liquid effluent is enriched in sugars and could be used for fermentation, producing ethanol, butanol, etc., where also compounds with antioxidant activity could be isolated. The solid effluent is enriched in lignin and Lignin-Carbohydrate Complex that could be further refined and potentially used for new plastics. As mentioned above the heat recovery is considered in all the process steps (Cantero et al., 2015b).

Conserve complexity. SCW allows for the quick disintegration of biopolymers. The control of the reaction time and reaction conditions allows high yield and selectivity toward desired products (Abad-Fernández et al., 2019; Cantero et al., 2013; Martínez et al., 2015). The operation at high P and T is an opportunity for heat integration (Cantero et al., 2015b).

Durability rather than immortality. The process can operate with different feedstocks, as different biomasses or biopolymers. This brings high diversity of obtained products that are nature based, so that they can be durable but also

biodegradable. The plant and devices used are improved with new materials that support operation at high pressures and temperatures.

Meet need, minimize excess. Reaction time is one of the main variables that influence the selectivity of the process (Cocero et al., 2018). The reaction time can be easily adjusted just by changing the length of the reactor or the flow of biomass and water streams. Innovative Sudden Expansion Micro Reactor (SEMR) supported in a tubular reactor concept allows operating with residence time from 0.1s.

Minimize material diversity. Innovative reactor design supported in conventional high-pressure devices is accessible and disassembly friendly.

Integrate material and energy flows. The process energy demand considers the heat recovery from the effluent to the SCW preheaters. The heat integration developed allows the recovery of effluent work and heat (Cantero et al., 2015c).

Design for commercial "afterlife". SCWH process is a continuous process easy to scale up (Martínez et al., 2019). A Demo plant is running for the production of commercial products (Renmatix). The production is very flexible due to the possibility of obtaining a wide range of products when biomass feedstock is changed or the operating conditions are varied.

Renewable rather than depleting. Biomass is a renewable material source, and the thermal and electrical energy can be easily produced from the renewable source too.

Approach to follow lignin depolymerization in Supercritical water

The depolymerization of lignin in supercritical water to the desirable monomers occurs in short reaction times. At longer reactions times, however, the production of char was observed in different studies. A system that can allow following the depolymerization reaction in real-time could significantly help to understand the mechanism of these ultra-fast reactions. Taking into account the high temperature and pressure conditions applied during SCW reactions, this system needs to be designed for these harsh conditions. Our primary idea on such system as well as some results obtained in the study are given in the following section.

Methodology

High-pressure visual cell

A high-pressure visual cell (HPVC) is designed for operating under supercritical water conditions, presented in Figure 9. The cell is made out of Inconel and provides optical access through two sapphire windows located in opposition to each other**.** The internal volume of the cell is 30 ml and the maximum operating conditions are 500 °C and 30 MPa. The design of the cell allows the instantaneous introduction of the reagents (lignin or lignin model compounds) into the supercritical water medium by a magnetic elevator (ME) that is separated from the cell body by a high-pressure ball valve (G). The magnetic agitator is installed at the top of the cell and provide operation with a uniform mixture. Once the desired conditions in the cell

are reached (water in the supercritical state) and the elevator holder is pressurized to the pressure equal to the pressure in the cell, the valve can be opened and the elevator that carries the reagent is lifted into the cell. This is a way to introduce a solid sample into the cell, while for a liquid sample a simple piston pump could be used. In this way, undesired reactions due to the heating step are avoided. By using the sapphire windows as optical access, *in situ* Raman spectroscopy could be utilized to monitor reactions in SCW.

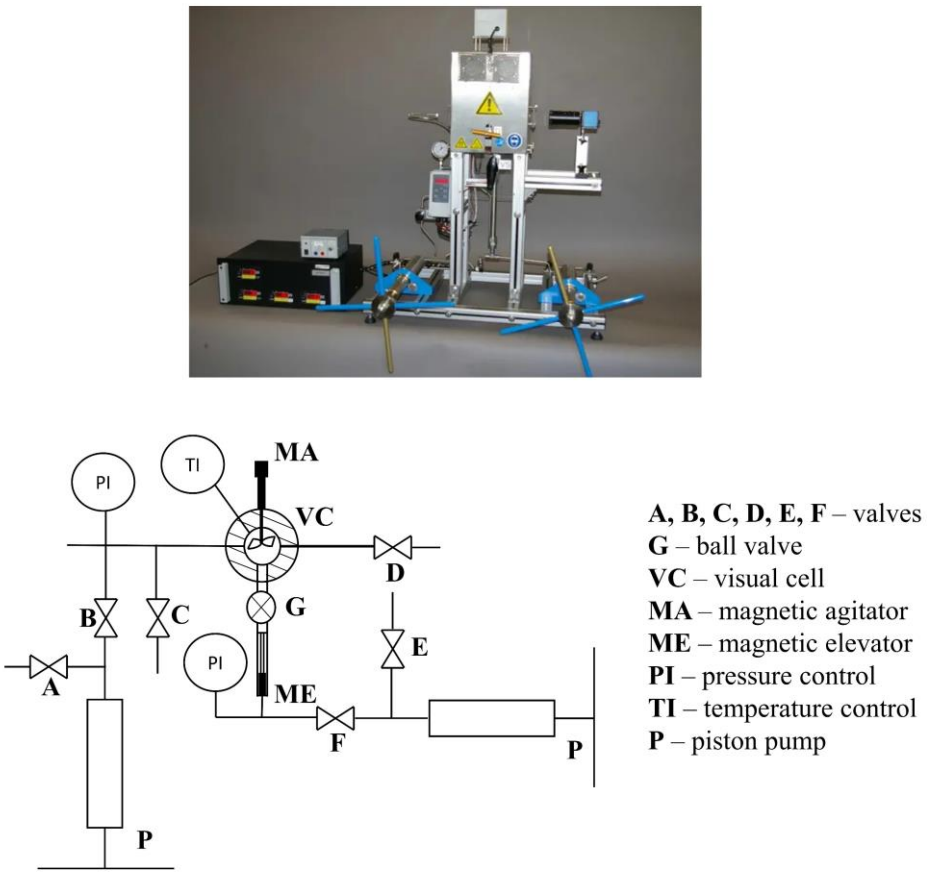

Figure 9. Photo and scheme of high-pressure visual cell

In situ Raman spectroscopy

Raman spectroscopy is based on an inelastic light scattering effect that was firstly discovered by C. V. Raman. When exciting a molecule with photons the vast part of the introduced energy is elastically scattered or absorbed, while a much smaller part is however inelastically scattered. This effect is known as Raman scattering, which can be separated in Stokes and anti-Stokes scattering. While the Stokes-scattered light is of a higher wavelength compared to the excitation source, the anti-Stokes-scattered light (not relevant in this study) is of a lower wavelength. This shift in wavelength is known as the Raman shift, (normally given in cm^{-1}) and is specific for each scattering effect (vibration, rotation etc.) of molecules. A Raman spectrum is obtained by plotting the detected intensity counts over the Raman shifts that correspond to pixels of the spectrometer (Braeuer, 2015).

The change of water properties as a function of temperature and pressure was already discussed in the text above and is again visualized in Figure 10. The spectra in Figure 10 are taken in a microcapillary setup at ITUN in Freiberg. Regarding the therein given spectra normalized by Raman signal area, the change in the shape of the OH stretch vibration of water caused by fading of hydrogen bonds is obvious. While the OH bands until a temperature of 350 °C tend to have a broad structure, a big change towards a single peak can be observed once supercritical conditions are reached (compare the spectrum of 400 °C).

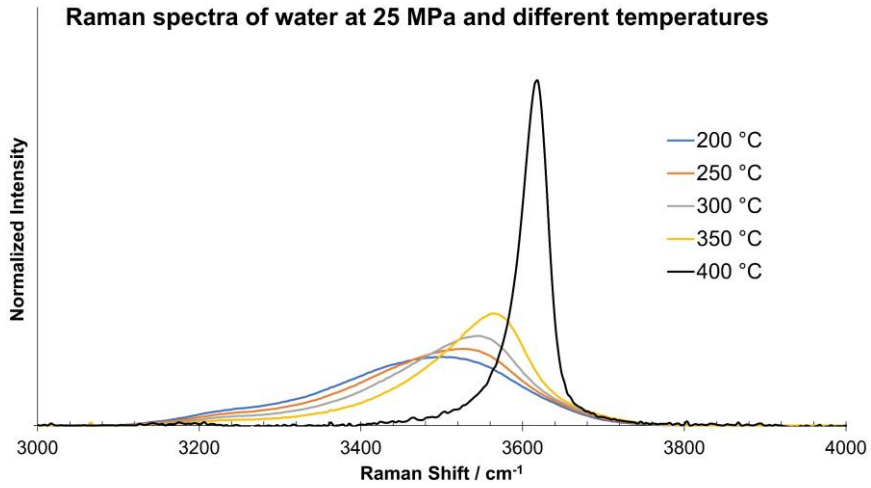

Figure 10. Raman spectra (532 nm excitation) of water at constant pressure of 25 Mpa and different temperatures taken in a microcapillary setup of ITUN TU Freiberg

When regarding water containing systems, Raman spectroscopy can be advantageous compared to infrared spectroscopy due to the tendency of strongly overlapping OH signals, especially in IR spectra. A setback of Raman analysis however is potentially disturbing fluorescence, especially in partly-turbid systems.

The high-pressure visual cell was coupled with the devices of the *in situ* Raman spectroscopy unit. The latter consists of a laser, a Raman gun in the design of Prof. Andreas Bräuer, two optical fibers and an Ocean View Qepro spectrometer. The Raman gun units optical parts for excitation and detection are described in detail in several publications (Braeuer, 2018; Fechter and Braeuer, 2020).

The described system was applied in experiments of depolymerization of eugenol as a lignin model compound in supercritical water. Hereby two different excitation wavelengths of 532 nm and of 785 nm were used. Unfortunately, few phenomena were found to be obstacles to successful experimentation. High

fluorescence was observed already when just water spectra was measured in HPVC. The spectra of water, recorded for different temperatures in HPVC are presented in Figure 11. Clear water spectra with OH stretch vibration in the range of 3100 – 3700 cm^{-1}can be observed at 100°C. With an increase in temperature, the fluorescence effect becomes more pronounced. In supercritical water conditions (380 °C) the whole spectrum is covered with high fluorescence and no OH stretch vibration can be observed. Two reasons can be behind this strong fluorescence effect:

1. As explained above, the properties of water change significantly from ambient to supercritical conditions and water changes its character from the ionic polar solvent as it is at ambient conditions to non-polar solvent at critical conditions. This means that once introduced in the reactor at ambient conditions and heated to supercritical conditions water covers a very wide range of solubility, dissolving probably all possible impurities presented in the cell. To exclude this possibility the reactor was disconnected from the setup and intensively cleaned with water and acetone. Before continuing measurements, the cell was few times cleaned heating water to the supercritical state.

2. The second possible reason could be high thermal radiation. As the cell is made out of stainless steel and embedded in the heating jacket, it accumulates and radiates a lot of heat that can interfere with Raman measurement.

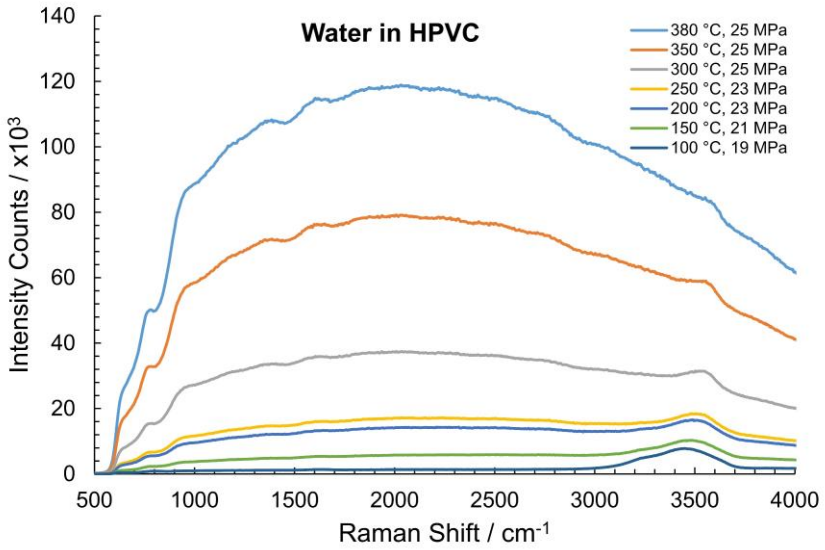

Figure 11. Raman spectra (532 nm excitation) of water at different temperatures taken in a HPVC setup

Unfortunately, the above listened problem was not solved by cell cleaning. The change of the laser wavelength could improve the decrease of fluorescence effect, but however, when the supercritical state was reached, no OH stretch vibration could be observed anymore.

The spectra of water presented in Figure 10 are, as mentioned, recorded using a capillary system. This system consists of a fused silica microcapillary reactor embedded in a steel heating block insulated by ceramic foam. The optical access is provided through spots where the polymer coating of the capillary is removed. The system has three pumps. Two feeding pumps for water and model compounds, one take-up pump for the conveyed mixture. The mixing of water and model compound streams is placed in the T-junction located prior to the heating block. A detailed explanation of the system can be found elsewhere (Fechter and Braeuer, 2020).

Although clear spectra with water were obtained up to 400 °C, few obstacles inhibited continuation of measurements with lignin model compound:

As the system consists of a capillary reactor, just a laminar flow of the system is possible, thus influencing the mixing in the system. Clear separation of two phases could be observed after the mixing point.

As pointed out in the text above, lignin monomers tend to upgrade to molecules with higher molecular weight in SCW. The char formation was observed as the microcapillary reactor was breaking due to the plug caused inside the reactor. This is probably due to the long residence time in the reactor, as reactor geometry cannot provide reaction times under 3s.

References:

Abad-Fernández, N., Pérez, E., Cocero, M.J., 2019. Aromatics from lignin through ultrafast reactions in water. Green Chem. 21, 1351–1360. https://doi.org/10.1039/C8GC03989E

Anastas, P.T., Zimmerman, J.B., 2007. Design Through the 12 Principles of Green Engineering. Environmental Science and Technology. 35, 16–16. https://doi.org/10.1109/EMR.2007.4296421

Arzami, A.N., Ho, T.M., Mikkonen, K.S., 2022. Valorization of cereal by-product hemicelluloses: Fractionation and purity considerations. Food Res. Int. 151, 110818. https://doi.org/10.1016/j.foodres.2021.110818

Balakshin, M., Capanema, E.A., Zhu, X., Sulaeva, I., Potthast, A., Rosenau, T., Rojas, O.J., 2020. Spruce milled wood lignin: linear, branched or cross-linked? Green Chem. 22, 3985–4001. https://doi.org/10.1039/D0GC00926A

Boerjan, W., Ralph, J., Baucher, M., 2003. Lignin Biosynthesis. Annu. Rev. Plant Biol. 54, 519–546. https://doi.org/10.1146/annurev.arplant.54.031902.134938

Bracmort, K., Gorte, R.W., 2010. Biomass: Comparison of definitions in legislation. Biomass Energy Data, Multi-Year Plan Legis. Defin. 1–18.

Braeuer, A.S., 2018. Prospects: Facing current challenges in high pressure high temperature process engineering with in situ Raman measurements. J. Supercrit. Fluids 134, 80–87. https://doi.org/10.1016/j.supflu.2017.11.026

Braeuer, A.S., 2015. In situ Spectroscopic Techniques at High Pressure. Elsevier. ISBN: 9780444634221

Bridgwater, A., 2013. Fast pyrolysis of biomass for the production of liquids, in: Biomass Combustion Science, Technology and Engineering. Elsevier, pp. 130–171. https://doi.org/10.1533/9780857097439.2.130

Brunner, G., 2014. Hydrothermal and Supercritical Water Processes. Elsevier. ISBN: 978-0-444-59413-6

Cantero, D.A., Bermejo, M.D., Cocero, M.J., 2015ª. Governing Chemistry of Cellulose Hydrolysis in Supercritical Water. ChemSusChem 8, 1026–1033. https://doi.org/10.1002/cssc.201403385

Cantero, D.A., Bermejo, M.D., Cocero, M.J., 2013. High glucose selectivity in pressurized water hydrolysis of cellulose using ultra-fast reactors. Bioresour. Technol. 135, 697–703. https://doi.org/10.1016/j.biortech.2012.09.035

Cantero, D.A., Vaquerizo, L., Mato, F., Bermejo, M.D., Cocero, M.J., 2015c. Energetic approach of biomass hydrolysis in supercritical water. Bioresour. Technol. 179, 136–143. https://doi.org/10.1016/j.biortech.2014.12.006

Capolupo, L., Faraco, V., 2016. Green methods of lignocellulose pretreatment for biorefinery development. Appl. Microbiol. Biotechnol. 100, 9451–9467. https://doi.org/10.1007/s00253-016-7884-y

Chen, G.-G., Qi, X.-M., Guan, Y., Peng, F., Yao, C.-L., Sun, R.-C., 2016. High Strength Hemicellulose-Based Nanocomposite Film for Food Packaging Applications. ACS Sustain. Chem. Eng. 4, 1985–1993. https://doi.org/10.1021/acssuschemeng.5b01252

Cherubini, F., 2010. The biorefinery concept: Using biomass instead of oil for producing energy and chemicals. Energy Convers. Manag. 51, 1412–1421. https://doi.org/10.1016/j.enconman.2010.01.015

Cherubini, F., Jungmeier, G., Wellisch, M., Willke, T., Skiadas, I., Van Ree, R., de Jong, E., 2009. Toward a common classification approach for biorefinery systems. Biofuels, Bioprod. Biorefining 3, 534–546. https://doi.org/10.1002/bbb.172

Cocero, M.J., Cabeza, Á., Abad, N., Adamovic, T., Vaquerizo, L., Martínez, C.M., Pazo-Cepeda, M.V., 2018. Understanding biomass fractionation in subcritical & supercritical water. J. Supercrit. Fluids 133, 550–565. https://doi.org/10.1016/j.supflu.2017.08.012

De Buck, V., Polanska, M., Van Impe, J., 2020. Modeling Biowaste Biorefineries: A Review. Front. Sustain. Food Syst. 4. https://doi.org/10.3389/fsufs.2020.00011

de Jong, E., Higson, A., Walsh, P., Wellisch, M., 2011. Bio-based chemicals Value Added Products from Biorefineries. IEA Bioenergy – Task 42 Biorefinery

Dong, H., Zheng, L., Yu, P., Jiang, Q., Wu, Y., Huang, C., Yin, B., 2020. Characterization and Application of Lignin–Carbohydrate Complexes from Lignocellulosic Materials as Antioxidants for Scavenging In Vitro and In Vivo Reactive Oxygen Species. ACS Sustain. Chem. Eng. 8, 256–266. https://doi.org/10.1021/acssuschemeng.9b05290

Ehara, K., Saka, S., 2002. A comparative study on chemical conversion of cellulose between the batch-type and flow-type systems in supercritical water. Cellulose 9, 301–311. https://doi.org/10.1023/A:1021192711007

Fechter, M.H.H., Braeuer, A.S., 2020. Vapor–Liquid Equilibria of Mixtures Containing Ethanol, Oxygen, and Nitrogen at Elevated Pressure and Temperature, Measured with In Situ Raman Spectroscopy in Microcapillaries. J. Chem. Eng. Data 65, 3373–3383. https://doi.org/10.1021/acs.jced.0c00184

Fernihough, A., O'Rourke, K.H., 2014. Coal and the European Industrial Revolution. The Economic Journal 131, 1135-1149. https://doi.org/10.1093/ej/ueaa117

Gallina, G., Cabeza, Á., Biasi, P., García-Serna, J., 2016. Optimal conditions for hemicelluloses extraction from Eucalyptus globulus wood: hydrothermal treatment in a semi-continuous reactor. Fuel Process. Technol. 148, 350–360. https://doi.org/10.1016/j.fuproc.2016.03.018

Giummarella, N., Lawoko, M., 2017. Structural Insights on Recalcitrance during Hydrothermal Hemicellulose Extraction from Wood. ACS Sustain. Chem. Eng. 5, 5156–5165. https://doi.org/10.1021/acssuschemeng.7b00511

Heitner, C., Dimmel, D., Schmidt, J. (Eds.), 2016. Lignin and Lignans Advances in Chemistry. CRC Press. ISBN 9781574444865

Hendriks, A.T.W.M., Zeeman, G., 2009. Pretreatments to enhance the digestibility of lignocellulosic biomass. Bioresour. Technol. 100, 10–18. https://doi.org/10.1016/j.biortech.2008.05.027

Himmel, M.E., Ding, S.-Y., Johnson, D.K., Adney, W.S., Nimlos, M.R., Brady, J.W., Foust, T.D., 2007. Biomass Recalcitrance: Engineering Plants and Enzymes for Biofuels Production. Science 315, 804–807. https://doi.org/10.1126/science.1137016

Holladay, J.E., White, J.F., Bozell, J.J., Johnson, D., 2007. Top Value-Added Chemicals from Biomass – Volume II—Results of Screening for Potential Candidates from Biorefinery Lignin. Pacific Northwest National Laboratory https://doi.org/10.2172/921839

Jiang, W., Lyu, G., Wu, S., Lucia, L.A., Yang, G., Liu, Y., 2016. Supercritical Water-induced Lignin Decomposition Reactions: A Structural and Quantitative Study. BioResources 11. https://doi.org/10.15376/biores.11.3.5660-5675

Jin, Z., Katsumata, K.S., Lam, T.B.T., Iiyama, K., 2006. Covalent linkages between cellulose and lignin in cell walls of coniferous and nonconiferous woods. Biopolymers 83, 103–110. https://doi.org/10.1002/bip.20533

John U, N., 1977. An Early Energy Crisis and Its Consequences. Sci. Am. Vol. 237, 140–151.

Jung, Y.H., Kim, K.H., 2015. Acidic Pretreatment, in: Pretreatment of Biomass. Elsevier, pp. 27–50. https://doi.org/10.1016/B978-0-12-800080-9.00003-7

Katahira, R., Elder, T.J., Beckham, G.T., 2018. Chapter 1: A Brief Introduction to Lignin Structure, in: Lignin Valorization: Emerging Approaches. RSC Energy Environ., pp 1-20. https://doi.org/10.1039/9781788010351-00001

Kumar, S., Gupta, R.B., 2008. Hydrolysis of Microcrystalline Cellulose in Subcritical and Supercritical Water in a Continuous Flow Reactor. Ind. Eng. Chem. Res. 47, 9321–9329. https://doi.org/10.1021/ie801102j

Lee, J.-B., Yamagishi, C., Hayashi, K., Hazashi, T., 2011. Antiviral and Immunostimulating Effects of Lignin-Carbohydrate-Protein Complexes from Pimpinella anisum. Biosci. Biotechnol. Biochem. 75, 459–465. https://doi.org/10.1271/bbb.100645

Li, M., Pu, Y., Ragauskas, A.J., 2016. Current Understanding of the Correlation of Lignin Structure with Biomass Recalcitrance. Front. Chem. 4. https://doi.org/10.3389/fchem.2016.00045

Liu, Z.-H., Hao, N., Wang, Y.-Y., Dou, C., Lin, F., Shen, R., Bura, R., Hodge, D.B., Dale, B.E., Ragauskas, A.J., Yang, B., Yuan, J.S., 2021. Transforming biorefinery designs with 'Plug-In Processes of Lignin' to enable economic waste valorization. Nat. Commun. 12, 3912. https://doi.org/10.1038/s41467-021-23920-4

Łukajtis, R., Rybarczyk, P., Kucharska, K., Konopacka-Łyskawa, D., Słupek, E., Wychodnik, K., Kamiński, M., 2018. Optimization of Saccharification Conditions of Lignocellulosic Biomass under Alkaline Pre-Treatment and Enzymatic Hydrolysis. Energies 11, 886. https://doi.org/10.3390/en11040886

Martínez, C.M., Adamovic, T., Cantero, D.A., Cocero, M.J., 2019. Scaling up the production of sugars from agricultural biomass by ultrafast hydrolysis in supercritical water. J. Supercrit. Fluids 143, 242–250. https://doi.org/10.1016/j.supflu.2018.08.017

Martínez, C.M., Cantero, D.A., Bermejo, M.D., Cocero, M.J., 2015. Hydrolysis of cellulose in supercritical water: reagent concentration as a selectivity factor. Cellulose 22, 2231–2243. https://doi.org/10.1007/s10570-015-0674-3

Naik, S.N., Goud, V. V., Rout, P.K., Dalai, A.K., 2010. Production of first and second generation biofuels: A comprehensive review. Renew. Sustain. Energy Rev. 14, 578–597. https://doi.org/10.1016/j.rser.2009.10.003

Nguyen, L.T., Phan, D.-P., Sarwar, A., Tran, M.H., Lee, O.K., Lee, E.Y., 2021. Valorization of industrial lignin to value-added chemicals by chemical depolymerization and biological conversion. Ind. Crops Prod. 161, 113219. https://doi.org/10.1016/j.indcrop.2020.113219

Pei, W., Chen, Z.S., Chan, H.Y.E., Zheng, L., Liang, C., Huang, C., 2020. Isolation and Identification of a Novel Anti-protein Aggregation Activity of Lignin-Carbohydrate Complex From Chionanthus retusus Leaves. Front. Bioeng. Biotechnol. 8. https://doi.org/10.3389/fbioe.2020.573991

Renmatix, available at https://renmatix.com, n.d.

Sakagami, H., Kushida, T., Oizumi, T., Nakashima, H., Makino, T., 2010. Distribution of lignin–carbohydrate complex in plant kingdom and its functionality as alternative medicine. Pharmacol. Ther. 128, 91–105. https://doi.org/10.1016/j.pharmthera.2010.05.004

Solarte-Toro, J.C., Romero-García, J.M., Martínez-Patiño, J.C., Ruiz-Ramos, E., Castro-Galiano, E., Cardona-Alzate, C.A., 2019. Acid pretreatment of lignocellulosic biomass for energy vectors production: A review focused on operational conditions and techno-economic assessment for bioethanol production. Renew. Sustain. Energy Rev. 107, 587–601. https://doi.org/10.1016/j.rser.2019.02.024

Tarasov, D., Leitch, M., Fatehi, P., 2018. Lignin–carbohydrate complexes: properties, applications, analyses, and methods of extraction: a review. Biotechnol. Biofuels 11, 269. https://doi.org/10.1186/s13068-018-1262-1

Tester, J.W., Cline, J.A., 1999. Hydrolysis and Oxidation in Subcritical and Supercritical Water: Connecting Process Engineering Science to Molecular Interactions. Corrosion 55, 1088–1100. https://doi.org/10.5006/1.3283946

Vinardell, M., Mitjans, M., 2017. Lignins and Their Derivatives with Beneficial Effects on Human Health. Int. J. Mol. Sci. 18, 1219. https://doi.org/10.3390/ijms18061219

Werpy, T., Petersen, G., 2004. Top Value Added Chemicals from Biomass: Volume I – Results of Screening for Potential Candidates from Sugars and Synthesis Gas. Pacific Northwest National Laboratory. https://doi.org/10.2172/15008859

Yedro, F.M., Grénman, H., Rissanen, J. V., Salmi, T., García-Serna, J., Cocero, M.J., 2017. Chemical composition and extraction kinetics of Holm oak (Quercus ilex) hemicelluloses using subcritical water. J. Supercrit. Fluids 129, 56–62. https://doi.org/10.1016/j.supflu.2017.01.016

Yong, T.L.-K., Matsumura, Y., 2012. Reaction Kinetics of the Lignin Conversion in Supercritical Water. Ind. Eng. Chem. Res. 51, 11975–11988. https://doi.org/10.1021/ie300921d

Yong, T.L.-K., Yukihiko, M., 2013. Kinetic Analysis of Guaiacol Conversion in Sub- and Supercritical Water. Ind. Eng. Chem. Res. 52, 9048–9059. https://doi.org/10.1021/ie4009748

Yu, Y., Wu, H., 2010. Significant Differences in the Hydrolysis Behavior of Amorphous and Crystalline Portions within Microcrystalline Cellulose in Hot-Compressed Water. Ind. Eng. Chem. Res. 49, 3902–3909. https://doi.org/10.1021/ie901925g

Zhao, Y., Lu, W.-J., Wang, H.-T., 2009. Supercritical hydrolysis of cellulose for oligosaccharide production in combined technology. Chem. Eng. J. 150, 411–417. https://doi.org/10.1016/j.cej.2009.01.026

Zhao, Y., Shakeel, U., Saif Ur Rehman, M., Li, H., Xu, X., Xu, J., 2020. Lignin-carbohydrate complexes (LCCs) and its role in biorefinery. J. Clean. Prod. 253, 120076. https://doi.org/10.1016/j.jclepro.2020.120076

Zoghlami, A., Paës, G., 2019. Lignocellulosic Biomass: Understanding Recalcitrance and Predicting Hydrolysis. Front. Chem. 7. https://doi.org/10.3389/fchem.2019.00874

Objectives of the work

This work is part of the project “Contributions to the development of a sustainable biorefinery. Dissolution/hydrolysis and polymerization of lignin by sub/supercritical water in ultra-fast reactors. Supported by the Ministry of Science and Innovation project CTQ 2016-79777-R.

The primary objective of this thesis was to follow lignin depolymerization in SCW using *in situ* Raman analysis. As explained above the idea was based on the possibility to use a high-pressure cell with optical access that allows the instantaneous start of reaction coupled with Raman spectroscopy to monitor the reaction online. However, due to the above explained limitation to perform that research, the thesis objectives were redirected. The new objectives were set as follows:

Hydrolysis of different biomass feedstocks, such as sugar beet pulp (SBP) and wheat bran (WB) had been previously conducted in our research group proving the feasibility of the SCW hydrolysis to convert these feedstocks into reducing sugars (PhD Thesis: Demonstration of a selective process to transform biomass into sugars by ultrafast hydrolysis in supercritical water, Celia María Martínez Fajardo Siendo, University of Valladolid 2018). However, both SBP and WB are feedstock with high carbohydrate content and very low content of insoluble lignin (2 % w/w and 4 % w/w, respectively).

In the industrial production of grape seed oil, defatted grape seed is produced as waste. This biomass has a lignin insoluble content of 36 % w/w. As discussed in the sections above lignin is an important contributor to biomass recalcitrance, thus it is expected that a high content of insoluble lignin would significantly influence defatted grape seed hydrolysis.

The first objective of this thesis investigates the feasibility of the process when defatted grape seed, as high lignin content biomass is used. The attention is also focused on the characterization of lignin enriched solid residue and understanding the changes that are happening on the lignin structure during the hydrolysis process. This objective is developed in **Chapter 1.**

Lignin is an aromatics-based polymer that is envisaged as the main source of removable aromatics. Lignin depolymerization to obtain aromatics is a challenge for which no solution is foreseen in the short term. The main challenge of depolymerization reaction is right the tendency of depolymerized products to further react in repolymerisation reaction. In a previous thesis from our group (PhD Thesis: Lignin depolymerization by supercritical water ultrafast reactions, Nerea Abad Fernández, University of Valladolid 2019.) it has been proved that SCW could be a good media for depolymerization, and the repolymerization could be reduced by the reduction of the reaction time.

The second objective of the thesis is understanding the repolymerization of lignin in SCW, to provide technology and operating conditions in order to minimize repolymerization impact. The hypothesis is that released monomeric compounds react among each other and lignin fragments yielding molecules with higher molecule weight, through repolymerization reaction. This hypothesis was investigated in **Chapter 2.** The repolymerization reaction is followed through the reaction of lignin model compounds in SCW and the reaction of model compounds with technical lignin. The focus is on understanding the structural changes that occur on the lignin structure after the hydrolysis reaction. The mechanism of the repolymerization reaction is proposed. A better understanding of undesired repolymerization reaction

would help to find the way for its suppression and provide a better recovery of aromatic compounds from lignin.

The objective of **Chapter 3** of the thesis is focused on the contribution to a better understanding of water behavior close to the critical point. In this chapter interfacial tension of water was measured using the pendant drop method as a suitable method for high pressure and temperature conditions. Measurements on the surface tension of water are already available in the literature in a big number of experimental sets, however, just a few experimental sets measure interfacial tension under high pressure and temperature conditions. The objective was to provide a detailed experimental procedure and explanation of the measurement method, as that information often do not supplement experimental results. The measurements of interfacial tension of water were performed in two systems: liquid water in its saturated vapor (water/water system) and liquid water in pressurized nitrogen atmosphere (water/nitrogen system). Two systems were compared and the influence of nitrogen on the interfacial tension of water was investigated. The data is further correlated using Macleod – Sugden equation and compared to available data in the literature.

Chapter 1.

Valorization of defatted grape seeds as high lignin content biomass through supercritical water treatment

This work discusses hydrolysis of defatted grape in supercritical water (SCW) at 380 °C and 260 bar from 0.18 s to 1 s focusing attention to sugars recovery in the liquid phase of the product and detailed characterization of remaining solid phase enriched in polyaromatics (e.g. lignin, flavonoids, etc.). After the longest reaction time of 1 s, 56 % of carbohydrates could be recovered in the liquid phase, as a result of carbohydrate hydrolysis. The high content of insoluble lignin in biomass (36 %), acts as a mass transfer limitation and presents an important feature in the hydrolysis process, slowing down the conversion of carbohydrate fraction, as after the maximum time of 1s, 10 % of carbohydrates still remained in the solid phase. Milled wood lignin, extracted from biomass and dioxane extract from the solid phase were characterized in order to understand the main structural changes during the SCW hydrolysis process. Dioxane (80 %) extraction of solids produces a very complex mixture of lipophilic extractives, flavonoids and lignin with a certain amount of chemically linked carbohydrates. 2D-NMR analysis of dioxane extract shows remarkably subtle changes in the amounts of main lignin moieties (β-O-4', β-β' (resinol) and β-5 (phenylcoumaran)).

Introduction

The focus of the current biorefinery are sugars or/and bioethanol production. Not enough attention is dedicated to other valuable biomass compounds including lignin and further polyphenols that are an alternative sustainable source of high value chemicals (Balakshin et al., 2021). The approach that targets just conversion of carbohydrate fractions loses the utility of remaining compounds and thus struggle with significant economic challenges that are preventing further industrial development. Those challenges can be overcome by the implementation of the advanced integrated biorefinery approach that puts forward valorization of every biomass stream for high value products (Balakshin et al., 2021).

One of the main challenges on the way of lignocellulosic biomass fractionization is its recalcitrance (Cocero et al., 2018). Biomass recalcitrance arises from three main constituents, cellulose, hemicellulose and lignin, and interaction between them (Lorenci Woiciechowski et al., 2020). Those three biopolymers create very compact, stable and resistant cell wall, so that significant force is required to separate them (Lorenci Woiciechowski et al., 2020). Conventional methods used to fractionate biomass described well in literature are acid and enzymatic hydrolysis. However, some of the main drawbacks of those methods are to use of hazardous material (acids), high yield of degradation products, the expensive price of the required chemicals (enzymes) and long reaction time. As an alternative to conventional methods, the use of Supercritical water technology is discussed as a clean and powerful method for fractionation and valorization of biomass to produce biorefinery lignin and to recover the carbohydrate fractions.

Attraction to use water as a reaction medium commence due to its environmentally friendly and non-expensive advantages over other solvents. At supercritical conditions, water has a character of a solvent for non-ionic species, in which many biomass compounds have enhanced solubility. The dipole moment of water in supercritical conditions decreases to a value typical for organic solvents. The value of pH significantly decreases in the subcritical region compared to ambient conditions as more H3O+ ions are produced, thus making these conditions good for acid catalyzed reactions. The ionic product changes remarkably close to the critical temperature, turning near-critical and supercritical water into a much less ionized compound compared to water at ambient conditions (Brunner, 2014). The opportunity to affect the water properties by changing the pressure and temperature, shifting from polar to non-polar solvent and from ionic to radical favorable medium, allows controlling selectivity in the process (Cocero et al., 2018). SCW environment provides an opportunity to conduct reactions in a single fluid phase, taking the advantage of having no interphase mass transport processes to decrease the reaction rate (Cantero et al., 2015a). As a result, reactions occur significantly faster. The reduction of reaction time allows a feasible scale-up of the process, using small reaction volumes.

Grape seeds are the main by-product from grape processing, such as the wine and grape juice industry. Above 3 Mt of grape seeds are discarded annually on the world base (Dávila et al., 2017). In the last few decades, there has been rising interest in the valorization of those products, to recover oil and phenolic compounds (Bravi et al., 2007; Duba et al., 2015; Fiori et al., 2014; Marqués et al., 2013). Oil from grape seeds is rich in unsaturated fatty acids such as linoleic acid and has furthermore a high content of tannins, which makes it more resistant to peroxidation (Cao and Ito, 2003).

Grape seeds have been also appreciated because of their content of phenolic compounds and their extracts have been a subject of intensive investigation due to their potential beneficial effects on human health, such as antioxidant activity (Maier et al., 2009). After the extraction of oil, defatted seeds are considered as a residue and can be used to produce energy by combustion. Considering that this residue still contains significant amounts of carbohydrates and high amounts of polyaromatics (lignin and other polyphenols), further exploitation to recover and use the remaining fractions could be more effective than energy recovery.

The practicability of sugar production from wheat bran and sugar beet pulp, in a continuous ultrafast supercritical hydrolysis pilot plant by the so-called FASTSUGAR process, has been demonstrated in the work of Martinez et al., where the challenges but also versatility and potential of the process are discussed (Martínez et al., 2019). This work discusses the feasibility of the SCW hydrolysis process for fractionation of biomass with high lignin content, as the amount of acid-insoluble lignin contained in defatted grape seeds is significantly higher compared to the amount in previously used biomass (36 % is defatted grape seeds compared to 4 % in sugar beet pulp and 2 % in wheat bran) (Martínez et al., 2019). High lignin content biomass presents an even greater challenge for the biorefinery, as lignin acts as a physical barrier that protects biomass from microorganism attack and chemical degradation, contributing significantly to biomass recalcitrance (Li et al., 2016b; Loow et al., 2016). Characterization of lignin contained in defatted grape seeds is presented, as characterization of this lignin has not been reported before. Attention is focused on understanding the structural changes of lignin due to the supercritical water hydrolysis (SCWH) process, using among others 2D-NMR as a powerful tool in lignin analysis.

Characterization of lignin residue after supercritical water and understanding of structural changes caused in lignin structure are the first steps on the way of targeting possible application of this lignin residue.

Experimental section

Materials

Defatted grape seeds were provided from Alvinesa Natural Ingredients (Spain). The grape seeds were defatted using hexane extraction. Deionized water was used as the reaction medium. The HPLC standards (cellobiose, galacturonic acid, glucuronic acid, glucose, mannose, xylose, fructose, arabinose, glyceraldehyde, glycolaldehyde, lactic, formic, acetic and acrylic acids, furfural and 5-hydroxymethylfurfural (5-HMF)) were purchased from Sigma Aldrich, as well as sulphuric acid and calcium carbonate for biomass characterization. For Kjeldahl determination of protein content, Kjeldahl catalyst (0.3 % $CuSO_4 \cdot 5H_2O$) tablets were purchased from PanReac. Dioxane was used for extraction of lignins from the sample's solid phase and deuterated dimethyl sulfoxide (DMSO-d6) as a solvent for 2D-NMR analysis.

Methods

Biomass and sample characterization

Prior to SCWH defatted grape seeds were ball milled using Retsch equipment, for 4 h. The composition was characterized using the Laboratory Analytical Procedure (LAP) of the National Renewable Energy Laboratory (NREL) (Hames et al., 2008; A

Sluiter et al., 2008b, 2008c; A. Sluiter et al., 2008). After the SCWH the sample was obtained as suspended solid and further centrifuged for 10 min at 7800 rpm and then separated into liquid and solid phases. The solid phase was dried at 50 °C and further analyzed. The composition of the solid and liquid phases was analyzed by LAP procedures. For analysis of the solid phase the procedure for determination of structural carbohydrates and lignin was used (A. Sluiter et al., 2008), while for the liquid phase the procedure for determination of sugars, by-products and degradation products was utilized (A Sluiter et al., 2008a).

The following analytical techniques were used in biomass and sample characterization:

High-Performance Liquid Chromatography (HPLC)

HPLC analysis was used to identify sugars and their derivatives. The sample was prepared using the before mentioned LAP procedures. Shodex SH-1011 column for components separation at 50 °C and RI-detector (Waters 2414) were used. The mobile phase was sulfuric acid (0.01 N) with a flow rate of 0.8 mL/min.

Total Organic Carbon (TOC)

TOC analysis was used to determine the concentration of total organic carbon in the liquid sample. The analyzer Shimadzu TOC-VCSH was used. The sample was prepared by diluting the liquid sample to the range of TOC standards.

Elemental analysis

Elemental analysis of the sample's solid phase was performed to determine carbon, hydrogen, nitrogen and sulfur content using Elemental C-S analyzer with a Leco CS-225.

Fourier-Transform Infrared Spectroscopy (FT-IR)

FT-IR analysis was utilized to follow the structural changes in biomass before and after hydrolysis using Bruker Tensor 27. The recorded spectra were baseline-subtracted and normalized to the maximum peak intensity. Each processed spectrum was hereby a mean of 64 single scans. The sample was analyzed without further preparation.

UV-VIS Spectroscopy

UV-VIS Spectroscopy was used to determine the total amount of soluble lignin after acid hydrolysis of biomass and solid sample. The absorbance was recorded at a wavelength of 280 nm, using an absorptivity coefficient of 17.08 $\mathrm{L\,g^{-1}cm^{-1}}$.

Scanning Electron Microscopy (SEM)

SEM experiments were conducted in a Hitachi FlexSEM 1000 to determine morphological changes on the sample surface.

Differential Scanning Calorimetry (DSC)

DSC analysis was used to determine the glass transition temperature of lignin in biomass and solid samples. The used device was a Mettler Toledo DSC 3+.

Milled Wood Lignin and dioxane-lignins preparation and characterization

For Milled Wood Lignin (MWL) isolation, a classical method was used (Björkman, 1956) with modifications described by Balakshin et al. (Balakshin et al., 2011). 4 g of defatted grape seeds were milled for 8 h in a jar of 80 mL volume by using 34 balls of ZrO2. The diameter of each ZrO2 ball is 10 mm. 15 minutes break has been used after every 30 minutes of milling to keep the temperature of the biomass

below 50 °C. The obtained meal was extracted with dioxane (96 % v/v) and the solvent was then evaporated under vacuum at 35 °C. Obtained solid was dried in a vacuum oven at 40 °C to obtain MWLs preparations. The supercritical water lignins were isolated by dioxane extraction, following a procedure described earlier (Capanema and Balakshin, 2015).

2D Nuclear Magnetic Resonance Spectroscopy (2D-NMR)

2D-NMR was conducted using a Bruker Avance 600 NMR with a magnetic flux density of 14.1 T and equipped with a cryogenically cooled 5 mm TCI probe head with inverse geometry (i.e., optimized for proton signal detection). A total of 36 transients (scans per block) were acquired using 1024 data points in the F2 (1H) dimension for and acquisition time of 77.8 ms and 256 data points in the F1 (13C) dimension for an acquisition time of 3.94 ms. The 2D data set was processed with 1024 × 1024 data points using the Qsine function in both dimensions. The sample was prepared for 2D-NMR by dissolving approximately 70 mg of lignin in 0.6 mL of DMSO-d6.

Supercritical water hydrolysis pilot plant

The experiments were performed in the ultrafast Supercritical Water Hydrolysis Pilot Plant with Sudden Expansion Micro Reactor (SEMR) (details of the reactor are given in Figure 8). The plant operates in continuous mode and the maximum operating conditions are 450 °C and 300 bar with a maximum capacity of 40 kg h^{-1} of biomass suspension. The flow diagram of the pilot plant is presented in Figure 12. The key parameter in biomass hydrolysis in SCW is time, thus the plant was designed to provide the precise control of reaction time and the possibility to

operate with a very short reaction time. Operation with a short reaction time is provided due to the small reactor volume and a fast flow through the reactor. The plant operates in the following manner: Biomass suspension and water streams are pumped and pressurized with two separate pumps. The water stream is passed through the heaters and heated to temperatures above the critical temperature of the water. Biomass stream could be optionally preheated passing through the heat exchangers, which was however not the case in this study. Biomass and SCW streams are mixed just in front of the reactor, in the mixing T-junction. The instantaneous mixing allows avoiding all degradation reactions that could occur during the heat-up. After passing through the reactor sample is directed to the valve for high temperature and pressure conditions based at the end of the reactor. This provides a decrease in temperature of the sample stream down to 150 °C, caused by the Joule-Thomson effect. Due to this immediate temperature decrease, all reactions are stopped. A heat exchanger is installed to cool the sample further down to room temperature just after the decompression valve. After the reactor sample (that is in the form of suspended solid) could be furtherly sent to the filters where the solid phase is separated from the liquid phase. The liquid phase can then optionally pass through the flash separators. Due to the nature of defatted grape seed biomass, this option was not used (nor filter or flash separators).

Regarding that one of the determining factors of hydrolysis is reaction time, its precise control is enabled by changing the length of the reactor or total flow, as mentioned earlier in this thesis. The reactor geometry and high flow rates provide a turbulent flow and thus ensure good mixing.

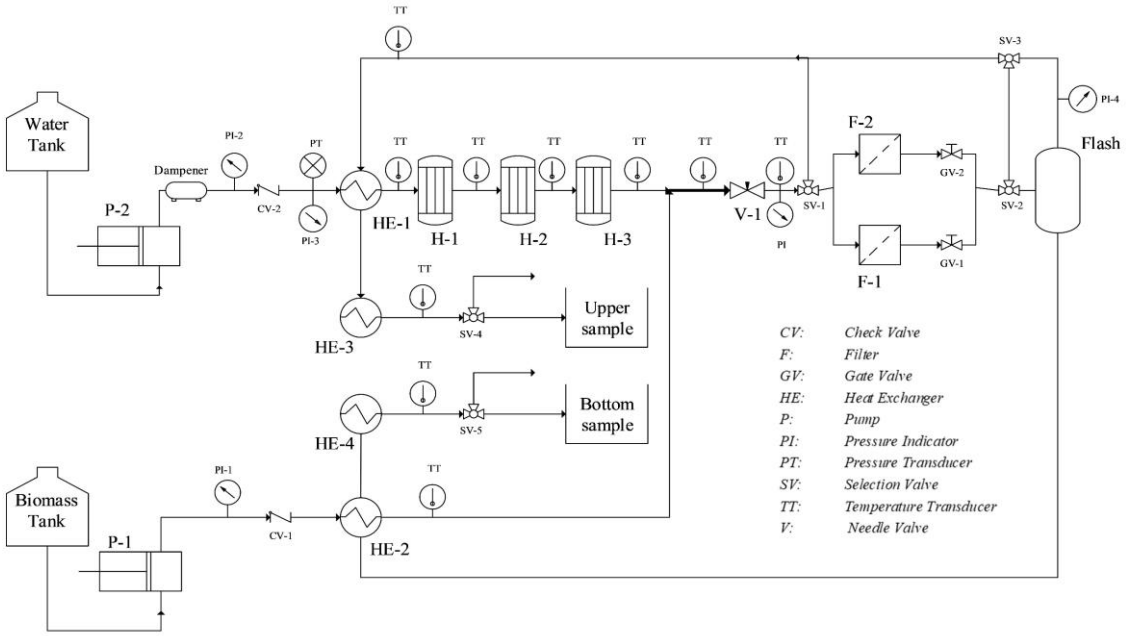

Figure 12. Flow diagram of ultrafast Supercritical Water Hydrolysis Pilot Plant. SEMR detail

Defatted grape seeds were hydrolysed in SCW at 380 °C and 260 bar for different reaction times, ranging from 0.18 s to 1 s, with a maximum biomass flow of 4.9 kg h^{-1}. The average fluctuation in experiments was around ±2 °C in terms of temperature and ± 5 bar in terms of pressure. The reaction temperature of 380 °C in the experiment was the same as the temperature in previous experiments with wheat bran, while in experiments with sugar beet pulp the temperature was 390 °C. Due to the high recalcitrance of grape seeds, a longer reaction time of up to 1 s was chosen, compared to 70eactionn time regarding wheat bran and sugar beet pulp hydrolysis (maximum reaction time of 0.17 s in the pilot-scale plant).

Results and discussion

Biomass characterization

The composition of the biomass as raw material is given in Table 1. This biomass is characteristic for a high lignin content that presents almost half of the biomass structure. As mentioned in the methods section, the biomass was firstly ball-milled before the hydrolysis and as such characterized. The resulting particle size of the ball-milled biomass was 180 μm. Reduction of particle size is necessary for the process due to possible pumping issues as particles with big diameters can cause plugging of the biomass line. This counts especially in the case of defatted grape seeds as the biomass with high lignin content and rigid structure. For the determination of extractives, water and ethanol were used (consequently) as solvents.

Table 1. Compositional analysis of defatted grape seeds

Substance	Composition (% w/w)
Ash	1.9 ± 0.5
Moisture	8.4 ± 0.05
Water extractives	12.7 ± 1.6
Ethanol extractives	2.7 ± 0.2
Proteins	3.2 ± 0.2
Acid Insoluble Lignin	36.5 ± 1.1
Acid Soluble Lignin	6.0 ± 0.4
Glucan	12.1 ± 0.12
Xylan	7.6 ± 0.2
Arabinan	1.3 ± 0.4

Carbohydrate recovery from the sample liquid phase

After SCW hydrolysis sample was centrifugated so that two phases, liquid and solid, were separated and analyzed. The liquid phase was subjected to acid hydrolysis adding 72 % sulfuric acid and diluting the acid concentration to 4 %. The sample was then hydrolyzed in the autoclave for one hour at 121 °C. During the SCWH process the cellulose and hemicellulose fractions are firstly hydrolyzed to oligomers, from oligomers to monomeric sugars and from monomers converted into further degradation products. Acid hydrolysis of the sample is necessary to bring oligomeric sugars into monomeric sugars that can be further analyzed and quantified. The carbohydrate fractions C6 (glucan) and C5 (arabinan and xylan) in the biomass, used for sugar yield calculation were obtained using the biomass without previous Soxhlet extraction. The hydrolysable base for sugars was calculated following eq.(1). Where c_{HS}^{C} is the concentration of hydrolysable to sugars in ppm of carbon, c_{C}^{in} is the concentration of carbon inside the reactor in ppm and $W_{C6}^{biomass}$ and $W_{C5}^{biomass}$ are the weight fractions of C6 and C5 carbohydrates referring to the biomass in % w/w.

$$c_{HS}^{C} = c_{C}^{in} \cdot \left(\frac{W_{C6}^{biomass} + W_{C5}^{biomass}}{100\ \%\ w/w} \right) \qquad (1)$$

The yield of total sugars (Y_{TS} in % w/w) was calculated in eq. (2) dividing the concentration of total sugars expressed in ppm of carbon (c_{TS}^{C}, see eq. (3)), that was determined in the liquid phase of the sample by HPLC analysis, by the concentration of hydrolysable to sugars (c_{HS}^{C}).

$$Y_{TS} = \frac{c_{TS}^{C}}{c_{HS}^{C}} \qquad (2)$$

$$c_{TS}^{C} = c_{C5}^{Cout} + c_{C6}^{Cout} \qquad (3)$$

The yields of each sugar fraction (Y_{C5} and Y_{C6} in % w/w) were calculated independently, dividing the concentrations of C5 and C6 sugars ($c_{C5}^{Cout}$and c_{C6}^{Cout}) determined in the liquid by the inlet concentrations of C5 and C6 carbohydrates fraction respectively (eq. (4) and (5)) (both concentrations presented with respect to carbon).

$$Y_{C5} = \frac{c_{C5}^{Cout}}{c_{C}^{in} \cdot W_{C5}^{biomass}} \cdot 100\ \% \qquad (4)$$

$$Y_{C6} = \frac{c_{C6}^{Cout}}{c_{C}^{in} \cdot W_{C6}^{biomass}} \cdot 100\ \% \qquad (5)$$

Carbohydrate fractions are considered as the liable fractions that undergo rapidly hydrolysis in SCW. In Figure 13, that presents the yield of total sugar in the liquid phase (Y_{TS}), it is shown that the highest yield was obtained for a short reaction time of 0.27 s, reaching 61 %. Martinez et al. and Cantero et al. showed that the maximum yield of sugars for the hydrolysis of sugar beet pulp and wheat bran were obtained for even shorter reaction times (0.11 s and 0.19 s respectively), operating in a laboratory-scale plant (Cantero et al., 2015b; Martínez et al., 2019). The recovery of sugars in the Supercritical water process is higher compared to work reported by Prado

et al. (Prado et al., 2016) where up to 40 % sugar was recovered from defatted grape seeds using Subcritical water hydrolysis, under 203 °C – 258 °C, 20Mpa for 30 min.

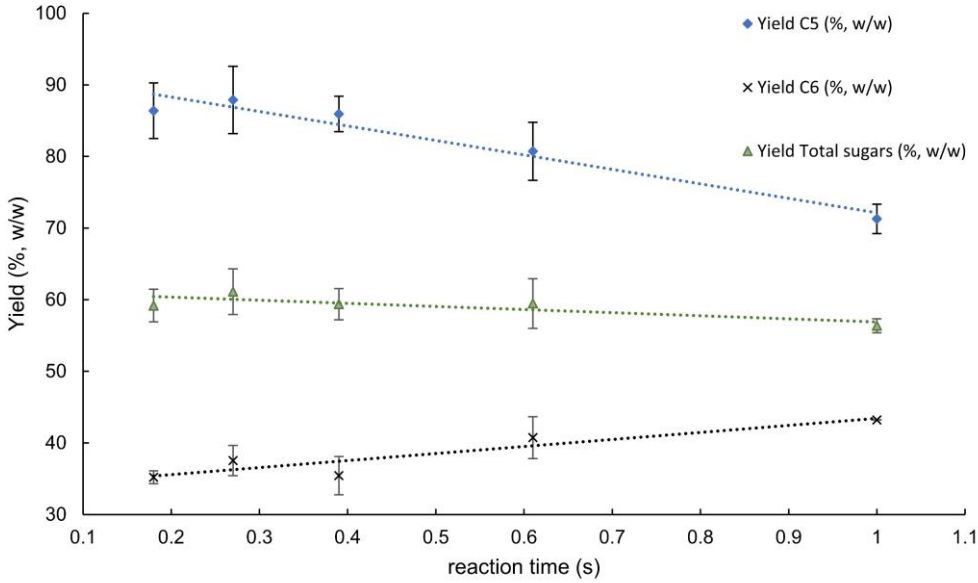

Figure 13. The yield of C5, C6 and total sugars over reaction time in the liquid phase; the error bars are the standard deviations; linear trendlines given

Differently from the case of sugar beet pulp (Martínez et al., 2018), where within 1 s of reaction time the main part of the carbohydrate fractions was already converted and the yield of sugars in the liquid phase rapidly decreased, the yield of the sugar in the case of grape seeds remained high (56 %). One of the natural factors that influence biomass recalcitrance is the amount of lignin and other polyphenols. The explanation for the slower gradual conversion of the carbohydrate fractions can lie in the high lignin content of the biomass. Lignin could act as a barrier for SCW to access the carbohydrate fractions, as some part of cellulose is less accessible in the inner structure of lignin (Gullón et al., 2012). The C5 conversion was higher than that

of C6. The C5 yield dropped from the maximum value of 88 % obtained for 0.27 to 43 % for 1s. The maximum yield of C6 sugars was 43 % obtained after 1 s.

Solid fraction characterization

The solid yield (Y_{solid} in % w/w) is calculated by eq. (6), where c_{SS} is the concentration of suspended solid in the sample in ppm and f_C^{Solid} is the solid carbon factor obtained with the elementary analysis of the solid.

$$Y_{solid} = \frac{c_{SS} \cdot f_C^{solid}}{c_C^{in}} \cdot 100\ \% \qquad (6)$$

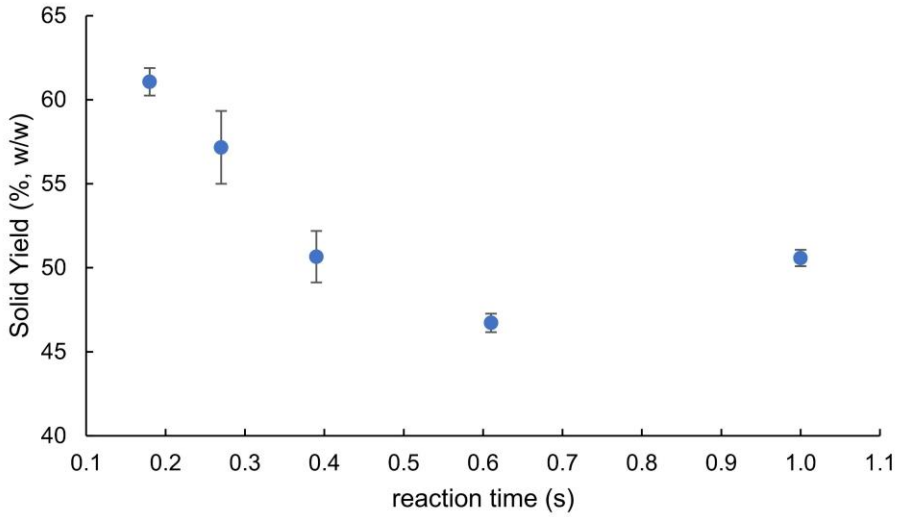

Figure 14. The yield of solid after SCWH over reaction time

The yield of the solid fraction (see Figure 14) decreases with reaction time up to 0.61 s. To obtain higher rates of liquefication, more severe conditions were needed, decreasing the yield from 60 % for a reaction time of 0.18 s to 46 % for the time of 0.61 s. A slight increase of the solid yield fraction for the longest reaction time of 1s

could be a result of the production of the water insoluble compounds as the reaction proceeds.

Solid characterization by LAP procedure for carbohydrate and lignin content is presented in Figure 15. It is important to note that extractives were not removed from the solid sample and that they could contribute to the total amount of the Klason lignin.

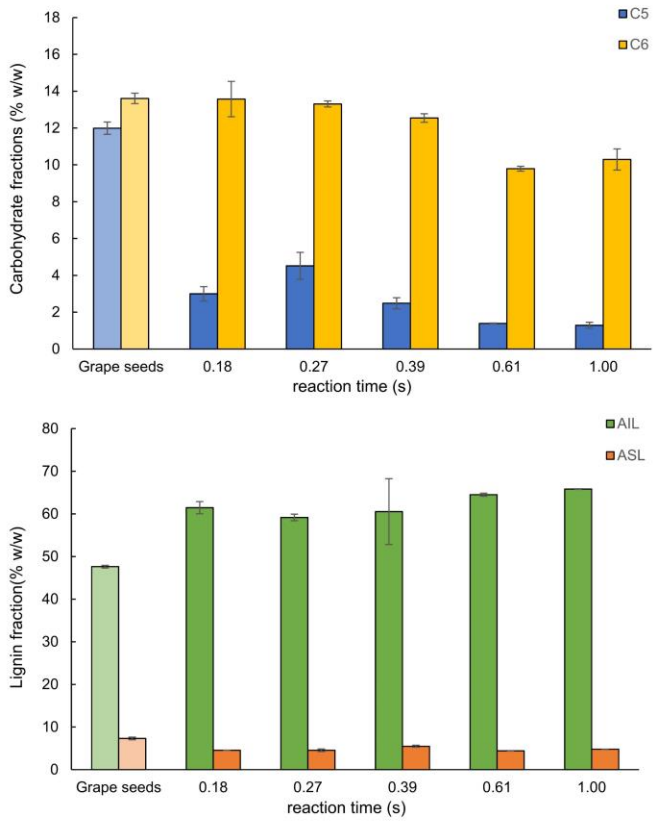

Figure 15. Solid sample composition over reaction time; top: carbohydrate fractions (where C6 refers to glucose and C5 to the sum of xylose and arabinose); bottom: acid insoluble lignin (AIL) and acid soluble lignin (ASL)

The amount of carbohydrates and lignin fractions in biomass presented in Figure 15 is also calculated for the biomass as received, without previous extraction.

As carbohydrate fractions are more labile fractions, they undergo to hydrolysis fast while the amount of acid insoluble solid increased in the solid fraction for the already shortest reaction time, to 61 %, and goes to 65 % for the longest reaction time. As mentioned above the biomass' high content of insoluble lignin increases its recalcitrance and reacts as a barrier to total hydrolysis of sugars fraction, as even for the longest reaction time of 1 s, the solid phase still contained 10 % of the carbohydrates fraction. This is different compared to the biomass composed mainly of the more labile fractions as above-mentioned sugar beet pulp (Martínez et al., 2018) as for this biomass high recovery of sugars was obtained in the liquid phase, and just 0.9 % of carbohydrates fraction was determined in solid phase after similar reaction time.

FT-IR signals for raw biomass and solids for different times (0.18 s, 0.39 s, 0.61 s) are presented in Figure 16 and assigned according to the literature (Ehara et al., 2005; Hemmilä et al., 2020; Sahoo et al., 2011; Wahyudiono et al., 2008a; Xu et al., 2013). The FT-IR signals of solids after hydrolysis showed increased intensity in the region related to lignin structure approving the increased aromaticity of the solid after the process. The increased intensity was observed for peaks at: $779\ cm^{-1}$ assigned to C-H out of plane vibration on the aromatic ring; $1270\ cm^{-1}$ assigned to the guaiacyl ring breathing and C=O stretching; $1315\ cm^{-1}$ assigned to aromatic ring breathing; $1617\ cm^{-1}$ and its shoulder at $1650\ cm^{-1}$ assigned to the aromatic ring vibration of phenylpropane groups and C=O bonds in conjugated ketones; $3430\ cm^{-1}$ assigned to O-H stretching specifically from lignin. The peak at $1050\ cm^{-1}$ assigned to the C–O–C ether linkage of the skeletal vibration of both pentose and hexose unit from

hemicellulose and cellulose decreased due to the hydrolysis of carbohydrate structures in the solid residue.

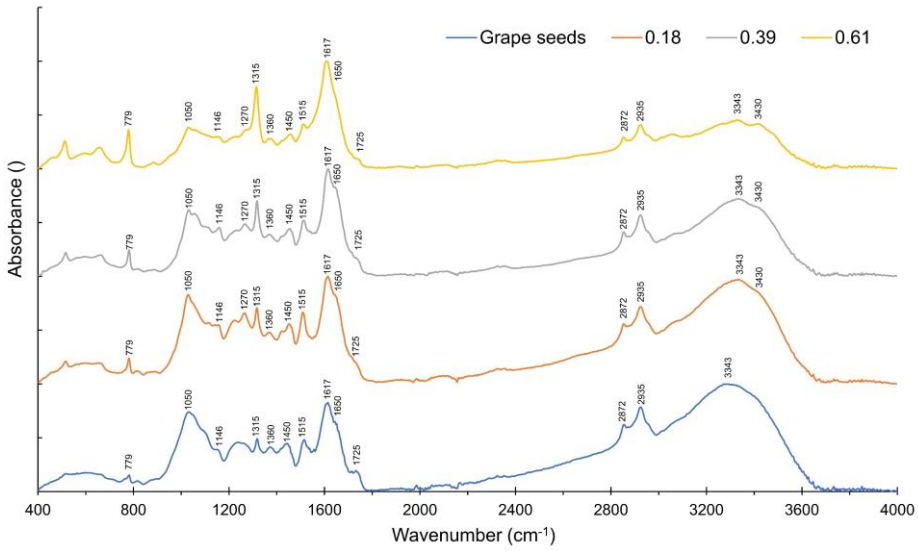

Figure 16. FT-IR spectrum of raw material and solid after hydrolysis at 0.18 s, 0.39 s and 0.61s

Reported Glass Transition Temperature (Tg) for different underivatized lignin lies between 100 °C to 180 °C (Daz et al., 2001). The DSC curves for the biomass sample and solid after SCWH at reaction times of 0.18 s, 0.39 s and 0.61 s are shown in Figure 17. The biomass sample shows a peak that could correspond to the lignin transition temperature at 152 °C, while the solid obtained after reaction times of 0.18 s, 0.39 s and 0.61 s have peaks shifted to a higher temperature, 162 °C, 165 °C and 167 °C respectively, which is higher compared to other lignins. The literature results report that the same molecular motion of in situ lignin has been observed at the temperature lower than that of the isolated lignin and that shifted Tg suggests that the amorphous structure of lignin could be affected by coexisting components in the

original biomass, but also by mechanical and thermal changes during the treatment (Hatakeyama et al., 2010). Higher Tg values of lignin obtained after processing even increased with the severity of the process. Determination of Tg value is important information for the potential application of lignin.

At temperatures above 250°C, peaks that correspond to the degradation of main constituents of samples (hemicellulose, cellulose and lignin) can be observed. These peaks can be seen in the temperature region of 285 °C–296 °C for hemicellulose, 347 °C-360 °C for cellulose and 402 °C – 417 °C for lignin. Similar degradation temperatures of main biomass constituents obtained by DSC analysis were reported by Brys et al., when different wood species were analyzed (Bryś et al., 2016). For the SCWH sample obtained after 0.61 s, the peak that corresponds to hemicellulose degradation was almost absent, as the main amount of hemicellulose was already hydrolyzed. The peak that corresponds to cellulose degradation was observed at 347 °C for GS, while for SCWH solids this peak was at 359 °C, 356 °C and 360 °C (for 0.18 s, 0.39 s, 0.61 s respectively). The higher degradation temperature of cellulose in solids after SCWH compared to GS might be due to the more crystalline structure of the cellulose that remained in the solid, as a more labile amorphous part is firstly hydrolyzed, or due to the part of cellulose chemically bonded to lignin polymer. The highest degradation temperatures correspond to lignin, as lignin is the most thermostable constituent of biomass (Bryś et al., 2016). Due to the complexity of the lignin structure, its thermal degradation happened over a wide temperature range (Yang et al., 2007).

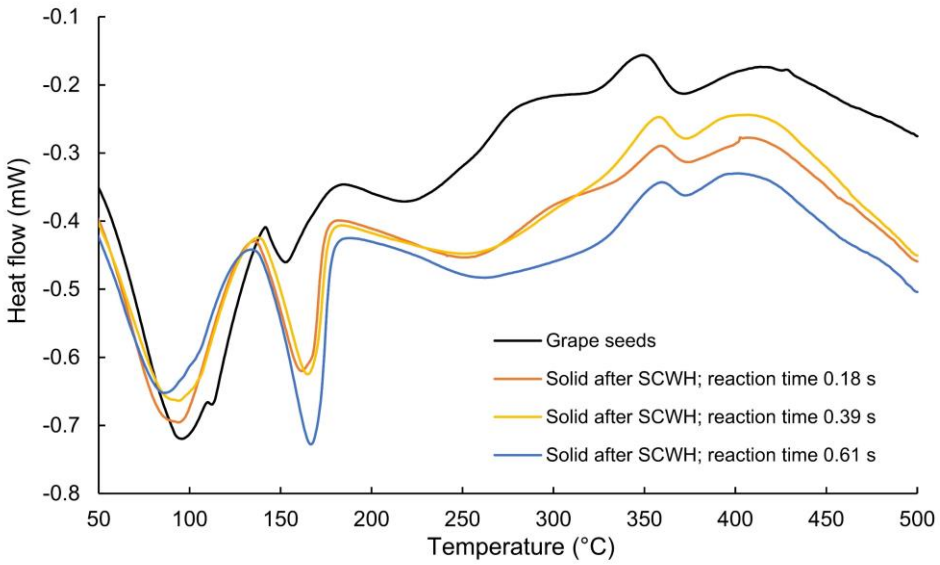

Figure 17. DSC curves for raw biomass and solid after SCWH for reaction times of 0.18 s, 0.39 s and 0.61 s

SEM analysis was performed for solid obtained at different reaction times to observe changes in the morphology of biomass caused by hydrolysis and the severity of the process (Figure 18). The sample before hydrolysis had a compact surface structure, while the influence of the SCWH clearly causes structural damage. These ruptures are more visible with longer reaction times. The surface of treated solid also shows the appearance of the small droplets that can be related to the molten lignin at high temperature and pressure (Donohoe et al., 2008; Kristensen et al., 2008; Pingali et al., 2010; Selig et al., 2007; Xiao et al., 2011). This is in accordance with the compositional analysis of solid fraction, as it is mainly composed of lignin. Since lignin plays a significant role in biomass recalcitrance this can be the reason for a slower rate of carbohydrate hydrolysis in SCW, compared to the biomass with a lower amount of lignin as explained above.

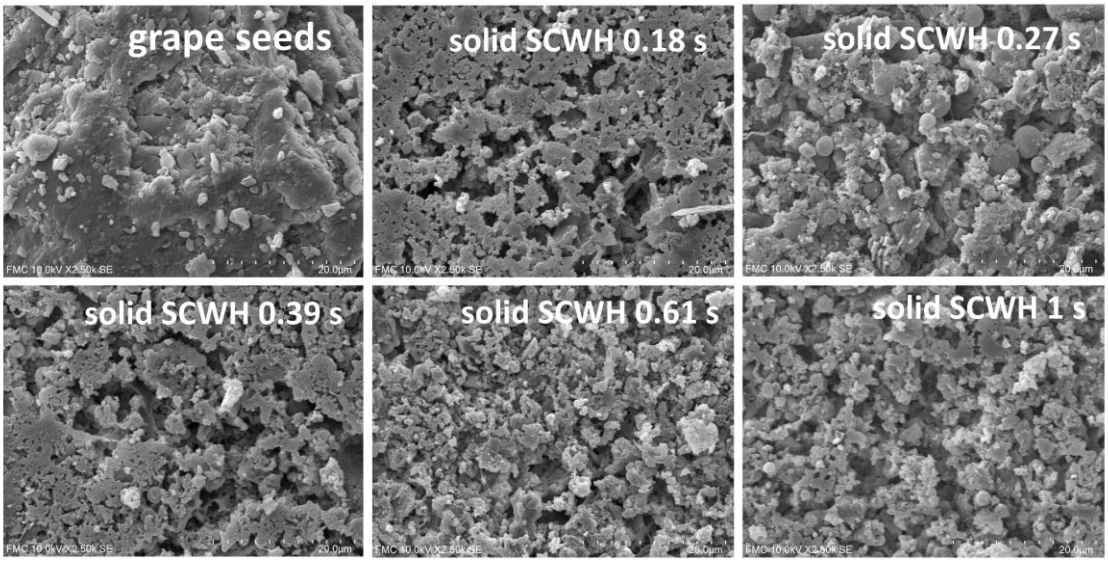

Figure 18. SEM images of raw material and solids after SCWH obtained for different reaction times (0.18 s, 0.27 s, 0,39, 0.61 s and 1 s)

Lignin is also specific to be relocated during the hydrothermal treatment so that upon melting, lignin in biomass becomes fluid and thus can move through the cell wall matrix observed as spherical formations on the surface of pretreated biomass (Selig et al., 2007). He et al. assign the appearance of aggregated droplets to pseudo lignin that originate from the condensation and aromatization reaction of sugar degradation products during dilute acid pretreatment (He et al., 2018). The released aromatic compounds from lignin degradation also affect the formation of pseudo lignin that has polyaromatic phenolic nature and contributes to the total amount of Klason lignin (He et al., 2020).

Structural analysis of grape seed MWL and extracted polyphenols mixture by 2D NMR

The supercritical water process produces solid enriched in lignin. This solid can be further refined to obtain a higher purity of lignin, named as SCWL in the text below (Capanema and Balakshin, 2015). For structural characterization with high-resolution NMR, lignins (with chemically linked carbohydrates) were extracted from the solids after SCWH with 80 % v/v dioxane. This solvent mixture allows for maximal solubility of lignin and LCC components (Mikhail Yu Balakshin et al., 2003) without possible chemical modification. This counts for instances in the case of NaOH extraction, especially for a very complex non-wood plant biomass containing significant amounts of ester and other labile moieties (e.g., polyphenols). The extraction yield (dioxane lignin) was about 55 to 57 % w/w per lignin content in the solids obtained after SCWH.

The extracted SCWL were analyzed by HSQC 2D-NMR method (shown in Figure 19), to obtain information on changes that occur in lignin structure during the hydrolysis process. The MWL isolated from grape seeds feedstock was used for comparison, as MWL is considered to be relatively close to the native lignin structure (Balakshin et al., 2020c).

The spectra (see Figure 19) show clearly that the extracted SCWL are very complex mixtures of different types of chemicals, such as lipophilic extractives, polyphenols (e.g., flavonoids) and true polymeric lignin, which is also linked to carbohydrates via chemical linkages. Detailed analysis of the SCWL is challenging

due to the high complexity of the mixture and significant signals overlap even in the 2D spectra. Therefore, only high-level conclusions are possible at the current stage.

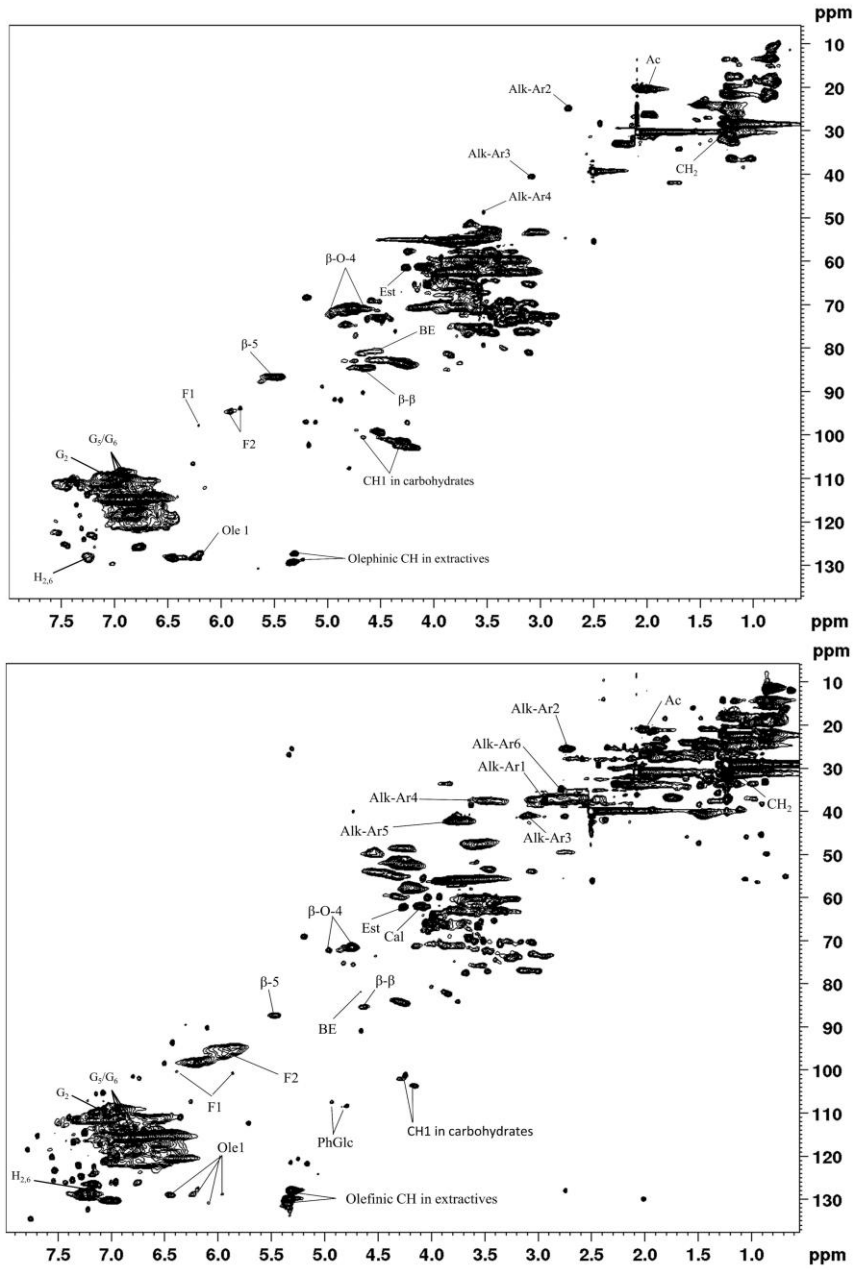

Figure 19. HSQC spectra; top: milled wood lignin; bottom: SCWHL (at reaction time of 0.39 s)

The assignments of main lignin cross-peaks and their quantification in the spectra of MWL and SCWL isolated after reaction times of 0.18 s, 0.27 s and 0.39 s are presented in Table 2.

Lignin from grape seeds consisted mainly of guaiacyl (G) type units, with a minor amount of p-hydroxyphenyl (H) units, while syringyl (S) units were practically absent. Main lignin signals were assigned according to the literature available (Balakshin et al., 2011; Mikhail Yu Balakshin et al., 2003; Lancefield et al., 2018a). Apart from main lignin units, the 2D-NMR data shows the presence of lignin-carbohydrate linkages, i.e., the presence of Lignin-Carbohydrate Complex (LCC). Three types of LCC linkages, namely benzyl ether (BE), phenyl glycoside (PhGlc) and γ-ester were detected (δC/δH 79.6-82.8/4.4-4.9, 99.4-103.7/4.8-5.1 and 60.8-62.9/4.2-4.4, respectively). Importantly, other BE (lignin-lignin) and esters moieties can also contribute to these resonances (Balakshin et al., 2020c, 2014, 2011), therefore they show only maximal possible amounts of LCC linkages. In addition, high varieties and high amounts of lipophilic extractives and flavonoids were detected in the spectra. Lignin from grape seeds differs from lignin isolated from the grape stalks, as the latter contains a significant amount of S units that were not found in the grape seeds MWL. Condensed structures of alkyl-aryl type were also determined in the lignin from grape stalks, and they are at least partially, assigned to the lignin−tannin condensed structures (Prozil et al., 2014).

For semiquantitative analysis, the resonance of methoxyl groups was used as a reference to normalize the resonance values of the other signals. It was set as 300 to express the value obtained close to 100 lignin monomeric units (i.e. expressed in mol % in respect to lignin). A more common approach (for lignins) using the resonance of

G2 cannot be used in our case as it is obscured with the resonance of non-lignin signals, apparently flavonoids. Very approximate calculation shows that lipophilic extractives, flavonoid and lignin are present in a similar mass proportion, i.e. lignin share in the extracted material is about 30 to 40 % w/w. In terms of advanced biorefinery, these valuable components might be further fractionated (if they are not linked chemically) e.g., by solvents of different polarities or/and other manners. Alternatively, the effect of the presence of non-lignin compounds and their potential synergism (Balakshin et al., 2020a), in typical lignin application may be also studied in terms of advanced biorefinery.

There is no clear tendency in the amounts of lipophilic extractives and flavonoids in the dioxane extracts of SCWL during the reaction course. The amounts of these components in MWL are dramatically less as the biomass was pre-extracted with toluene-ethanol prior to lignin isolation according to the classical procedure (Balakshin et al., 2011) indicated that they are not chemically linked to lignin in the original biomass. In contrast, the amounts of residual LCC (evaluated by the amounts of carbohydrates in the samples) was lower in the SCWL indicating cleavage of LCC linkages during the SCWH. Interestingly, the amounts of ester and BE moieties do not correlate with the amount of carbohydrates in the samples, indicating potential presence of ester and ether linkages of different types (e.g., acetyl groups, lignin-lignin ethers etc). Notably, the amount of labile acetyl groups (from carbohydrates and/or lignin) does not decrease during SCWH.

The amounts of main moieties of native lignin, e.g., β-O-4, β-5 and β-β structures, decrease very slightly during the SCWH process (compare Table 2) at least in the range of 0 to 0.39 s when the major changes in biomass component separation

occur. Such, the content of the main lignin reaction centres, β-O-4 moieties, decrease by only ca 30 %. This is in strict contrast to other biorefinery processes when the amount of β-O-4 linkages decreases by 3-10 times (Balakshin and Capanema, 2015).

Moon et al., reported a significant decrease in β-O-4 amount specifically and in the oxygenated aliphatic moieties in general after SCWH but under much severe process conditions (380 °C and 60 s), which sound very unreasonable in the light of our results. They also claim strong demethylation, which, however, cannot be justified due to clearly insufficient processing of the 13C NMR spectra obtained; no quantification was performed and the spectra were compared at rather different intensities that do not allow any reliable conclusion unless the changes were dramatic (such as a decrease in the oxygenated aliphatic region) (Moon et al., 2011).

Significant resonance in the saturated aliphatic region of the SCWL, specifically in different moieties of Alkyl-Aryl types, was observed. These signals likely belong to flavonoids of different types. Some lignin condensed moieties also resonate in this region, but their amounts are usually in the order of magnitude lower even after significant lignin conversion (Balakshin et al., 2003; Balakshin and Capanema, 2015), which is not the case here. Main lignin linkages and LCC linkages are given in Figure 20.

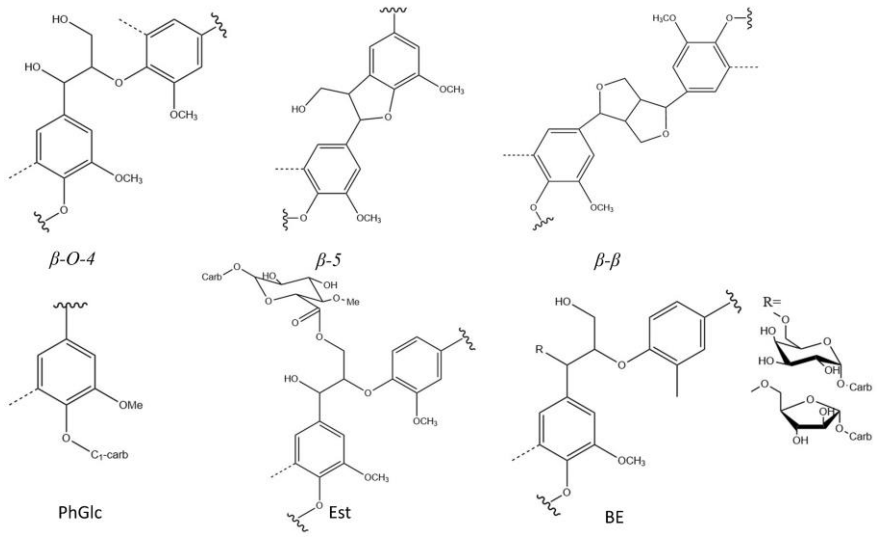

Figure 20. Main lignin and LCC linkages in Grape seed MWL and SCWL

Table 2. Relative amounts of different moieties of milled wood lignin (MWL) and supercritical water lignins (SCWL) at different reaction times (0.18 s, 0.27 s and 0.39 s);

δ_C/δ_H	MWL	0.18 s	0.27 s	0.39 s	assignment
69.3-73.6/4.6-5.0	33.9	26.0	26.7	24.4	*β – aryl ether (β-O-4)*
84.0-86.0/4.5-4.8	6.7	4.7	5.3	4.8	*resinol (β-β)*
86.1-88.5/5.4-5.6	10.3	7.8	7.6	6.9	*phenyl-coumaran (β-5)*
60.7-62.9/4.0-4.2	14.4	14.9	17.8	16.5	*coniferyl alcohol (Calk)*
60.8-62.9/4.2-4.4	3.4	5.6	9.1	6.4	*γ – esters (Est)*
79.6-82.8/4.4-4.9	7.5	12.8	12.6	11	*benzyl ethers (BE)*
99.4-103.7/4.8-5.1	4.1	2.0	0.5	1.4	*Phenyl glycosides (PhGlc)*
19.2-22.0/1.8-2.1	32.4	43.4	26.1	38.6	*Acetyl groups (Ac)*
97.0-100.5/5.8-6.4	1.7	35.5	35.0	38.8	*Flavonoids (F1)*
93.6-96.9/5.7-6.3	6.7	55.3	49.4	35.0	*Flavonoids (F2)*
98.9-105.1/4.0-4.8	28.4	17.5	7.3	13.1	*CH1 in carbohydrates*

35.9-39.2/2.9-3.0	1.1	14.2	11.0	22.5	*Alkyl-Aryl moieties (Alk-Ar1)*
23.2-26.3/2.6-2.8	2.3	50.6	69.4	60.8	*Alk-Ar2*
39.6-43.9/3.0-3.2	1.6	20.9	11.9	10.1	*Alk-Ar3*
35.4-39.6/3.3-3.7	0.8	23.3	21.0	24.8	*Alk-Ar4*
45.5-49.3/3.4-3.8	1.9	36.3	30.4	34.0	*Alk-Ar4*
39.9-44.9/3.6-3.9	1.9	64.3	27.9	42.9	*Alk-Ar5*
33.4-36.3/2.7-2.9	0.7	7.0	5.8	11.9	*Alk-Ar6*
125.6-133.2/5.8-6.5	16.8	30.3	24.5	29.5	*Olephinic 1*
133.2-150.8/7.1-8.2	4.7	19.7	17.9	23.3	*Olephinic 2*
27.7-33.1/1.0-1.3	120.3	748.4	1043.6	972.3	*CH2 (mainly extractives)*
125.9-133.9/5.1-5.5	8.7	149.2	192.8	180.8	*olephinic CH in extractives*

Conclusion

Defatted grape seeds were hydrolyzed in supercritical water where the recovered yield of sugars in the liquid phase reaches 61 % for 0.27 s and solid enriched in polyaromatics is produced. High content of insoluble lignin in grape seeds biomass creates additional mass transfer limitation that acts as a barrier to higher recovery of sugars. After the longest reaction time of 1s still 10% of carbohydrates remained in the solid, differently from the result obtained with biomass that has a low content of insoluble lignin where almost all carbohydrate fractions could be extracted. The solid phase of the sample consists of a very complex mixture that partially belongs to lignin with a certain amount of chemically linked carbohydrates, residual lipophilic extractives and flavonoids. The influence of supercritical water hydrolase on lignin structure was investigated by 2D-NMR analysis that indicates that cleavage of β-O-4

linkages and other native lignin moieties during the supercritical water process is very subtle, that can be beneficial in the valorization of this lignin residue.

Mass balance data

Mass balance is presented per carbon unit from carbohydrates following eqn. (7).

$$\frac{c_{Carb}^{C_{out}}}{c_{Carb}^{C_{in}}} \qquad (7)$$

Where:

$c_{Carb}^{C_{out}}$- total concentration of carbon from carbohydrates OUT

$c_{Carb}^{C_{in}}$- total concentration of carbon from carbohydrates IN

The total concentration of carbon from carbohydrates IN is calculated following eqn. (8)

$$c_{Carb}^{C_{in}} = c_{TC}\ x \sum W_{C5;C6;Cdeg}^{biomass} \qquad (8)$$

Where:

c_{TC} – concentration of total carbon in the sample

$W_{C5;C6;Cdeg}^{biomass}$- mass fraction of hemicellulose; cellulose and sugar degradation product in biomass

The total concentration of carbon in the sample is calculated following eqn. from (9) to (11)

$$c_{TC} = c_S^C + c_L^C \qquad (9)$$
$$c_L^C = TOC \qquad (10)$$
$$c_S^C = c_{ss} x f_C^{Solid} \qquad (11)$$

Where:

c_L^C- concentration of carbon in liquid phase obtained from total organic carbon analysis (TOC)

c_S^C- concentration of carbon in solid phase

c_{ss} – concentration of suspended solid in sample

f_C^{Solid} – carbon factor of the solid phase

The total concentration of carbon OUT is the sum of carbon concentration out from the solid and liquid phase as in eqn. (12)

$$c_{Carb}^{C_{out}} = c_{Carb_S}^{C_{out}} + c_{Carb_L}^{C_{out}} \qquad (12)$$

$c_{Carb_S}^{C_{out}}$- concentration of carbon from carbohydrates out from solid phase

$c_{Carb_L}^{C_{out}}$- concentration of carbon from carbohydrates out from liquid phase

This concentration is in the case of solid-phase calculated following eqn. (13)

$$c_{Carb\_s}^{C_{out}} = c_S^C \, x \sum W_{C5;C6}^S \qquad (13)$$

Where:

$W_{C5;C6}^S$- a mass fraction of hemicellulose and cellulose in solid phase

The concentration of carbon out from the liquid phase is calculated following eqn. (14)

$$c_{Carb\_L}^{C_{out}} = \sum c_{C5;C6;Cdeg}^C \qquad (14)$$

Where:

$c_{C5;C6;Cdeg}^C$- carbon concentration from cellulose, hemicellulose and sugar degradation products in liquid phase from HPLC

The concentration of carbon from cellulose, hemicellulose and degradation products in the liquid phase is calculated following eqn. from (15) to (17):

$$c_{C5}^{C} = \sum c_{C5}^{L} \, x \, f_c^{C5} \qquad (15)$$

$$c_{C6}^{C} = \sum c_{C6}^{L} \, x \, f_c^{C6} \qquad (16)$$

$$c_{Deg}^{C} = \sum c_{Deg}^{L} \, x \, f_c^{Deg} \qquad (17)$$

Where:

c_{C5}^{L} – unit con. of carbon originating from C5 sugars,

c_{C6}^{L} – unit con. of carbon originating from C6 sugars,

c_{CDeg}^{L} – unit con. of carbon originating from sugars degradation products;

f_c^{C5} – carbon factor of C5 sugars unit,

f_c^{C6} – carbon factor of C6 sugars unit,

f_c^{deg} – carbon factor of sugars degradation unit;

c_{C5}^{C} – total con. of carbon originating from C5 sugars,

c_{C5}^{C} – total con. of carbon originating from C6 sugars,

c_{Deg}^{C} – total con. of carbon originating from sugars degradation products.

Finally, the results obtained are presented in Table 3 where mass balance for the different experiments was closed in the range from 0.94 to 1.05:

$$\frac{c_{Carb}^{C_{out}}}{c_{Carb}^{C_{in}}} = [0.97 \; - \; 1.05]$$

Table 3. Mass balance closure data

	Reaction time / s	**0.18**	**0.27**	**0.39**	**0.61**	**1**
	c_L^C	1107 ± 57	1073 ± 12	1465 ± 78	1312 ± 50	1612 ± 19
	f_C^{Solid}	0.52	0.46	0.52	0.52	0.55
	ODW Solid	0.97	0.97	0.97	0.98	0.97
carbon IN	c_{ss}	3323 ± 143	2762 ± 177	2916 ± 334	2200 ± 133	3092 ± 24
	c_S^C	1690 ± 73	1340 ± 44	1471 ± 168	1129 ± 68	1650 ± 21
	c_{TC}	2798 ± 125	2413 ± 31	2936 ± 247	2442 ± 119	3261 ± 40
	$c_{Carb}^{C_{in}}$	939 ± 42	810 ± 11	986 ± 83	820 ± 40	1095 ± 10
carbon OUT	$c_{Carb_L}^{C_{out}}$	705 ± 60	585 ± 30	765 ± 100	687 ± 11	876 ± 91
	$c_{Carb_S}^{C_{out}}$	280 ± 12	239 ± 8	221 ± 25	126 ± 8	191 ± 3
	$c_{Carb}^{C_{out}}$	985 ± 71	824 ± 34	986 ± 126	813 ± 14	1066 ± 97
Mass balance	$\frac{c_{Carb}^{C_{out}}}{c_{Carb}^{C_{in}}}$	1.05 ± 0.04	1.02 ± 0.03	1.00 ± 0.04	0.99 ± 0. 05	0.97 ± 0.9

ODW Solid – Owen dried weight of the solid sample in per cent

**note all concentrations are presented in ppm

References:

Balakshin, M., Capanema, E., Berlin, A., 2014. Isolation and Analysis of Lignin–Carbohydrate Complexes Preparations with Traditional and Advanced Methods. Studies in natural products chemistry, 83–115. https://doi.org/10.1016/B978-0-444-63281-4.00004-5

Balakshin, M., Capanema, E., Gracz, H., Chang, H. min, Jameel, H., 2011. Quantification of lignin-carbohydrate linkages with high-resolution NMR spectroscopy. Planta 233, 1097–1110. https://doi.org/10.1007/s00425-011-1359-2

Balakshin, M., Capanema, E.A., Sulaeva, I., Schlee, P., Huang, Z., Feng, M., Borghei, M., Rojas, O.J., Potthast, A., Rosenau, T., 2020a. New opportunities in the valorization of technical lignins. ChemSusChem 14, 1–22. https://doi.org/10.1002/cssc.202002553

Balakshin, M., Capanema, E.A., Zhu, X., Sulaeva, I., Potthast, A., Rosenau, T., Rojas, O.J., 2020b. Spruce milled wood lignin: Linear, branched or cross-linked? Green Chem. 22, 3985–4001. https://doi.org/10.1039/d0gc00926a

Balakshin, M.Y., Capanema, E.A., 2015. Comprehensive structural analysis of biorefinery lignins with a quantitative 13C NMR approach. RSC Adv. 5, 87187–87199. https://doi.org/10.1039/c5ra16649g

Balakshin, M.Y., Capanema, E.A., Chen, C.L., Gracz, H.S., 2003. Elucidation of the structures of residual and dissolved pine kraft lignins using an HMQC NMR technique. J. Agric. Food Chem. 51, 6116–6127. https://doi.org/10.1021/jf034372d

Björkman, A., 1956. Studies on finely divided wood. Part 1. Extraction of lignin with neutral solvents. Sven. Papperstidn 59, 477–485.

Bravi, M., Spinoglio, F., Verdone, N., Adami, M., Aliboni, A., D'Andrea, A., De Santis, A., Ferri, D., 2007. Improving the extraction of α-tocopherol-enriched oil from grape seeds by supercritical CO2. Optimisation of the extraction conditions. J. Food Eng. 78, 488–493. https://doi.org/10.1016/j.jfoodeng.2005.10.017

Brunner, G., 2014. Hydrothermal and Supercritical Water Processes. Elsevier. ISBN: 978-0-444-59413-6

Bryś, A., Bryś, J., Ostrowska-Ligęza, E., Kaleta, A., Górnicki, K., Głowacki, S., Koczoń, P., 2016. Wood biomass characterization by DSC or FT-IR spectroscopy. J. Therm. Anal. Calorim. 126, 27–35. https://doi.org/10.1007/s10973-016-5713-2

Cantero, D.A., Bermejo, M.D., Cocero, M.J., 2015a. Governing Chemistry of Cellulose Hydrolysis in Supercritical Water. ChemSusChem 8, 1026–1033. https://doi.org/10.1002/cssc.201403385

Cantero, D.A., Martínez, C., Bermejo, M.D., Cocero, M.J., 2015b. Simultaneous and selective recovery of cellulose and hemicellulose fractions from wheat bran by supercritical water hydrolysis. Green Chem. 17, 610–618. https://doi.org/10.1039/C4GC01359J

Cao, X., Ito, Y., 2003. Supercritical fluid extraction of grape seed oil and subsequent separation of free fatty acids by high-speed counter-current chromatography. J. Chromatogr. A 1021, 117–124. https://doi.org/10.1016/j.chroma.2003.09.001

Capanema, E.A., Balakshin, M., 2015. Plantrose lignins: a new type of technical lignins. 18th Int. Symp. Wood, Fibre Pulping Chem. 120–123.

Cocero, M.J., Cabeza, Á., Abad, N., Adamovic, T., Vaquerizo, L., Martínez, C.M., Pazo-Cepeda, M.V., 2018. Understanding biomass fractionation in subcritical & supercritical water. J. Supercrit. Fluids 133, 550–565. https://doi.org/10.1016/j.supflu.2017.08.012

Dávila, I., Robles, E., Egüés, I., Labidi, J., Gullón, P., 2017. The Biorefinery Concept for the Industrial Valorization of Grape Processing By-Products, in: Handbook of Grape Processing By-Products. Elsevier, pp. 29–53. https://doi.org/10.1016/B978-0-12-809870-7.00002-8

Daz, F.R., Godoy, A., Moreno, J., Bernde, J.C., Snchez, C.O., Opazo, A., Gargallo, L., 2001. Blends of vinylic copolymer with plasticized lignin: Thermal and mechanical properties. J. Appl. Polym. Sci. 81, 861–874. https://doi.org/10.1002/app.1505

Donohoe, B.S., Decker, S.R., Tucker, M.P., Himmel, M.E., Vinzant, T.B., 2008. Visualizing lignin coalescence and migration through maize cell walls following thermochemical pretreatment. Biotechnol. Bioeng. 101, 913–925. https://doi.org/10.1002/bit.21959

Duba, K.S., Casazza, A.A., Mohamed, H. Ben, Perego, P., Fiori, L., 2015. Extraction of polyphenols from grape skins and defatted grape seeds using subcritical water: Experiments and modeling. Food Bioprod. Process. 94, 29–38. https://doi.org/10.1016/j.fbp.2015.01.001

Ehara, K., Takada, D., Saka, S., 2005. GC-MS and IR spectroscopic analyses of the lignin-derived products from softwood and hardwood treated in supercritical water. J. Wood Sci. 51, 256–261. https://doi.org/10.1007/s10086-004-0653-z

Fiori, L., Lavelli, V., Duba, K.S., Sri Harsha, P.S.C., Mohamed, H. Ben, Guella, G., 2014. Supercritical CO2 extraction of oil from seeds of six grape cultivars:

Modeling of mass transfer kinetics and evaluation of lipid profiles and tocol contents. J. Supercrit. Fluids 94, 71–80. https://doi.org/10.1016/j.supflu.2014.06.021

Gullón, P., Romaní, A., Vila, C., Garrote, G., Parajó, J.C., 2012. Potential of hydrothermal treatments in lignocellulose biorefineries. Biofuels, Bioprod. Biorefining 6, 219–232. https://doi.org/10.1002/bbb.339

Hames, R., Scarlata, C., Sluiter, A., 2008. Determination of Protein Content in Biomass - NREL/TP-510-42625. NREL.

Hatakeyama, H., Tsujimoto, Y., Zarubin, M.J., Krutov, S.M., Hatakeyama, T., 2010. Thermal decomposition and glass transition of industrial hydrolysis lignin. J. Therm. Anal. Calorim. 101, 289–295. https://doi.org/10.1007/s10973-010-0698-8

He, J., Huang, Caoxing, Lai, C., Huang, Chen, Li, M., Pu, Y., Ragauskas, A.J., Yong, Q., 2020. The effect of lignin degradation products on the generation of pseudo-lignin during dilute acid pretreatment. Ind. Crops Prod. 146, 1–8. https://doi.org/10.1016/j.indcrop.2020.112205

He, J., Huang, Caoxing, Lai, C., Huang, Chen, Li, X., Yong, Q., 2018. Elucidation of structure-inhibition relationship of monosaccharides derived pseudo-lignin in enzymatic hydrolysis. Ind. Crops Prod. 113, 368–375. https://doi.org/10.1016/j.indcrop.2018.01.046

Hemmilä, V., Hosseinpourpia, R., Adamopoulos, S., Eceiza, A., 2020. Characterization of Wood-based Industrial Biorefinery Lignosulfonates and Supercritical Water Hydrolysis Lignin. Waste and Biomass Valorization 11, 5835–5845. https://doi.org/10.1007/s12649-019-00878-5

Kristensen, J.B., Thygesen, L.G., Felby, C., Jørgensen, H., Elder, T., 2008. Cell-wall structural changes in wheat straw pretreated for bioethanol production. Biotechnol. Biofuels 1, 1–9. https://doi.org/10.1186/1754-6834-1-5

Lancefield, C.S., Wienk, H.J., Boelens, R., Weckhuysen, B.M., Bruijnincx, P.C.A., 2018. Identification of a diagnostic structural motif reveals a new reaction intermediate and condensation pathway in kraft lignin formation. Chem. Sci. 9, 6348–6360. https://doi.org/10.1039/c8sc02000k

Li, M., Pu, Y., Ragauskas, A.J., 2016. Current understanding of the correlation of lignin structure with biomass recalcitrance. Front. Chem. 4, 1–8. https://doi.org/10.3389/fchem.2016.00045

Loow, Y.L., Wu, T.Y., Jahim, J.M., Mohammad, A.W., Teoh, W.H., 2016. Typical conversion of lignocellulosic biomass into reducing sugars using dilute acid hydrolysis and alkaline pretreatment. Cellulose 23, 1491–1520. https://doi.org/10.1007/s10570-016-0936-8

Lorenci Woiciechowski, A., Dalmas Neto, C.J., Porto de Souza Vandenberghe, L., de Carvalho Neto, D.P., Novak Sydney, A.C., Letti, L.A.J., Karp, S.G., Zevallos Torres, L.A., Soccol, C.R., 2020. Lignocellulosic biomass: Acid and alkaline pretreatments and their effects on biomass recalcitrance – Conventional processing and recent advances. Bioresour. Technol. 304, 122848. https://doi.org/10.1016/j.biortech.2020.122848

Maier, T., Schieber, A., Kammerer, D.R., Carle, R., 2009. Residues of grape (Vitis vinifera L.) seed oil production as a valuable source of phenolic antioxidants. Food Chem. 112, 551–559. https://doi.org/10.1016/j.foodchem.2008.06.005

Marqués, J.L., Porta, G. Della, Reverchon, E., Renuncio, J.A.R., Mainar, A.M., 2013. Supercritical antisolvent extraction of antioxidants from grape seeds after vinification. J. Supercrit. Fluids 82, 238–243. https://doi.org/10.1016/j.supflu.2013.07.005

Martínez, C.M., Adamovic, T., Cantero, D.A., Cocero, M.J., 2019. Scaling up the production of sugars from agricultural biomass by ultrafast hydrolysis in supercritical water. J. Supercrit. Fluids 143, 242–250. https://doi.org/10.1016/j.supflu.2018.08.017

Martínez, C.M., Cantero, D.A., Cocero, M.J., 2018. Production of saccharides from sugar beet pulp by ultrafast hydrolysis in supercritical water. J. Clean. Prod. 204, 888–895. https://doi.org/10.1016/j.jclepro.2018.09.066

Moon, S.J., Eom, I.Y., Kim, J.Y., Kim, T.S., Lee, S.M., Choi, I.G., Choi, J.W., 2011. Characterization of lignin-rich residues remaining after continuous super-critical water hydrolysis of poplar wood (Populus albaglandulosa) for

conversion to fermentable sugars. Bioresour. Technol. 102, 5912–5916. https://doi.org/10.1016/j.biortech.2011.02.091

Pingali, S.V., Urban, V.S., Heller, W.T., McGaughey, J., ONeill, H., Foston, M., Myles, D.A., Ragauskas, A., Evans, B.R., 2010. Breakdown of cell wall nanostructure in dilute acid pretreated biomass. Biomacromolecules 11, 2329–2335. https://doi.org/10.1021/bm100455h

Prado, J.M., Lachos-Perez, D., Forster-Carneiro, T., Rostagno, M.A., 2016. Sub- and supercritical water hydrolysis of agricultural and food industry residues for the production of fermentable sugars: A review. Food Bioprod. Process. 98, 95–123. https://doi.org/10.1016/j.fbp.2015.11.004

Prozil, S.O., Evtuguin, D. V., Silva, A.M.S., Lopes, L.P.C., 2014. Structural characterization of lignin from Grape Stalks (Vitis vinifera L.). J. Agric. Food Chem. 62, 5420–5428. https://doi.org/10.1021/jf502267s

Sahoo, S., Seydibeyoĝlu, M.Ö., Mohanty, A.K., Misra, M., 2011. Characterization of industrial lignins for their utilization in future value added applications. Biomass and Bioenergy 35, 4230–4237. https://doi.org/10.1016/j.biombioe.2011.07.009

Selig, M.J., Viamajala, S., Decker, S.R., Tucker, M.P., Himmel, M.E., Vinzant, T.B., 2007. Deposition of lignin droplets produced during dilute acid pretreatment of maize stems retards enzymatic hydrolysis of cellulose. Biotechnol. Prog. 23, 1333–1339. https://doi.org/10.1021/bp0702018

Sluiter, A, Hames, B., Ruiz, R., Scarlata, C., Sluiter, J., Templeton, D., 2008a. Determination of Sugars , Byproducts , and Degradation Products in Liquid Fraction Process Samples - NREL/TP-510-42623. NREL.

Sluiter, A., Hames, B., Ruiz, R., Scarlata, C., Sluiter, J., Templeton, D., Crocker, D., 2008. Determination of Structural Carbohydrates and Lignin in Biomass - NREL/TP-510-42618. NREL.

Sluiter, A, Hames, R., Ruiz, R., Scarlata, C., Sluiter, J., Templeton, D., 2008b. Determination of Ash in Biomass - NREL/TP-510-42622. NREL.

Sluiter, A, Ruiz, R., Scarlata, C., Sluiter, J., Templeton, D., 2008c. Determination of Extractives in Biomass - NREL/TP-510-42619. NREL.

Wahyudiono, Sasaki, M., Goto, M., 2008. Recovery of phenolic compounds through the decomposition of lignin in near and supercritical water. Chem. Eng. Process. Process Intensif. 47, 1609–1619. https://doi.org/10.1016/j.cep.2007.09.001

Xiao, L.P., Sun, Z.J., Shi, Z.J., Xu, F., Sun, R.C., 2011. Impact of hot compressed water pretreatment on the structural changes of woody biomass for bioethanol production. BioResources 6, 1576–1598. https://doi.org/10.15376/biores.6.2.1576-1598

Xu, F., Yu, J., Tesso, T., Dowell, F., Wang, D., 2013. Qualitative and quantitative analysis of lignocellulosic biomass using infrared techniques: A mini-review. Appl. Energy 104, 801–809. https://doi.org/10.1016/j.apenergy.2012.12.019

Yang, H., Yan, R., Chen, H., Lee, D.H., Zheng, C., 2007. Characteristics of hemicellulose, cellulose and lignin pyrolysis. Fuel 86, 1781–1788. https://doi.org/10.1016/j.fuel.2006.12.013

Chapter 2.

Sulfonated kraft lignin repolymerization in supercritical water medium

Repolymerization reactions are a commonly reported issue on the way to the higher recovery of monomers from lignin. The reactivity of monomers obtained from lignin depolymerization and their contribution to the repolymerization in supercritical water (SCW) was investigated. In this study Sulfonated kraft lignin (SKL) was used along with four monomers: vanillin, vanillic acid, vanillyl alcohol and acetovanillone. Indulin kraft lignin was also employed as the reference to understand the repolymerization of SKL in SCW. The formation of diarylmethane structures was detected in HSQC spectra of solid residue after the SCW process. Lignin released fragments with free phenolic β-O-4 structures, as well as the monomeric product vanillyl alcohol are involved with the formation of o-o´ and o-p´ diarylmethane structures. Chemical structure of kraft lignin and its polymeric product after the SCW process was remarkably similar, as shown by HSQC, indicating that repolymerization reactions occur through cross-linking polymerization, mainly in their fractions of low molecular weight products.

Introduction

Lignin is the most abundant aromatic polymer in nature. Its aromatic moieties attract remarkable attention as lignin could play an important role as a sustainable source for aromatic chemicals. The scientific community has recognized this potential, shown by the big number of articles discussing different technologies and strategies of lignin valorization. Among all possible lignin applications, its efficient conversion to low molecular weight aromatics is very popular. However, it is also the most challenging and complex objective due to the lignin technology barriers (Holladay et al., 2007) as well as economic issues (Wenger et al., 2020). Those barriers arise from the very complex and recalcitrant lignin nature, influenced by many factors, among which are the methods used to isolate lignin from biomass.

Kraft process is the dominant pulping procedure used to separate cellulose fibers from lignin, with an estimated global production of 130 Mt/y (as extracted in black liquor; about 5-15% of it can be isolated from black liquor while the rest is needed to be incinerated for the kraft chemicals recovery) (Rinaldi et al., 2016). Advantages of Kraft process over others in the Pulp and Paper Industry are: high quality of the pulp, insensitivity to the wood species and possibility of recovery of chemicals and energy (Mboowa, 2021). In the kraft process, lignin and part of hemicelluloses of the wood chips are dissolved in the solution of sodium hydroxide and sodium sulphide resulting in the isolation of cellulose fibers. During the treatment, the hydroxide and hydrosulfide anions react with the lignin causing the polymer to break into smaller fragments (Azadi et al., 2013). Isolated lignin from the Kraft process undergoes many degradation and condensation reactions (Mikhail Yu.

Balakshin et al., 2003; Chakar and Ragauskas, 2004; Kyosti V Sarkanen, 1971; Lancefield et al., 2018b). One of the obstacles to the further processing of Kraft lignin is its limited solubility in water. As solubility is an important factor that facilitates lignin handling, sulfonation of Kraft lignins has become practice (Aro and Fatehi, 2017).

Numerous strategies have been utilized to break down the lignin molecule in order to obtain valuable aromatic compounds. Methods used for lignin depolymerization can be listed as thermochemical methods (pyrolysis, hydrogenolysis, hydrolysis, etc.), microwave-assisted depolymerization, methods using chemicals or catalysts (acid-catalyzed, base-catalyzed, metallic-catalyzed, ionic liquid-assisted catalyzed, methods using hydrogen peroxide as a catalyst) and biological methods (bacteria, fungi, enzymes) (Chio et al., 2019). Despite the availability of lignin and all the effort involved in obtaining aromatic compounds from it, its deconstruction has not reached the pilot plant scale, because of the difficulties in depolymerization and product separation (Xu et al., 2014). Process limitations and complex lignin structure are the main difficulties to the successful valorization of lignin into high-value aromatic chemicals. Behling et al. and Xu et al. identified those difficulties as: harsh conditions in the sense of long reaction time, high pressure and temperature; use of expensive (noble metal-based catalyst) or/and toxic catalysts; use of non-eco-friendly solvents; the lack of mass transfer from lignin feedstocks to the catalytic surface leading to moderate conversions; low yield of generated products; possible recombination/repolymerization of lignins and lignin fragments; the feasibility of product separation and isolation issues due to the low amount of generated products; the recyclability of the heterogeneous catalyst involved in the

process: separation issues and surface saturation/deactivation of the catalyst (Behling et al., 2016; Xu et al., 2014).

Water at elevated temperature and in the supercritical state has been recognized as a potential reaction medium for lignin depolymerization (Ahlbom et al., 2021; Cocero et al., 2018; Jiang et al., 2016; Pérez and Tuck, 2018; Saisu et al., 2003a; Wahyudiono et al., 2008b; Yong and Matsumura, 2012). This green technology that uses water as solvent overcomes many limitations of applied conventional processes, firstly regarded to use of toxic and expensive catalysts and solvents. The properties of supercritical water differ from those of ambient liquid water. SCW behaves as many organic solvents due to the low value of the dielectric constant (Cantero et al., 2015a). One of the important advantages of the use of water as a reaction medium is that the properties of subcritical and supercritical water vary over a wide temperature and pressure range, giving the possibility to optimize medium identity simply by adjusting those parameters (Brunner, 2014). Another important benefit of SCW is its ability to dissolve both the organic compounds and gases, so that the reaction occurs in a single phase overcoming the limitation of mass transfer. Moreover, high temperatures can greatly enhance the reaction kinetics so a small continuous reactor can be used for very short reaction times.

Different works discussing depolymerization of lignin in SCW reported an increased yield of solid residue and decreased yield of monomers over reaction time due to the repolymerization reaction. They also reported that liberated formaldehyde could promote repolymerization and proposed the use of capping against as phenol and p-cresol to prevent undesired repolymerization and increase the yield of oil enriched in monomers (Okuda et al., 2008, 2004a, 2004b; Saisu et al., 2003). Keeping

reaction time short is essential in lignin depolymerization to avoid undesired repolymerization reactions and to favor monomer recovery. Previous results demonstrated that SKL can be successfully converted into aromatic monomers via ultrafast depolymerization in SCW, keeping the reaction time under 500 ms (Abad-Fernández et al., 2019). The results showed that the total aromatic yield based on lignin was 10.5 % w/w. It was found that the optimum reaction time for lignin depolymerization was 0.3 s. At longer reactions times, however, the yield of the monomeric fraction decreases, followed by an increase in the yield of the heavier fraction, as a result of possible products recombination and repolymerization. The yield of monomeric units starts to decrease after the optimum point, suggesting that these units play an active role in repolymerization (Abad-Fernández et al., 2019).

Repolymerization reactions present an important limiting factor on the way to higher recovery of aromatics from lignin, that face every depolymerization method. The mechanism of repolymerization reactions in SCW is still unclear and its understanding is one way to prudently govern the depolymerization reaction towards the high yield of monomers. In this work, the focus is right on the better understanding of repolymerization processes in SCW. In particular on the reactivity of a mixture of model compounds in presence of lignin, in order to find out if they react between themselves or if they react with other lignin fragments. On the other hand, it was desired to understand the main changes that occur in SKL structure during the SCW process. This was analyzed using FTIR, Gel Permeation Chromatography (GPC) and 2D HSQC NMR.

Experimental section

Materials

Technical lignins and model compounds with their specification used in the experiments are listed in Table 4. Sodium hydroxide used as a catalyst, and ethyl acetate (>99%) used for sample fractionation were purchased from PanReac. Distillate water type III was used as a reaction medium. Acetic acid, sodium acetate, acetonitrile and methanol used in HPLC and GPC analysis were all purchased from Sigma Aldrich.

Table 4. Technical lignins and model compounds used in the study

Compound	CAS	Purchased from	Purity
Vanillin	121-33-5	Sigma Aldrich	99.9
Vanillic acid	121-34-6	Sigma Aldrich	99.8
Vanillyl alcohol	498-00-0	Sigma Aldrich	99.9
Acetovanillon	498-02-0	Sigma Aldrich	99.8
Sulfonated Kraft Lignin	8068-05-1	Sigma Aldrich	Lot MKCG9481
Kraft Lignin (Indulin AT)		Ingevity (formerly MeadWestvaco)	

Methods

Experimental procedure

The chosen model compounds for these experiments were four guaiacyl type monomers: vanillin, vanillin acid, vanillyl alcohol and acetovanillone. Vanillin and acetovanillone are the main model compounds isolated in the previous studies of our

research group. Vanillyl alcohol is one model compound of lignin moieties and a reactive intermediate that has been proposed to play an important role in repolymerization. Aromatic acids such as vanillic acid have been usually found in hydrothermal reactions. The water solutions of reagents were prepared in 0.1M sodium hydroxide. Two reference experiments were performed, one just with 5% w/w SKL, and another with an equimolar mixture of the four model compounds (MC) with a total concentration of 2 % w/w. The total concentration (MC+SKL) for the rest of the experiments was 5 % w/w, with two different lignin to model compounds (SKL:MC) ratios of 1:4 and 2:3. The temperature in every experiment was 385 ±1 ºC, the pressure was 254±2 bar and the residence time 360±20 ms. After the reaction samples were fractionated following a procedure similar to one reported by Perez and Tuck (Pérez and Tuck, 2018). The sample was acidified to pH=2 using sulphuric acid, followed by centrifugation to separate the precipitated solid (s) and the aqueous (aq) fractions. The solid was then washed three times with acidified water (pH=2), which was collected and added to the liquid fraction. The solid was further extracted three times with ethyl acetate. The solvent after extraction was removed by rotary evaporator and the solid obtained as the extract is called heavy oil fraction (s-E). The residue obtained after the extraction is called solid residue (s-R). The aqueous fraction was also extracted three times with ethyl acetate. The solvent of the organic phase of this fraction was removed in a rotary evaporator and the obtained extract is named light oil (aq-E). The water phase fraction is called aqueous residue (aq-R), and it was discarded as usually does not provide significant information (Pérez and Tuck, 2018).

The procedure of samples fractionation explained here is simplify presented in Figure 21.

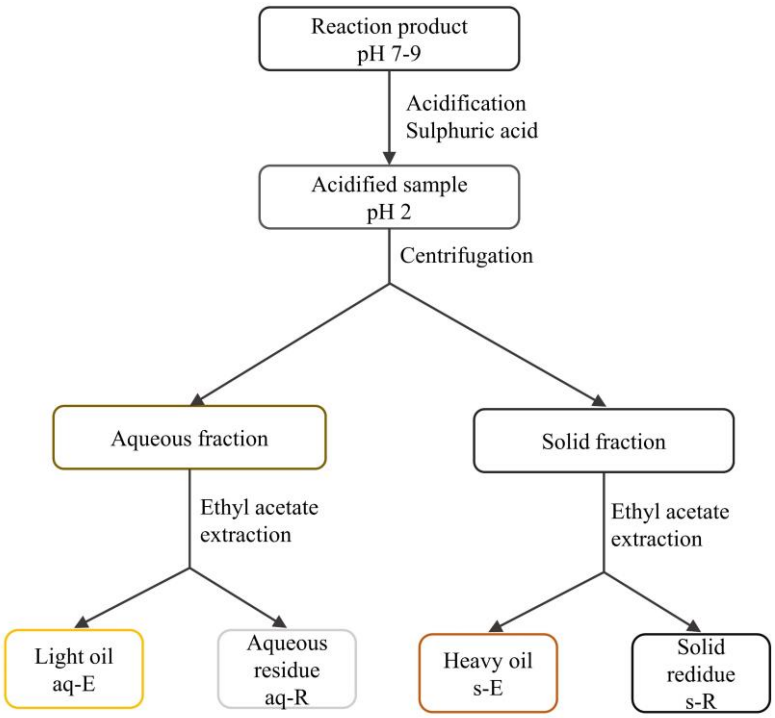

Figure 21. The procedure of sample fractionation after the reaction

Sample analysis

The analytical techniques used in sample characterization are described as follows:

High-performance liquid chromatography (HPLC)

The concentration of the monomeric compounds after the SCW process was determined by HPLC. The analysis was performed using a method based on work from Perez and Tuck (Pérez and Tuck, 2018). An Agilent TM 1100 series with an

XterraTM C-18 column and a single wavelength UV detector at 230 nm were used. The mobile phase was the mixture of acetic acid/sodium acetate buffer and acetonitrile (ACN). The flow rate was 0.7 mL/min. Isocratic method (10 % ACN) for the first 10 min; 10 – 20 min gradient method (10 to 50 % ACN); 20-21 min, quickly decrease to initial conditions (50 to 10 %); 21-30 isocratic method (10% ACN). The sample injection volume was 10 µL.

Gel Permeation Chromatography (GPC)

The molecular weight distribution of the samples was determined by gel permeation chromatography (GPC) with the Jordi Gel Sulphonated Plus 10000 A 250 x 10 mm column and using Waters IR detector 2414 (210 mm) and Waters dual λ absorbance detector 2487 (254 nm). The mobile phase was a solution of water and methanol in the ratio of 90:10 v/v, adjusted to pH = 12 at a flow rate of 1 mL/min (Perez and Tuck, 2018). Samples were dissolved directly in the eluent with a concentration between 2 and 6 mg/ml. The injection volume was 25 µl.

Fourier Transform Infrared Spectroscopy (FTIR)

The equipment used for FT-IR analysis of lignin and s-R was a Bruker Tensor 27 with a diamond crystal. The analysis was performed at room temperature. The spectra are recorded in mode Attenuated Total Reflection (ATR). The baseline was corrected, and the peaks were normalized to the maximum peak.

2D HSQC NMR analysis

Two-dimensional 1H-13C correlation HSQC NMR experiments were performed with Bruker AVNEO 600 MHz spectrometers equipped with a cryogenically cooled 5 mm TCI probe head to identify and quantify the structure of

lignin and their reaction product samples. Except for the 80 mg of SKL that was fully dissolved in 0.6 ml of DMSO-d6/D2O mixture (5:1, vol.), 80 mg of other samples were fully dissolved only in 0.6 ml of DMSO-d6. A sensitivity-enhanced pulse program (hsqcetgpsisp.2) that utilizes shaped pulses for all 180° pulses on the proton channel was used in the acquisition. 1024 data points were acquired from 11 to 0 ppm in F2 (1H), with an acquisition time of 77.8 ms, and from 215 to 0 ppm in F1 (13C) with 256 increments, 36 scans, and a 2.0 s interscan delay, with a total acquisition time of 5 h 50 min in 298 K. The average value for one-bond J-coupling between protons and carbons was set as 145 Hz. All data were processed using Bruker BioSpin's Topspin 3.5 software. The spectra were calibrated using the central peak of the DMSO-d6 (δH 2.49 ppm, δc 39.5 ppm). Processing the final matrix to 2 k by 1 k data points was performed by QSINE window functions in both F2 and F1. The known correlation peaks appearing in the HSQC spectra were assigned by referring to the NMR data of lignin model compounds in the NMR database of lignin model compounds and previous studies. The integrals were normalized to the integral of C2-H2 correlation at the 2-position of guaiacyl ring (G2), which are representative of all G-units as internal standard. Therefore, the results were relatively expressed per aromatic ring keeping in mind the semiquantitative character of the HSQC method. According to the integral value of G2 signal, the number of structural units could be relatively estimated by the following eqn. (18):

$$Ix\% = \frac{Ix}{I_{G2}}\ x\ 100\ \% \qquad (18)$$

Where *Ix* is the integral value of corresponding structural units. The integration was made in the same contour level condition (number of positive contour levels = 50, highest contour level = 100%, lowest contour level = 20).

Experimental setup

Experiments were carried out in the Ultrafast supercritical water hydrolysis plant with a Sudden Expansion Micro Reactor (SEMR) shown in Figure 22 (note: this plant has lab-scale differently from Chapter 1 where the pilot-scale plant was used). The maximum operating conditions for this plant are 425 °C and 300 bar, with a maximum capacity of 3.6 kg/h of lignin solution.

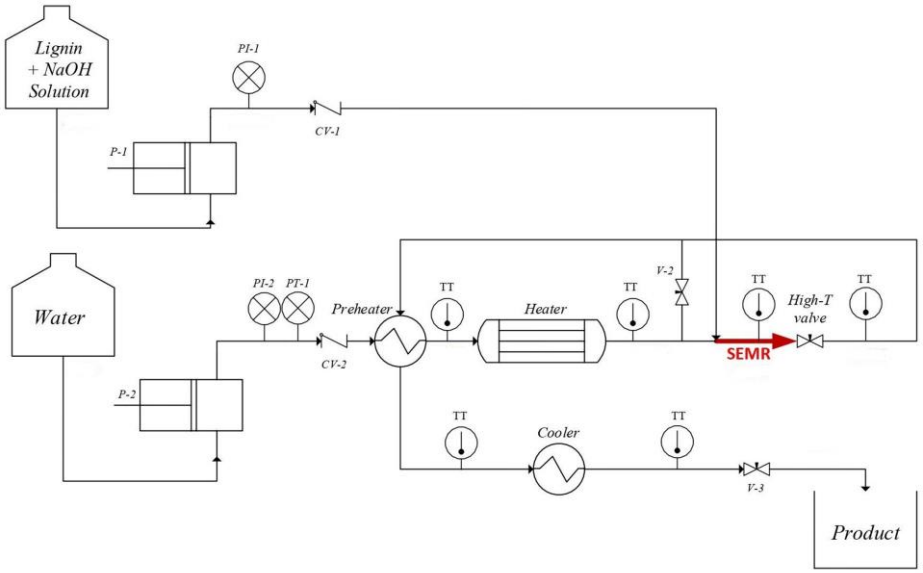

Figure 22. Flow diagram of continuous plant with SEMR reactor, lab-scale

The design of the plant provides sudden start and termination of the reaction by sharp temperature changes. The sudden start is proved by the mixing of SCW and the

compressed solution in T junction just on the entrance of the reactor while termination is proved by sudden decompression using a high temperature and pressure needle valve, resulting in a Joules-Thomson effect. In this way is possible to provide a short reaction time and avoid heating and cooling slopes that prevent its accurate control. After the decompression valve, a heat exchanger is installed to cool the sample further down to room temperature. Differently from the pilot plant (compare Figure 12 and Figure 22), this plant does not have installed filters and flash separators. Mass balance based on carbon for every experiment is presented in the text after the conclusion.

Results and Discussion

Model compounds conversion

In the first experimental set, the solution of the MC mixture was processed in SCW. The reactivity of the four model compounds is followed by the conversion rate (X). The conversion rate of each compound in every experiment is calculated by eqn. (19).

$$X = \frac{(c_{in}^{MC} - c_{out}^{MC})}{c_{in}^{MC}} \qquad (19)$$

Where is:

c_{in}^{MC} – inlet concentration of model compounds

c_{out}^{MC} – outlet concentration of model compounds

In the MC experiment, the highest conversion rate is obtained in the order vanillyl alcohol > vanillin > vanillic acid > acetovanillone. High conversion rates of model compounds presented in Figure 23 signify their high reactivity in the SCW medium. Guaiacol is detected in the HPLC chromatogram after the reaction as a product. This is expected as guaiacol also is a reaction product derived from the decomposition of some of the model compounds in SCW, for example, the decomposition of vanillic acid by decarboxylation reaction (González et al., 2004). It has been proposed that other units could yield guaiacol by radicalary scissions (Abad-Fernández et al., 2020; Liu et al., 2016). Another type of degradation would involve the reaction between monomers, leading to higher molecular weight compounds.

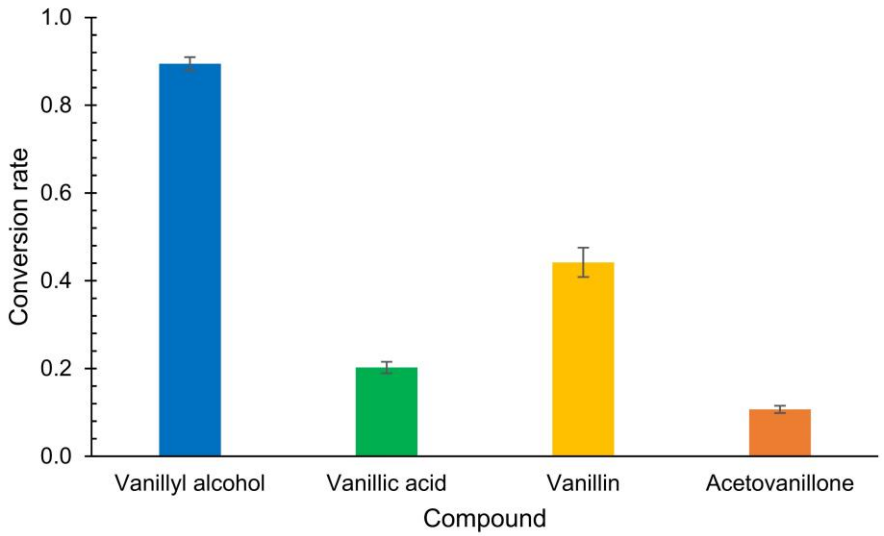

Figure 23. The conversion rate of different model compounds

The conversion rate of each model compound changed when SKL is introduced into the reaction mixture. During the lignin depolymerization reactions in SCW, it was observed that the yield of obtained monomers decreases over reaction time as a

result of repolymerization reactions (Abad-Fernández et al., 2019). The new conversion rates of model compounds in our system are thus influenced by the presence of SKL, either by reacting with SKL fragments or the latter inhibiting the monomer degradation.

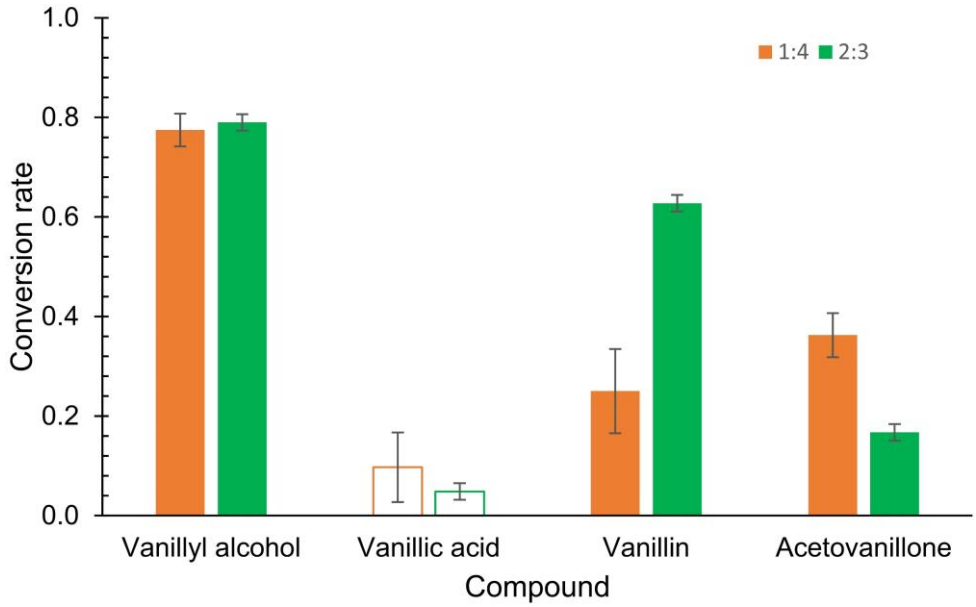

Figure 24. The conversion rate of model compounds for different L:MC ratios

Figure 24 presents the conversion rate of model compounds in experiments with different SKL:MC ratios (1:4 vs 2:3) suggesting that SKL introduced has a significant influence on the conversion rate of model compounds. Conversion of vanillyl alcohol remain the highest one and is similar for different SKL:MC ratios, as well as with the experiment where SKL is not present. The conversion of vanillic acid decreases significantly when SKL was introduced into the reactor, indicating vanillic acid production due to the presence of SKL (the conversion rate has a negative value, presented with not filled columns in the chart). This could be explained by a certain

amount of homovanillic acid production from SKL (Abad-Fernández et al., 2019), which interferes with the HPLC signal of vanillic acid. In any case, these results suggest that SKL has a protector effect over vanillic acid. Conversion of vanillin increases from 0.25 to 0.63 when the concentration of SKL is higher so that more lignin promotes vanillin conversion. The opposite trend is observed for acetovanillone where the reaction rate is lower when more SKL is present.

Sample fractionation

After the reaction, the sample was fractionated into four fractions: aqueous residue (aq-R), aqueous extract (aq-E) called light oil, solid residue (s-R) and solid extract (s-E) called heavy oil. s-R and s-E fraction together are marked as total solid and present heavier fractions of the sample. It is expected that s-R is the fraction that contains the products from the repolymerization reactions (Abad-Fernández et al., 2019) for reaction times higher than the optimum. From Figure 25a, it can be seen that s-R yield reaches the highest value for the experimental run just with SKL. The yield decreases when MC are introduced into the reaction mixture, i.e., decrease by lowering the SKL concentration compared to the concentration of MC. The yield of s-E fraction is around 35% and thus similar for every experiment (Figure 25c). This yield is based on the total mass inside the reactor (MC + SKL). If we however present this yield based on the mass of SKL inside the reactor (Figure 25d), it can be seen that for the ratio SKL:MC = 1:4 the yield of s-E fractions exceeds 100%, confirming that MC upgrade to a solid fraction. This contributes mainly to s-E. As mentioned above, MC are undergoing reaction in SCW when SKL was not present inside the reaction mixture, as shown by their high conversion rates.

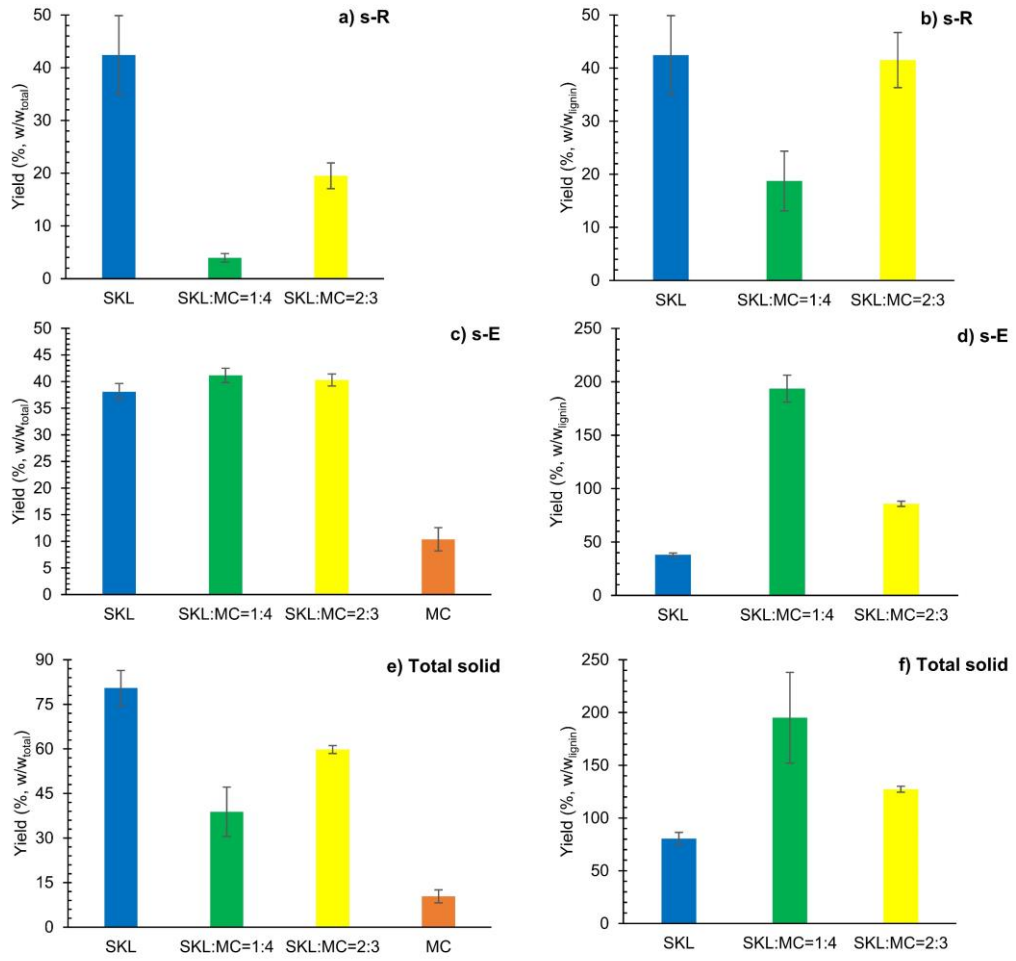

Figure 25. The yield of heavier fraction: s-R a) based on total mass b) based on lignin mass;
s-E c) based on total mass d) based on lignin mass; total solid yield e) based on total mass f) based on lignin mass

After performing fractionation steps of the sample obtained with MC, the whole solid fraction was dissolved in ethyl acetate and thereby no s-R fraction is obtained while the yield of s-E fraction is around 10 % (Figure 25c). It is difficult to confirm whether the model compounds react between each other or with SKL fragments, but the experiment where the SKL:MC ratio was 2:3, yields more s-R

compared to the experiment with just lignin, denoting that MC could polymerize with lignin fragments.

GPC spectrum of samples obtained with MC, SKL and mixture of MC and SKL are presented in Figure 26.

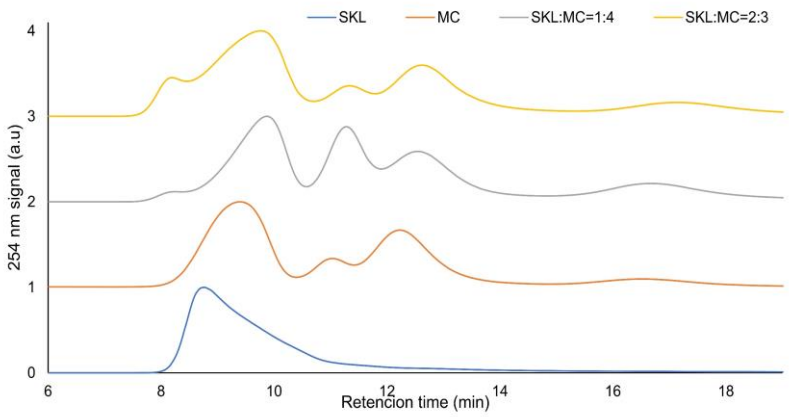

Figure 26. GPC spectrums of the samples

Spectrum from a sample of MC shows peaks at diverse retention times, confirming a certain degree of polymerization among them, as has already been observed previously for vanillin (Pérez and Tuck, 2018). Samples obtained with a mixture of MC and SKL (SKL:MC = 1:4 and 2:3) have peaks appearing at shorter reaction times ($t \approx 8$ min) compared to the sample obtained with SKL. These results suggest that, at least partially, MC have reacted with SKL fragments to yield higher molecular weight compounds.

Analysis and characterization of solid fraction

FT-IR analysis

FT-IR analysis of original SKL, s-R fraction of SKL, s-R fraction of mixture of MC and SKL and s-E fraction of MC is presented in Figure 27. Every sample shows the typical lignin signals, where the list of vibrations and their assignments is presented in Table 5.

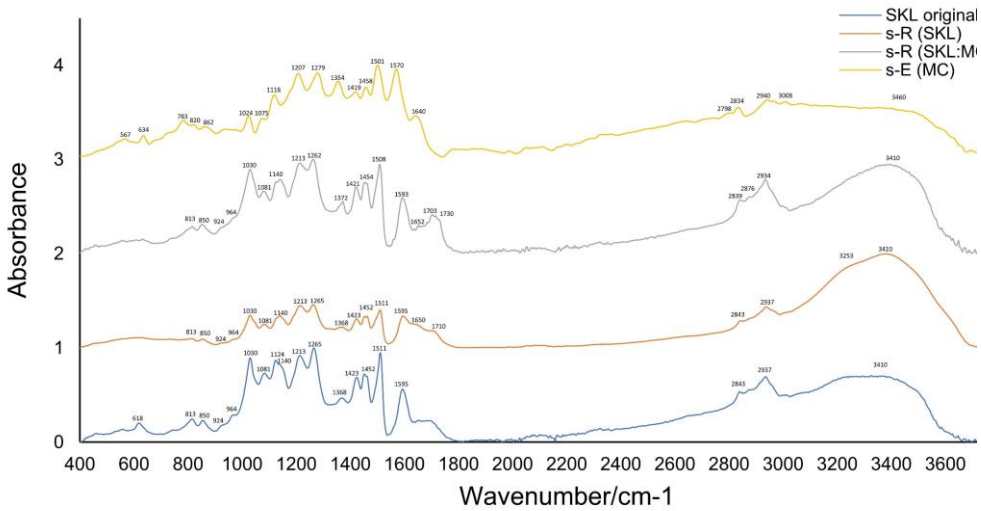

Figure 27. FT-IR spectrum of original SKL, s-R (SKL, SKL:MC=1:1) and s-E (MC)

The main change obtained in spectra of s-R fractions of SKL compared to the original SKL is the disappearance of a peak at 618 cm^{-1}, characteristic for sulphonic groups due to the de-sulphonation. The peaks between 2938 cm^{-1} and 2842 cm^{-1}, assigned to C-H stretching frequencies of aromatic methoxy group, methyl and methylene groups of the side chain have decreased intensity in s-R fraction compared to original SKL. s-E fraction of MC had the shift in the wavenumber for most of the

bands. For example, aromatic skeleton vibration that appears for every s-R fraction at 1600 cm-1 and 1511 cm^{-1} is shifted to 1570 cm^{-1} and 1501 cm^{-1}, respectively. Guaiacol ring vibration and C=O stretching was shifted from 1265 cm^{-1} to 1279 cm^{-1}.

Table 5. FT-IR spectrum of original SKL, s-R (SKL, SKL:MC=1:1) and s-E (MC)

Assignments	**Band (cm^{-1})**
Sulphonic groups (Hemmilä et al., 2020)	620
Out-of-plane vibration of aromatic ring (Constant et al., 2016)	815.850
C-H out of plane bending (aromatic ring) (Hemmilä et al., 2020)	915-925
Out-of-plane deformation of trans double band (stilbene units) (Constant et al., 2016)	965
Aliphatic-OH (Boeriu et al., 2014)	1030
Guaiacyl units (Constant et al., 2016)	1032, 1271, 1514
Aliphatic ether groups (Boeriu et al., 2014) C-O deformation (secondary alcohols and aliphatic esters) (Hemmilä et al., 2020)	1075-1081
Aromatic C-H in-plane deformation with C-O deformation (primary alcohol and ether) and C=O stretching (unconjugated)	1030-1035
Aromatic C-H in-plane deformation (G-ring) (Hemmilä et al., 2020)	1140
C-C with C-O and C=O stretching (Hemmilä et al., 2020)	1215-1220
G-ring breathing with C-O stretching (Hemmilä et al., 2020)	1266-1270
H-O in-plane deformation (phenolic OH) and C-H in methyl groups (Hemmilä et al., 2020)	1365-1370
C-H in plane deformation (Pang et al., 2017)	1421
C-H stretching of methylene groups (Pang et al., 2017)	1456
C=C stretching of the aromatic ring skeleton (Pang et al., 2017)	1501/1506

Aromatic ring vibration of phenyl propane 9C skeleton (Hemmilä et al., 2020)	1425, 1515, 1600
Conjugated / non-conjugated C=O (Boeriu et al., 2014)	1658 / 1710
C-H stretching of methyl groups (Pang et al., 2017)	2931
O–H stretching vibration in aromatic and aliphatic structure (Hemmilä et al., 2020)	3410 - 3460

HSQC analysis

Solid residue fraction (s-R) is the heaviest fraction that should contain possible repolymerization products and unreacted lignin. Taking a detailed structural study on s-R fraction should help us to understand the side reaction happening on SKL during the SCW process. The signals in the spectra were assigned according to previous publications (Heitner et al., 2016; Gierer and Pettersson, 1977; Komatsu and Yokoyama, 2021; Lancefield et al., 2018b; Yelle and Ralph, 2016)

As shown in Figure 28a HSQC spectrum of the original SKL was overlaid with that of its s-R fraction obtained after the SCW process. It can be seen that there is a significant change happened on SKL structure after the SCW process. The main reaction of SKL in the SCW system was lignin de-sulphonation as the spectrum of s-R was very similar to a typical spectrum of a softwood Kraft lignin i.e., Indulin (Figure 28c, f vs d, g). The other structural changes in SKL were rather minor and could not be investigated as they were strongly obscured by the intensive changes due to lignin de-sulphonation.

To investigate the transformation of SKL and its monomer products during SCW process, the s-R fraction from SKL and s-E fraction of MC were compared to each other in HSQC spectra (Figure 28b).

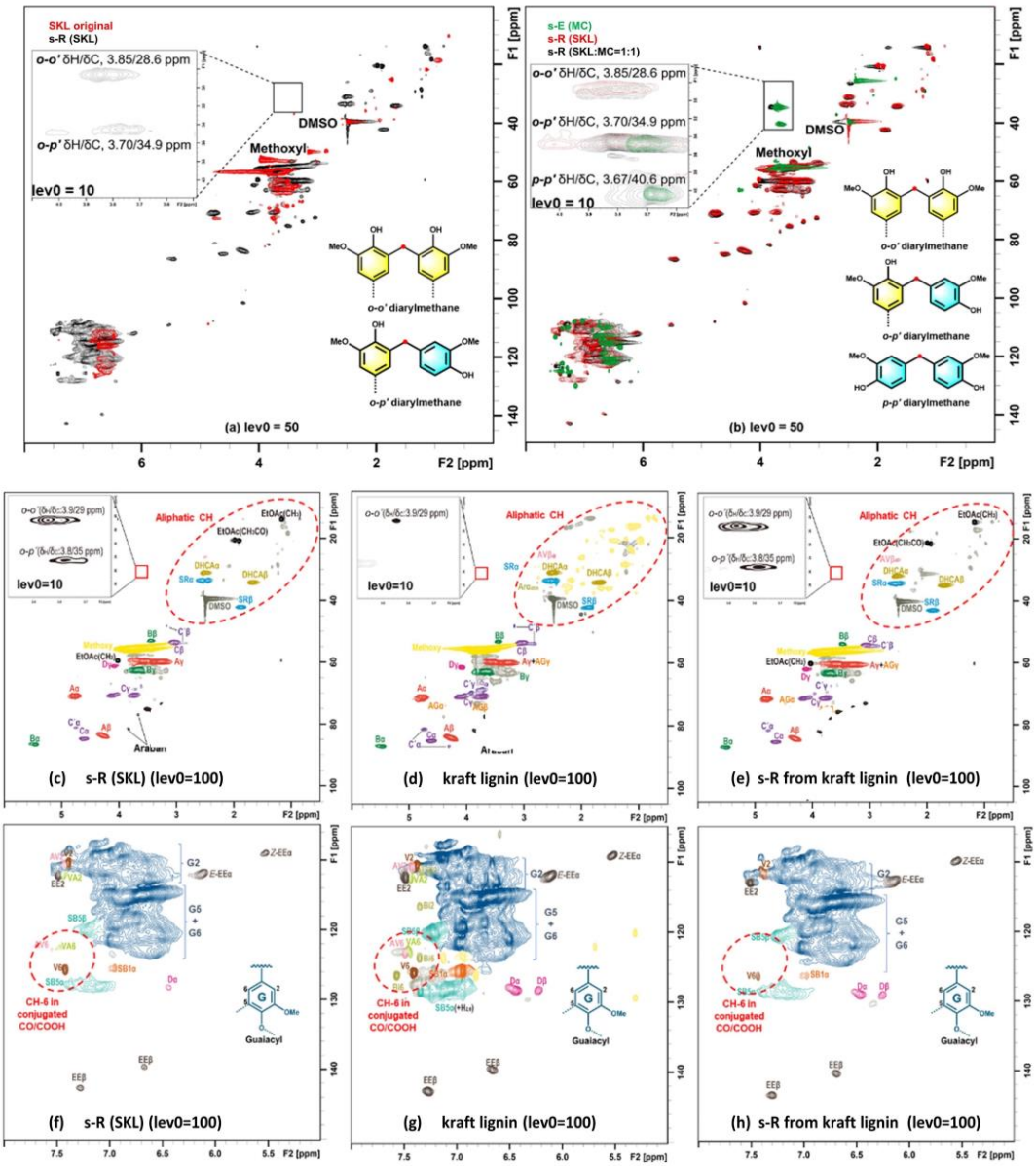

Figure 28. 2D HSQC NMR spectra of lignin samples: SKL overlaid with its s-R fraction after SCW process (a); the s-E fraction of model compounds, s-R fraction of SKL and their mixture after SCW process overlaid with each other (b); aliphatic region of s-R from SKL (c), kraft lignin (d) and its s-R fraction (e); aromatic region of s-R from SKL (f), kraft lignin (g) and its s-R fraction (h), the lev0 is the value of lowest contour level in the spectrum, the coloured structures are used to show main structural linkages in lignin samples

The formation of o-o´ and o-p´ diarylmethane structures with minor amounts can be observed in the s-R fraction of SKL (Figure 28a). In contrast, the o-p´ and p-p´ diarylmethane structures were found in the s-E fraction of MC after the SCW process (Figure 28b). This indicated that the repolymerization can be related to the formation of diarylmethane structures, but the formation mechanism for MC and SKL is different during the SCW process, as proposed in Figure 30. As shown in Figure 30a, vanillyl alcohol plays an important role in the formation of o-p´ and p-p´ diarylmethane structures. In detail, vanillyl alcohol transforms in para-quinone methide under alkaline conditions (Komatsu and Yokoyama, 2021).

This para-quinone methide reacts at any ortho or the para position to the guaiacol generated from other monomers, finally resulting in the o-p´ and p-p´ diarylmethane, respectively. Whereas, the formation of o-o´ and o-p´ diarylmethane structures during SCW treatment on SKL may be due to the liberated formaldehyde from some structures of SKL during the SCW process, e.g., γ-position of free phenolic β-O-4 structures in the alkaline condition. Gierer and Pettersson ever reported that formaldehyde liberated from terminal hydroxymethyl groups in β-O-4 bonded quinone methide intermediates during alkaline treatment reacts with the added phenols affording the corresponding diarylmethane (Gierer and Pettersson, 1977).

Therefore, we can see that the formation of p-p´ diarylmethane is limited to monomer products, but hardly occur to any significant extent with polymeric lignins. On the contrary, the o-o´ diarylmethane structure was not formed among monomers. However, the formation of o-p´ and p-p´ diarylmethane structures could occur between two monomer products or/and a lignin fragment. These reactions are unlikely to directly contribute to the generation of s-R fraction from SKL during the SCW

process, but are beneficial on the oil fractions. Product fractionation also shows that MC contribute to the yield of total solid mainly through increased yield of s-E fraction. However, it cannot be excluded that the resultant dimeric p-p´ diarylmethane structures or low molecular lignin fragments with o-p´ diarylmethane structures would react furtherly to contribute the s-R fractions. We assumed that the produced monomer products from SKL could involve the formation of s-R fraction during SCW. To confirm this, an experiment with the mixture of SKL and MC was analyzed by 2D-NMR (SKL:MC = 1:1, Figure 28b). Interestingly, all three types of diarylmethane structures were observed in their s-R fraction, indicating all of them are related to the production of s-R fraction during SCW. Nevertheless, p-p´ diarylmethane structures were still not found in the s-R fraction of SKL after the SCW process. It is possible that the transformation to vanillic acid for vanillic alcohol is easier than the para quinone methide during the SCW process on SKL, thus leaving few opportunities to form the p-p´ diarylmethane structures. Detailed kinetic studies with MC is therefore needed to address this hypothesis. The main structures determined in the study are presented in Figure 29.

As it was very difficult to elucidate lignin repolymerization using SKL, we performed an experiment on kraft lignin with much simpler structure. The structural assignment of HSQC spectra of original kraft lignin (Indulin), and its s-R fraction after the SCW process are presented in Figure 28 (d/g, e/h). Their main structural quantitative data are shown in Table 6.

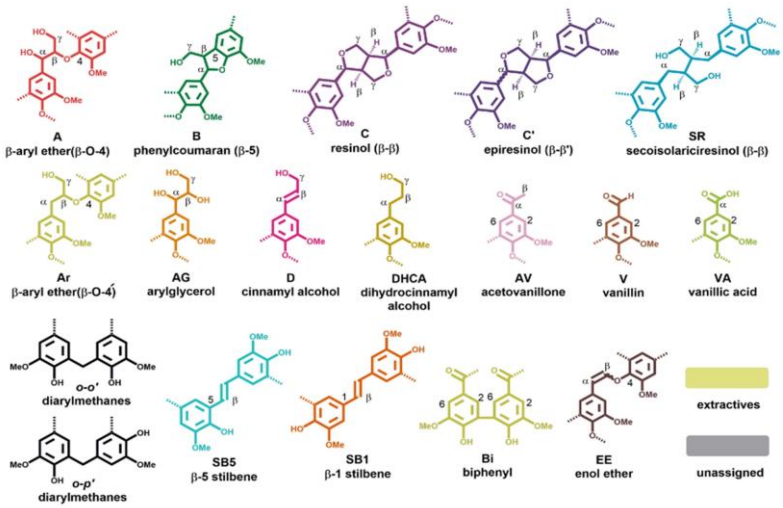

Figure 29. The main structures determined in the study

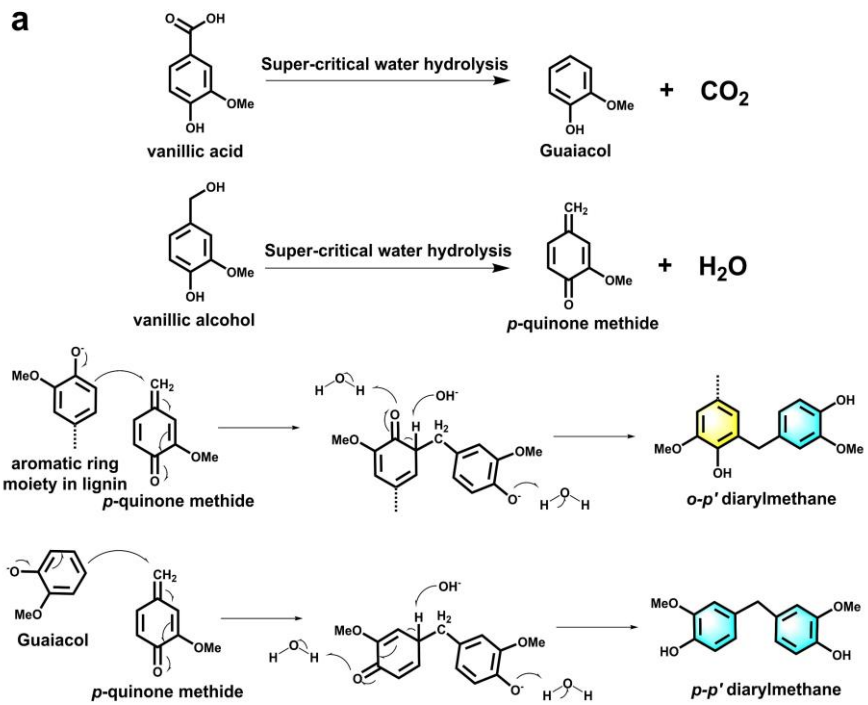

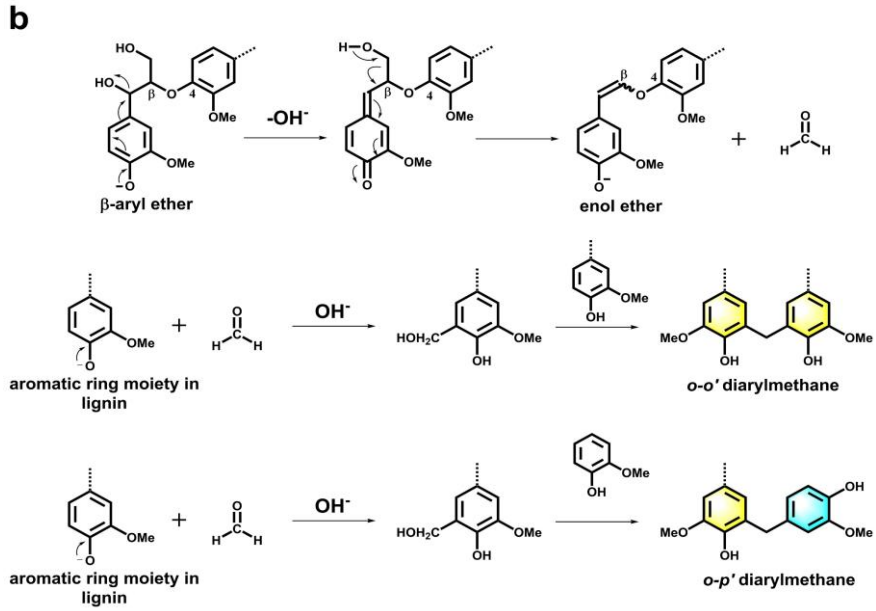

Figure 30. Proposed mechanism for the formation of diarylmethane structures in SCW process: from MC (a); from SKL (b)

In the s-R fractions obtained from kraft lignin after the SCW process, a small amount of o-o´ diarylmethane structures as crosslinked bridges between two lignin fragments can be observed. Therefore, these diarylmethane structures may contribute to the formation of s-R fractions from kraft lignins after the SCW process. Although our data in Table 6 shows a small amount of o-o´ diarylmethane structure (0.5%) in the s-R from kraft lignin, they are sufficient to cross-link the lignin fragments to double the molecular weight of resultant solid residue. Also, no new Alk-Ar structures were observed in the spectrum of kraft lignin after the reaction. However, the formation of Ar-Ar and/or Ar-O-Ar (e.g., 5-5', 4-O-5') moieties contributing to the production of s-R fraction during the SCW process cannot be excluded as the HSQC technique does not allow their reliable analysis.

There is no significant difference observed in the oxygenated alkyl region between kraft lignin and its s-R fractions after the SCW process (Figure 28d, e). This indicates that the cross-polymerization may happened between lignin fragments after the SCW process. Consequently, their main inter-structural linkages were preserved. Figure 28 shows a remarkable similarity between the original kraft lignin and its s-R fraction after the reaction. Most of the differences were within the experimental error or/and related to very minor lignin moieties. The only noticeable difference was a decrease in the amount of stilbene moieties (from ca 25/100 Ar to about 10/100Ar), which apparently underwent degradation in the SCW process.

Table 6. Amount of typical inter-unit linkages in samples (nlev=50, lev0=20, toplev=100 %)

No.	HSQC peaks	Indulin/100 aromatic ring	s-R from Indulin/100 aromatic ring	Assignment
1	Methoxyl	105.5	110.6	-OCH3
2	G2	100.0	100	CH-2 in Guaiacyl ring
3	Aα	9.8	7.9	β-O-4
4	Bα	3.0	3.2	β-5
5	Cα	2.1	1.8	β-β
6	C'α	0.9	0.9	epiresinol
7	SRβ	2.5	2.5	secoisolariciresinol
8	Arα	0.7	0.8	Reduced β-O-4
9	AGα	0.5	1.2	arylglycerol
10	Dγ	1.7	1.6	cinnamyl alcohol
11	DHCAβ	3.9	4.3	dihydrocinnamyl
12	AVβ	0.5	0.8	acetovanillone

13	*o-o´*	0.1	0.3	diarylmethane
14	*o-p´*	ND	0.1	diarylmethane
15	V6	1.8	0.9	vanillin
16	VA6	0.8	ND	Vanillic acid
17	E-EEα	2.4	3.0	E-Enol ether
18	Z-EEα	1.2	1.1	Z-Enol ether
19	SB1α	2.5	0.7	β-1 stilbene
20	SB5β	19.8	8.2	β-5 stilbene

Conclusion

Lignin model compounds tend to furtherly react in SCW as shown by their high conversion rates, both between themselves and with lignin fragments. The yield of solid fraction increase when the mixture of SKL and MC is processed in SCW, compared to processing of just SKL, signifying that MC contribute to solid formation. To reduce the repolymerization and recover the high yield of monomers in the SCW process, light oil fraction enriched in monomers should be separated from the reaction mixture as soon as it is produced.

One of the products found in the solid extract fraction of MC and solid residue fraction obtained with SKL are diarylmethanes structures. The formation of those moieties contributes to the repolymerization but their mechanism pathway is different for SKL and MC. After SCW processing SKL residue has a structure similar to softwood kraft lignin and the main reaction that occurred is SKL de-sulphonation. Noteworthy, the chemical structure of Indulin kraft lignin and its solid residue after

the SCW process was remarkably similar indicating that the main reactions occurred in the fractions of low molecular weight products.

Mass balance data

Mass balance data presented here are based on carbon and are calculated as the ratio between total carbon concentration measured in the outlet and inlet of the reactor by eq. (20).

$$\frac{c_{out}^{C}}{c_{in}^{C}} \qquad (20)$$

Where is:

c_{in}^{C}- concentration of carbon in the inlet of the reactor

c_{out}^{C}-concentration of carbon in the outlet of the reactor

The concentration of carbon in the inlet of the reactor (c_{in}^{C}) is measured as the sum of carbon concentration originated from model compounds and sulfonated kraft lignin used in the study (eq.

(21)).

$$c_{in}^{C} = \sum c_{VA;VCOCH3;VCOOH;VCOH;SKL}^{C} \qquad (21)$$

Where is:

c_{VA}^{C} – concentration of carbon from vanillin

c_{VCOCH3}^{C}- concentration of carbon from acetovanillone

c_{VCOOH}^{C} − concentration of carbon from vanillic acid

c_{VCOH}^{C}- concentration of carbon from vanillyl alcohol

c_{SKL}^{C}- concentration of carbon from sulfonated kraft lignin

note: The following example shows the further calculation for vanillin while the same equations are applied for each compound.

The concentration of carbon from each compound in the inlet of the reactor is calculated as the product of compound concentration in the inlet (c_{VA}^{C}) and carbon factor of that compound (f_{VA}^{C}), as presented by eq. (22). The concentration of the compound in the inlet is calculated as shown by eq. (23).

$$c_{VA}^{C} = c_{VA}\, x\, f_{VA}^{C} \qquad (22)$$

$$c_{VA}(ppm) = \frac{c_{VA}^{solution}\left(\frac{g}{g}\right) x F_{solution}\left(\frac{ml}{s}\right)}{F_{total} x 10^{6}\left(\frac{ml}{s}\right)} \qquad (23)$$

Where:

$c_{VA}^{solution}$- concentration of vanillin in the starting solution

$F_{solution}$ – the flow of the starting solution

F_{total} – the total flow of the product

The concentration of carbon in the outlet of the reactor is calculated using Total Organic Carbon analysis.

c_{out}^{C}=TOC

The data of the mass balance are presented in Table 7.

Table 7. Mass balance data based on carbon

Experiment	c^C_{VA}(ppm)	c^C_{VCOOH}(ppm)	c^C_{VCOH}(ppm)	c^C_{VOCH3}(ppm)	c^C_{SKL}(ppm)	c^C_{in} (ppm)	c^C_{out} (ppm)	$\frac{c^C_{out}}{c^C_{in}}$
SKL						10878.2±235.0	10136±277.2	**0.93±0.005**
MC	1014.3±45.8	860.2±4.4	859.7±4.4	964.2±4.9		3698±32.9	3626.7±18.5	**1.0±0.2**
SKL:MC=1:4	1513.2±49.1	1512.4±49.0	1512.4±49.0	1700.6±55.1	1238.7±40.2	7477.3±242.5	7278.5±126.6	**0.97±0.01**
SKL:MC=2:3	1500.9±57.0	1499.6±57.0	1499.6±57.0	1686.8±64.1	3275.6±124.6	9049.0±359.8	8917.3±569.7	**0.94±0.03**

References:

Abad-Fernández, N., Pérez, E., Cocero, M.J., 2019. Aromatics from lignin through ultrafast reactions in water. Green Chem. 21, 1351–1360. https://doi.org/10.1039/C8GC03989E

Abad-Fernández, N., Pérez, E., Martín, Á., Cocero, M.J., 2020. Kraft lignin depolymerisation in sub- and supercritical water using ultrafast continuous reactors. Optimization and reaction kinetics. J. Supercrit. Fluids 165. https://doi.org/10.1016/j.supflu.2020.104940

Ahlbom, A., Maschietti, M., Nielsen, R., Hasani, M., Theliander, H., 2021. Towards understanding kraft lignin depolymerisation under hydrothermal conditions. Holzforschung 76. https://doi.org/10.1515/hf-2021-0121

Aro, T., Fatehi, P., 2017. Production and Application of Lignosulfonates and Sulfonated Lignin. ChemSusChem 10, 1861–1877. https://doi.org/10.1002/cssc.201700082

Azadi, P., Inderwildi, O.R., Farnood, R., King, D.A., 2013. Liquid fuels, hydrogen and chemicals from lignin: A critical review. Renew. Sustain. Energy Rev. 21, 506–523. https://doi.org/10.1016/j.rser.2012.12.022

Balakshin, M.Y., Capanema, E.A., Chen, Gracz, H.S., 2003. Elucidation of the Structures of Residual and Dissolved Pine Kraft Lignins Using an HMQC NMR Technique. J. Agric. Food Chem. 51, 6116–6127. https://doi.org/10.1021/jf034372d

Behling, R., Valange, S., Chatel, G., 2016. Heterogeneous catalytic oxidation for lignin valorization into valuable chemicals: What results? What limitations? What trends? Green Chem. 18, 1839–1854. https://doi.org/10.1039/c5gc03061g

Boeriu, C.G., Fiţigău, F.I., Gosselink, R.J.A., Frissen, A.E., Stoutjesdijk, J., Peter, F., 2014. Fractionation of five technical lignins by selective extraction in green solvents and characterisation of isolated fractions. Ind. Crops Prod. 62, 481–490. https://doi.org/10.1016/j.indcrop.2014.09.019

Brunner, G., 2014. Hydrothermal and Supercritical Water Processes. Elsevier. ISBN: 978-0-444-59413-6

Cantero, D.A., Bermejo, M.D., Cocero, M.J., 2015. Governing Chemistry of Cellulose Hydrolysis in Supercritical Water. ChemSusChem 8, 1026–1033. https://doi.org/10.1002/cssc.201403385

Chakar, F.S., Ragauskas, A.J., 2004. Review of current and future softwood kraft lignin process chemistry. Ind. Crops Prod. 20, 131–141. https://doi.org/10.1016/j.indcrop.2004.04.016

Chio, C., Sain, M., Qin, W., 2019. Lignin utilization: A review of lignin depolymerization from various aspects. Renew. Sustain. Energy Rev. 107, 232–249. https://doi.org/10.1016/j.rser.2019.03.008

Cocero, M.J., Cabeza, Á., Abad, N., Adamovic, T., Vaquerizo, L., Martínez, C.M., Pazo-Cepeda, M.V., 2018. Understanding biomass fractionation in subcritical & supercritical water. J. Supercrit. Fluids 133, 550–565. https://doi.org/10.1016/j.supflu.2017.08.012

Constant, S., Wienk, H.L.J., Frissen, A.E., Peinder, P. De, Boelens, R., Van Es, D.S., Grisel, R.J.H., Weckhuysen, B.M., Huijgen, W.J.J., Gosselink, R.J.A., Bruijnincx, P.C.A., 2016. New insights into the structure and composition of

technical lignins: A comparative characterisation study. Green Chem. 18, 2651–2665. https://doi.org/10.1039/c5gc03043a

Gierer, J., Pettersson, I., 1977a. Studies on the condensation of lignins in alkaline media. Part II. The formation of stilbene and arylcoumaran structures through neighbouring group participation reactions. Can. J. Chem. 55, 593–599. https://doi.org/10.1139/v77-084

González, G., Salvadó, J., Montané, D., 2004. Reactions of vanillic acid in sub- and supercritical water. J. Supercrit. Fluids 31, 57–66. https://doi.org/10.1016/j.supflu.2003.09.015

Heitner, C., Dimmel, D., Schmidt, J. (Eds.), 2016. Lignin and Lignans Advances in Chemistry. CRC Press. ISBN 9781574444865

Hemmilä, V., Hosseinpourpia, R., Adamopoulos, S., Eceiza, A., 2020. Characterization of Wood-based Industrial Biorefinery Lignosulfonates and Supercritical Water Hydrolysis Lignin. Waste and Biomass Valorization 11, 5835–5845. https://doi.org/10.1007/s12649-019-00878-5

Holladay, J.E., White, J.F., Bozell, J.J., Johnson, D., 2007. Top Value-Added Chemicals from Biomass - Volume II—Results of Screening for Potential Candidates from Biorefinery Lignin. Pacific Northwest National Laboratory. https://doi.org/10.2172/921839.

Jiang, W., Lyu, G., Wu, S., Lucia, L.A., Yang, G., Liu, Y., 2016. Supercritical Water-induced Lignin Decomposition Reactions: A Structural and Quantitative Study. BioResources 11. https://doi.org/10.15376/biores.11.3.5660-5675

Komatsu, T., Yokoyama, T., 2021. Revisiting the condensation reaction of lignin in alkaline pulping with quantitativity part I: the simplest condensation between vanillyl alcohol and creosol under soda cooking conditions. J. Wood Sci. 67, 45. https://doi.org/10.1186/s10086-021-01978-4

Lancefield, C.S., Wienk, H.L.J., Boelens, R., Weckhuysen, B.M., Bruijnincx, P.C.A., 2018. Identification of a diagnostic structural motif reveals a new reaction intermediate and condensation pathway in kraft lignin formation. Chem. Sci. 9, 6348–6360. https://doi.org/10.1039/C8SC02000K

Liu, C., Deng, Y., Wu, S., Mou, H., Liang, J., Lei, M., 2016. Study on the pyrolysis mechanism of three guaiacyl-type lignin monomeric model compounds. J. Anal. Appl. Pyrolysis 118, 123–129. https://doi.org/10.1016/j.jaap.2016.01.007

Mboowa, D., 2021. A review of the traditional pulping methods and the recent improvements in the pulping processes. Biomass Convers. Biorefinery. https://doi.org/10.1007/s13399-020-01243-6

Okuda, K., Man, X., Umetsu, M., Takami, S., Adschiri, T., 2004a. Efficient conversion of lignin into single chemical species by solvothermal reaction in water-p-cresol solvent. J. Phys. Condens. Matter 16. https://doi.org/10.1088/0953-8984/16/14/045

Okuda, K., Ohara, S., Umetsu, M., Takami, S., Adschiri, T., 2008. Disassembly of lignin and chemical recovery in supercritical water and p-cresol mixture. Studies on lignin model compounds. Bioresour. Technol. 99, 1846–1852. https://doi.org/10.1016/j.biortech.2007.03.062

Okuda, K., Umetsu, M., Takami, S., Adschiri, T., 2004b. Disassembly of lignin and chemical recovery—rapid depolymerization of lignin without char formation in water–phenol mixtures. Fuel Process. Technol. 85, 803–813. https://doi.org/10.1016/j.fuproc.2003.11.027

Pang, B., Yang, S., Fang, W., Yuan, T.Q., Argyropoulos, D.S., Sun, R.C., 2017. Structure-property relationships for technical lignins for the production of lignin-phenol-formaldehyde resins. Ind. Crops Prod. 108, 316–326. https://doi.org/10.1016/j.indcrop.2017.07.009

Pérez, E., Tuck, C.O., 2018. Quantitative analysis of products from lignin depolymerisation in high-temperature water. Eur. Polym. J. 99, 38–48. https://doi.org/10.1016/j.eurpolymj.2017.11.053

Rinaldi, R., Jastrzebski, R., Clough, M.T., Ralph, J., Kennema, M., Bruijnincx, P.C.A., Weckhuysen, B.M., 2016. Paving the Way for Lignin Valorisation: Recent Advances in Bioengineering, Biorefining and Catalysis. Angew. Chemie - Int. Ed. 55, 8164–8215. https://doi.org/10.1002/anie.201510351

Saisu, M., Sato, T., Watanabe, M., Adschiri, T., Arai, K., 2003. Conversion of Lignin with Supercritical Water−Phenol Mixtures. Energy & Fuels 17, 922–928. https://doi.org/10.1021/ef0202844

Wahyudiono, Sasaki, M., Goto, M., 2008. Recovery of phenolic compounds through the decomposition of lignin in near and supercritical water. Chem. Eng. Process. Process Intensif. 47, 1609–1619. https://doi.org/10.1016/j.cep.2007.09.001

Wenger, J., Haas, V., Stern, T., 2020. Why Can We Make Anything from Lignin Except Money? Towards a Broader Economic Perspective in Lignin Research. Curr. For. Reports 6, 294–308. https://doi.org/10.1007/s40725-020-00126-3

Xu, C., Arancon, R.A.D., Labidi, J., Luque, R., 2014. Lignin depolymerisation strategies: Towards valuable chemicals and fuels. Chem. Soc. Rev. 43, 7485–7500. https://doi.org/10.1039/c4cs00235k

Yelle, D.J., Ralph, J., 2016. Characterizing phenol–formaldehyde adhesive cure chemistry within the wood cell wall. Int. J. Adhes. Adhes. 70, 26–36. https://doi.org/10.1016/j.ijadhadh.2016.05.002

Yong, T.L.-K., Matsumura, Y., 2012. Reaction Kinetics of the Lignin Conversion in Supercritical Water. Ind. Eng. Chem. Res. 51, 11975–11988. https://doi.org/10.1021/ie300921d

Chapter 3.

Interfacial tension of liquid water in a pressurized nitrogen atmosphere and of liquid water in its saturated vapor – measured for temperatures up to 350 °C

The interfacial tension of water was measured in two systems: liquid/vapor water (further in the text as water/water system) following the saturation line and liquid in a pressurized nitrogen atmosphere (water/nitrogen system). The applied measurement technique used was the pendant drop method as an adequate method for measurements of the interfacial tension at elevated temperature and pressure. Interfacial tension of the water/nitrogen system was investigated at 10, 15 and 18 MPa and up to the temperatures of 325 °C. For the water/water system the temperature was up to 350 °C, close to the critical temperature of water. The equation of Macleod-Sugden was used to describe the measured interfacial tensions of the water/nitrogen system, as well as the water/water system. The equation is hereby in good agreement with the measurement results, showing an AAD of 4.97 % for the water/nitrogen system and 3.02 % for the water/water system. The obtained experimental results are in good agreement with comparable literature data.

Introduction

This work is dedicated to the measurement of interfacial tension (IFT) of water in two systems: liquid water in its saturated vapor (water/water) following the saturation line and of liquid water in a pressurized nitrogen atmosphere (water/nitrogen).

According to Patek et al. (Pátek et al., 2016) there are 211 data sets regarding water IFT values in the archival literature, wherein different measurement methods are used. The most applied technique is the capillary-rise method, followed by the maximum bubble pressure. The technique applied in this work is the pendant drop method. Patek et al. point further out, that many authors of the considered data do not provide necessary information about their measurements, such as details regarding the experimental setup. Most data points were furthermore acquired for moderate temperatures, while IFT data above the atmospheric boiling point of water (100 °C) are scarce. The data sets of major relevance regarding the comparison of the here acquired data are given in Table 8. In these publications the capillary rise method was employed.

Table 8. IFT data for temperatures high than the atmospheric boiling temperature (Pátek et al., 2016); all measurements performed by capillary rise method, no uncertainty given.

author(s)	**Temperature range** **T / °C**
Ramsay and Shields (Ramsay and Shields, 1893)	0 – 140
Sohet (Sohet, 1898)	15 – 150.5
Voljak (Voljak, 1950)	0 – 370

Heiks et al.(Heiks et al., 1954)	101.8 – 224.4
Vargaftik et al. (Vargaftik et al., 1973)	0.4 – 370.39

There are only a few, clearly labelled data sets for the IFT of liquid water in a pressurized nitrogen atmosphere, of which the information is provided in Table 9. Leonard et al. as well as Grenoble and Trabelsi (Grenoble and Trabelsi, 2021; Leonard et al., 2018) measured further IFT for the water/nitrogen system. The data is however not accessible in tabular form and is thus not considered in Table 9.

Table 9. IFT data for liquid water in pressurized nitrogen atmosphere (water/nitrogen system); all measurements performed by the pendant drop method

author(s)	**Temperature range T / K**	**Pressure range MPa**
Chow et al. (Chow et al., 2016)	25 – 175	2 - 40
Wiegand and Franck (Wiegand and Franck, 1994)	25 – 300	0.1 - 280
Yan et al. (Yan et al., 2001)	25 – 100	1 - 30
Yiling et al. (Yiling, T., 1997)	25 – 200	0.1 - 100

In the following work new IFT data are provided at high temperature conditions and to compare furthermore the influence of the surrounding atmosphere, as in many works that report IFT data of water, additional components such as nitrogen, air, argon or helium are present inside the measurement system (Pátek et al., 2016). For this reason, we compare the IFT values of water in a system with its saturated vapor, as well as in the atmosphere with pressurized nitrogen. The equation of Macleod-Sugden was correlated to the obtained experimental results for both discussed systems. To our

knowledge this is the first work to report IFT pendant-drop measurements at temperatures above the atmospheric boiling temperature in the water/water system.

Experimental section

Materials

The water used in the experiments is type I ultrapure, as defined by the American Society for Testing and Materials (ASTM). The nitrogen was purchased from Linde in the purity of 5.0 (>99.999 $\%_v$).

Methods

The interfacial tension was measured by the pendant drop method using a high-pressure visual cell (HPVC) purchased from Eurotechnica GmbH (Bargteheide, Germany). This cell is already described in the introduction part, however modification of the cell was necessary in order to measure interfacial tension using the pendant drop method. The new scheme of HPVC with modification and coupled mini-dosing device can be seen in Figure 31.

The drop was recorded using a CCD camera and the evaluation was carried out by a drop-shape analysis software that is commercially available from Krüss (Hamburg, Germany). The program adopts a theoretical drop profile according to the Young-Laplace equation (given in eqn. (24)), which describes the curvature of the surface of a liquid drop (Knauer et al., 2017). Detailed theoretical background about the pendant drop technique can be found elsewhere (Song and Springer, 1996).

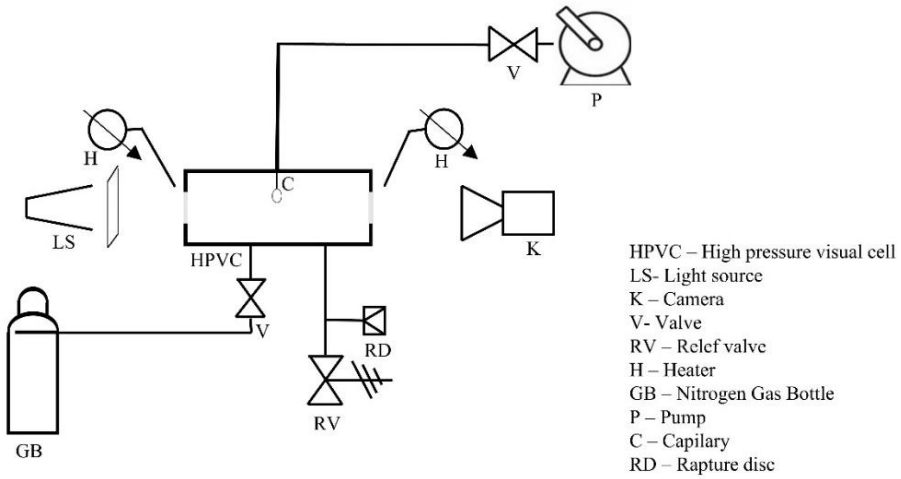

Figure 31. Scheme of the HPVC applied for the IFT pendant drop experiments

In eqn. (24), γ is the interfacial tension, $\Delta\rho$ is the density gradient between the respective saturated liquid and vapor phases (see eqn. (25)), g is the gravitational acceleration, h is the distance from the apex and R_1 as well as R_2 are the radii of the curvature. For the water/nitrogen system the saturated mixture densities were obtained using the Perturbed Chain-Statistical Associating Fluid Theory (PC-SAFT) equation of state, while for the water/water system the densities of pure liquid and vapor water at saturation from NIST are used. More details can be found in the results section.

$$\gamma = \frac{\Delta\rho^s g h}{(\frac{1}{R_1} + \frac{1}{R_2})} \qquad (24)$$

$$\Delta\rho = \rho^{liq} - \rho^{vap} \qquad (25)$$

Relating the classical Young-Laplace equation to the hydrostatic pressure between the point *P* and the apex shown in Figure 32, one obtains:

$$\frac{1}{R_1}+\frac{1}{R_2}=\frac{2}{R_0}-\frac{\Delta\rho^s\cdot g\cdot h}{\gamma} \qquad (26)$$

This equation combines the radius of curvature R_1 and R_2 with the radius at the apex R_0 (see Figure 32), $\Delta\rho^s$, g, γ and the height difference (h) between the apex and the point P. Replacing eqn. (26) by a set of three first-order differential equations to apply it to a non-steady state for the interfacial site *X* as well as *Z* and turning angle ϕ of the interface as a function of the arc length *s* (s comes from the variable change where $\phi=\frac{dx}{ds}$), leads to (Sutjiadi-Sia et al., 2007) eqn. (27):

$$\frac{d^2Z}{dX^2}+\frac{1}{X}\cdot\frac{dZ}{dX}\cdot\left[1+\left(\frac{dZ}{dX}\right)^2\right]=(2-B\cdot Z)\cdot\left[1+\left(\frac{dZ}{dX}\right)^2\right]^{3/2} \qquad (27)$$

Two dimensionless variables are introduced:

- $X=\frac{x}{R_0}$
- $Z=\frac{z}{R_0}$

The capillary constant *B* is defined by material properties, the gravity constant *g* and the drop radius R_0 (see eqn. (28)):

$$B=\frac{\Delta\rho\cdot g\cdot R_0^2}{\sigma} \qquad (28)$$

The shape of a drop is mathematically fitted and the eqn. (27) is solved by using parameters including the location of the apex (X_0, Z_0), the radius of curvature at the apex R_0 and the capillarity constant *B*.

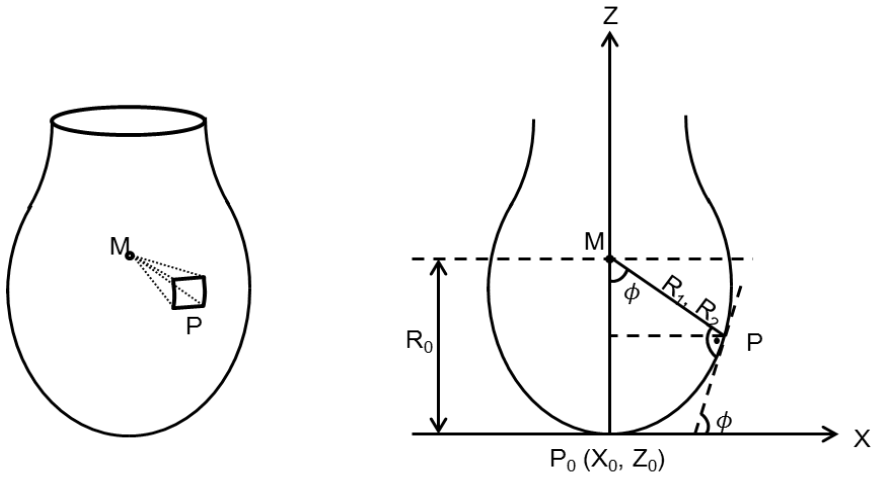

Figure 32. Pendant drop (left) and the geometry of a two dimensionally projected pendant drop (right). Redrawn (Sutjiadi-Sia et al., 2007)

The drop was generated with a mini dosing device developed by Eurotechnica GmbH, that consists of a piston pump, valve, 1/16 capillary tube. The capillary is placed through one opening inside the HPVC. The second opening is used for water or nitrogen supply and the third one is used for a safety burst disc and relief valve. The cell has two sapphire windows located in opposition to each other, so that optical access is provided. The light source is placed in front of one window and the camera is placed in front of the second. The design of the cell allows measurements at pressures up to 30 MPa and temperatures of 500 °C (see also Figure 9 in the introduction part).

The measurement procedure for water/nitrogen is described as follows: the cell is purged with nitrogen and preheated to the desired temperature. When the desired temperature is reached the cell is pressurized with nitrogen to the operating pressure. Once the temperature and pressure become stable, a drop is generated inside the cell using a mini-dosing device. For each pressure-temperature combination measurements were done at least in triplicate. Experiments were performed at pressures of 10, 15 and 18 MPa and temperatures ranging from 50 °C up to 325 °C.

For the water/water system the procedure used was slightly different. Due to the difference in the temperature between the internal and external sides of the sapphire windows, water condensed on the internal side and thus interrupted the measurements. To suppress water condensation, both windows were constantly heated with external heaters. Once the temperature and pressure conditions were stabilized, the drop was generated inside the cell. For the water/water system the temperatures range from 150 °C, up to 350 °C.

Results and discussion

Applied equations and correlations

The saturated densities for the water/water system were obtained from the NIST chemistry Webbook, where the correlations of Wagner and Pruß are used (P.J. Linstrom and W.G. Mallard, n.d.; Wagner and Pruß, 2002). The saturated mixture densities of the water/nitrogen system were however obtained by the Pert PC-SAFT (see eqn. (29)), which is described briefly in the following.

$$Z = 1 + Z^{hc} + Z^{disp} + Z^{assoc} \qquad (29)$$

The PC-SAFT equation of state is expressed by the compressibility factor Z, which is computed by the sum of separate contributions according to Gross and Sadowski (Gross and Sadowski, 2002, 2001). In eqn. (29) Z^{hc} is the hard-chain term, Z^{disp} the dispersion term and Z^{assoc} the contribution term resulting from association. Nitrogen, as a non-associating molecule, is only defined by the number of segments per chain m, the segment diameter σ and the depth of the pair potential ε/k_b, with k_b being the Boltzmann constant.

For water, the 2B scheme of Huang and Radosz (Huang and Radosz, 1990) was used, wherein two further pure-component parameters are necessary for the associating interactions of the molecule: $\varepsilon^{A_iB_i}/k_b$ as the association energy and $\kappa^{A_iB_i}$ as the effective association volume between association sites A of molecule i and B of molecule i. The mixing rules applied in the PC-SAFT equation are given in eqn. (30) and (31). Therein k_{ij} is a single binary interaction parameter that is however set to 0 for the system nitrogen/water, making it a predictive model. The relevant PC-SAFT parameters are given in Table 10 (Martín et al., 2009).

$$\sigma_{ij} = \frac{1}{2}(\sigma_i + \sigma_j) \qquad (30)$$

$$\varepsilon_{ij} = \left(\varepsilon_i \cdot \varepsilon_j\right)^{0.5} \cdot (1 - k_{ij}) \qquad (31)$$

Table 10. PC-SAFT parameters for the considered binary system water/nitrogen (Gross and Sadowski, 2002, 2001)

compound	m	$\sigma/10^{-10}\mathrm{m}$	$\varepsilon/k_b/\ \mathrm{K}$	$\varepsilon^{A_iB_i}/k_b/\ \mathrm{K}$	$\kappa^{A_iB_i}$
water	1.0953	2.8898	365.96	2515.7	0.03487
nitrogen	1.2053	3.3130	90.96	-	-

The saturated pure and mixture densities are relevant for obtaining both the experimental values of the interfacial tension by eqn. (24), as well as for the correlation values coming from the Macleod-Sugden equation. In the case of a system consisting of a single component (water/water system; see eqn. (32)), the Macleod-Sugden correlation is fitted by a single temperature-independent adjustable parameter $[P]$, which is named parachor in the literature (Poling et al., 2001). Inside the Macleod-Sugden correlation, the interfacial tension is expressed in the unit $\mathrm{mN \cdot m^{-1}}$ (equals $\mathrm{dyne \cdot cm^{-1}}$).

Considering a binary mixture as the experimental system (water/nitrogen; see eqn. (33)), $[P]$ are calculated by the mixing rules given in eqn. (34) and (35), wherein x_i are liquid phase and y_i are vapor phase mole fractions. The binary Parachor is obtained by eqn. (36). Therein λ_{ij} is an interaction coefficient, that is however set to 1 in this study. The exponent of 4 in eqn. (33) is recommended by Weinaug-Katz (Weinaug, Charles F., 1943). Different exponents can be introduced for other binary systems (Poling et al., 2001). The pure component parachors are given in Table 11. $[P_{water}]$ was obtained by fitting the Macleod-Sugden correlation towards our experimental interfacial tensions of water/water. $[P_{Nitrogen}]$ was however considered

as a fit parameter in eqn. (36), in order to obtain an accurate description of the experimental interfacial tensions of the nitrogen/water system by eqn. (33). $[P_{Nitrogen}]$ could only be obtained from a fit towards literature interfacial tensions at conditions below its critical point ($T_{crit} = -145.9$ °C K, $p_{crit} = 3.4$ MPa). However, this parameter is not applicable since pure nitrogen is supercritical at the here considered experimental conditions and does thus not have an interfacial tension.

$$\gamma = \left[[P] \cdot (\rho^{liq,s} - \rho^{vap,s})\right]^4 \qquad (32)$$

$$\gamma_m = \left[\left[P_m^{liq}\right]\rho_m^{liq,s} - [P_m^{vap}]\rho_m^{vap,s}\right]^4 \qquad (33)$$

$$[P_m^{liq}] = \sum_{i=1}^{N}\sum_{j=1}^{N} x_i x_j [P_{ij}] \qquad (34)$$

$$[P_m^{vap}] = \sum_{i=1}^{N}\sum_{j=1}^{N} y_i y_j [P_{ij}] \qquad (35)$$

$$[P_{ij}] = \lambda_{ij}\frac{[P_i] + [P_j]}{2} \qquad (36)$$

Table 11. Pure component parachors of water and nitrogen

component	**[P]**
water	$2.8608 \cdot 10^{-3}$
nitrogen	$1.9377 \cdot 10^{-4}$

The difference between the experimental interfacial tensions and those stemming from the Macleod-Sugden correlation is quantified by the average absolute deviation (*AAD*), given in eqn. (37). The results are given in Table 12.

$$AAD = \frac{1}{N}\sum_{i=1}^{N}\left|\frac{\gamma_i^{exp} - \gamma_i^{corr}}{\gamma_i^{exp}}\right| \cdot 100\ \% \qquad (37)$$

Table 12. Average absolute deviations between Macleod-Sugden correlation and experimental data

system	**AAD/%**
water/water	3.02
water/nitrogen	4.97

Experimental results

The obtained interfacial tensions for the water/water system are given in Table 13 and for the water/nitrogen system in Table 14. For the water/water system the experimental results are compared to the literature data obtained experimentally (summarized in Table 8) in Figure 33, from which good agreement, especially at higher temperatures, can be observed.

Table 13. Interfacial tensions of water/water system

***T* / °C**	***γ*/ 10^{-3} N m^{-1}**	***st.dev.***
150	45.28	0.12
175	40.67	0.10

200	35.85	0.06
225	29.88	0.09
250	24.76	0.12
275	20.22	0.13
300	13.86	0.21
325	7.95	0.00
350	2.89	0.10

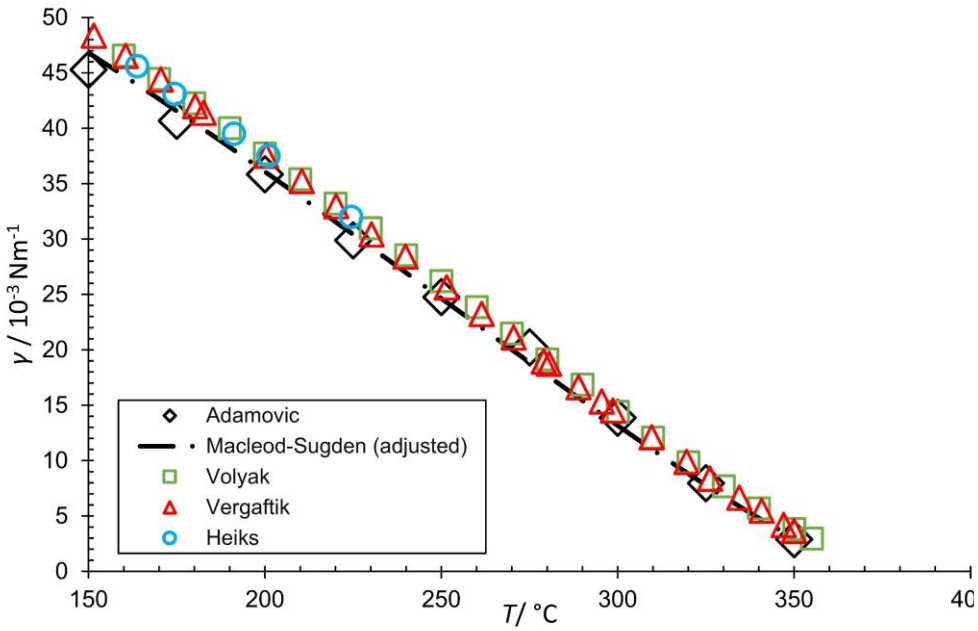

Figure 33. Interfacial tensions for the water/water system and comparison to literature data (Heiks et al., 1954; Vargaftik, N. B.; Voljak, L. D.; Volkov, 1973; Voljak, 1950) (compare Table 8)

Absolute deviations (AD for $N = 1$ in eqn. (38)) between our experimental interfacial tensions and comparable literature values for temperatures of 423.15 K to 573.15 K range from 7.40 % to 3.89 considering the data of Voljak et al. (Voljak,

1950), and from 6.78 % to 4.75 % considering the values of Vergaftik et al. (Vargaftik et al., 1983). The deviations close to the critical point are significantly higher, regarding the small magnitude of interfacial tension. However, the available literature values deviate from each other as well.

Table 14. Interfacial tensions of water/nitrogen system

***P*/MPa**	***T* / °C**	**$\Delta\rho$/ Kg m^{-1}**	**γ_{exp}/ 10^{-3} N m^{-1}**	***st.dev.***
10.06	50	884.93	61.24	0.20
10.02	100	869.77	55.26	0.51
9.94	150	848.06	49.02	0.46
10.10	200	818.79	40.64	0.55
10.04	250	782.56	31.42	0.14
10.07	300	731.84	21.92	0.97
15.00	50	837.42	59.77	0.63
15.14	150	811.63	46.85	0.62
15.12	200	787.46	38.59	1.01
15.06	250	753.88	30.69	0.78
15.09	325	669.43	15.46	0.80
17.96	50	810.52	58.43	0.17
17.98	100	806.65	51.78	0.34
18.01	150	792.24	45.34	0.32
18.04	200	770.06	36.56	0.68
18.01	250	737.71	29.91	0.52
18.02	300	689.11	18.76	0.21
17.98	325	654.47	13.81	0.13

For water/nitrogen system data are compared with available literature experimental data in Figure 34. Good agreement is found as the absolute deviations between our experimental interfacial tensions and data from Chow, Yan and Yiling is 0.62 %, 1.85 % and 2.07 % respectively, for the same measurement point (10 MPa,

373 K). From Figure 34 slight decrease of interfacial tension with pressure and temperature increment can be seen, as expected.

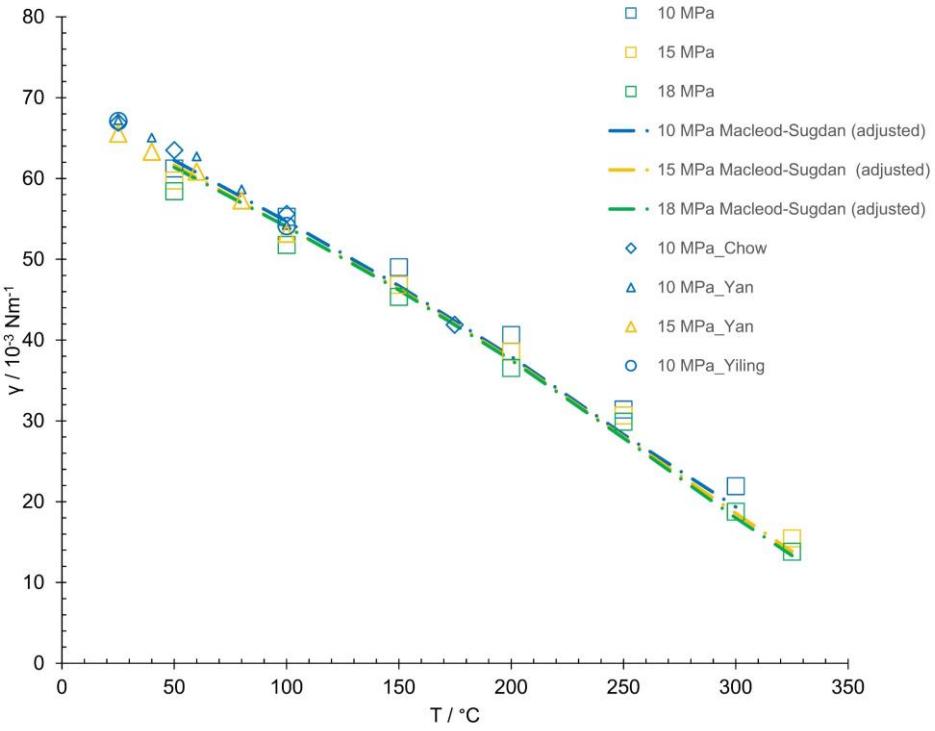

Figure 34. Interfacial tensions of water/nitrogen system and comparable literature data(Yan et al., 2001; Yi-Ling et al., 1997; Yiling, T., Yanfan, X., Hongxu, Z., Xi-Jing, D., Xiao-Wen, R., & Feng-Cai, 1997) (compare Table 9)

As already mentioned in the introduction part in some of the experimental sets that report interfacial tension of water additional inert atmospheres is used, such as nitrogen. Comparison of experimental data obtained in this study in water/water system and water/nitrogen system is presented in Figure 35. Good agreement of interfacial tension of water in water/water system compared to water nitrogen system could be observed under 18 MPa and temperature up to 200 °C: However, at higher temperature significant deviations could be observed. This is expected as the

solubility of nitrogen in water changes significantly at higher temperatures and thus the densities of the liquid and vapor phase taken in the calculation for the final interfacial tension value.

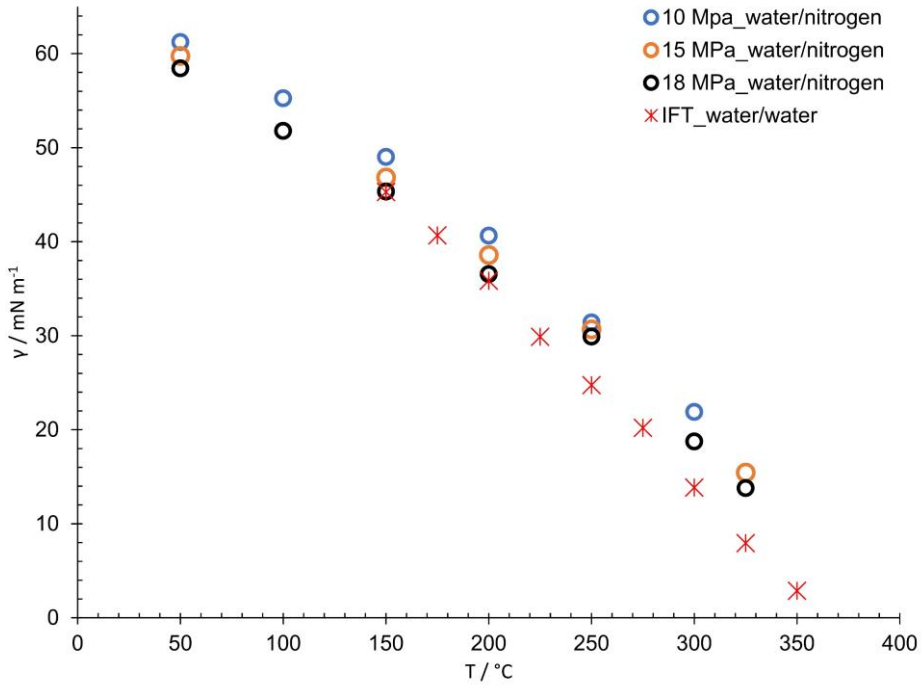

Figure 35. Comparison of experimental values obtained in this work for water/water and water/nitrogen system

Conclusion

Interfacial tensions have been measured for which data at elevated temperatures are scarce in the archival literature. Good agreement in comparison with available literature data was found, as maximum absolute deviation was 7.40 % and 2.07 % for water/water and water/ nitrogen system, respectively. The Macleod-Sugden equation for a single component was used to describe water/water experimental data while the

equation for the mixture was used to describe the water/nitrogen system. AAD of 4.97 % for the water/nitrogen system and 3.02 % for the water/water system shows that the Macleod-Sugden equation is in good agreement with the measurement results. Comparing the values of interfacial tension of water obtained in the water/water system and water/nitrogen system under 18 MPa and up to 200 °C good agreement is observed. However, at temperatures above 200 °C significant deviation of interfacial tension of water in those two systems is observed due to the change of nitrogen solubility.

References:

Chow, Y.T.F., Maitland, G.C., Trusler, J.P.M., 2016. Interfacial tensions of the (CO 2 + N 2 + H 2 O) system at temperatures of (298 to 448) K and pressures up to 40 MPa. J. Chem. Thermodyn. 93, 392–403. https://doi.org/10.1016/j.jct.2015.08.006

Grenoble, Z., Trabelsi, S., 2021. Interfacial Tension Measured at Nitrogen–Liquid and Liquid–Liquid Interfaces Using Model Microemulsions at High-Pressure and High-Temperature Conditions. Energy & Fuels 35, 13055–13064. https://doi.org/10.1021/acs.energyfuels.1c01358

Gross, J., Sadowski, G., 2002. Application of the Perturbed-Chain SAFT Equation of State to Associating Systems. Ind. Eng. Chem. Res. 41, 5510–5515. https://doi.org/10.1021/ie010954d

Gross, J., Sadowski, G., 2001. Perturbed-Chain SAFT: An Equation of State Based on a Perturbation Theory for Chain Molecules. Ind. Eng. Chem. Res. 40, 1244–1260. https://doi.org/10.1021/ie0003887

Heiks, J.R., Barnett, M.K., Jones, L. V., Orban, E., 1954. The Density, Surface Tension and Viscosity of Deuterium Oxide at Elevated Temperatures. J. Phys. Chem. 58, 488–491. https://doi.org/10.1021/j150516a010

Huang, S.H., Radosz, M., 1990. Equation of state for small, large, polydisperse, and associating molecules. Ind. Eng. Chem. Res. 29, 2284–2294. https://doi.org/10.1021/ie00107a014

Knauer, S., Schenk, M.R., Köddermann, T., Reith, D., Jaeger, P., 2017. Interfacial Tension and Related Properties of Ionic Liquids in CH_4 and CO_2 at Elevated Pressures: Experimental Data and Molecular Dynamics Simulation. J. Chem. Eng. Data 62, 2234–2243. https://doi.org/10.1021/acs.jced.6b00751

Leonard, C., Ferrasse, J.-H., Boutin, O., Lefevre, S., Viand, A., 2018. Measurements and correlations for gas liquid surface tension at high pressure and high temperature. AIChE J. 64, 4110–4117. https://doi.org/10.1002/aic.16216

Martín, Á., Pham, H.M., Kilzer, A., Kareth, S., Weidner, E., 2009. Phase equilibria of carbon dioxide + poly ethylene glycol + water mixtures at high pressure: Measurements and modelling. Fluid Phase Equilib. 286, 162–169. https://doi.org/10.1016/j.fluid.2009.08.010

P.J. Linstrom and W.G. Mallard, E., n.d. NIST Chemistry WebBook, NIST Standard Reference Database Number 69. https://doi.org/10.18434/T4D303

Pátek, J., Součková, M., Klomfar, J., 2016. Generation of Recommendable Values for the Surface Tension of Water Using a Nonparametric Regression. J. Chem. Eng. Data 61, 928–935. https://doi.org/10.1021/acs.jced.5b00776

Poling, B. E., Prausnitz, J. M., O´Connell, J. P. 2001. The properties of gases and liquids. McGraw Hill. Vol. 5, 693–696.

Ramsay, W., Shields, J., 1893. LXXXI.—The molecular complexity of liquids. J. Chem. Soc., Trans. 63, 1089–1109. https://doi.org/10.1039/CT8936301089

Sohet, A., 1898. Variations des hauteurs capillaires et des tensions superficielles de l'eau de l'alcool et des solutions d'eau et d'alcool avec la tempˆerature. Mem. Soc. R. Sci. Liege 20, 1–56.

Song, B., Springer, J., 1996. Determination of Interfacial Tension from the Profile of a Pendant Drop Using Computer-Aided Image Processing. J. Colloid Interface Sci. 184, 64–76. https://doi.org/10.1006/jcis.1996.0597

Sutjiadi-Sia, Y., Marckmann, H., Eggers, R., Holzknecht, C., Kabelac, S., 2007. Zum Einfluss von in Flüssigkeiten unter Druck gelösten Gasen auf Grenzflächenspannungen und Benetzungseigenschaften. Forsch. im Ingenieurwes. 71, 29–45. https://doi.org/10.1007/s10010-006-0042-4

Vargaftik, N. B.; Voljak, L. D.; Volkov, B.N., 1973. Issledovanije poverchnostnogo natjazenia pri temperaturach, blizkich k krititcheskoj. Teploenergetika 8, 80–84.

Vargaftik, N.B., Volkov, B.N., Voljak, L.D., 1983. International Tables of the Surface Tension of Water. J. Phys. Chem. Ref. Data 12, 817–820. https://doi.org/10.1063/1.555688

Voljak, L.D., 1950. Issledovanie temperaturnoj zavisimosti poverchnostnogo natjazhenija vody. Dokl. Akad. Nauk SSSR 1–20.

Wagner, W., Pruß, A., 2002. The IAPWS Formulation 1995 for the Thermodynamic Properties of Ordinary Water Substance for General and Scientific Use. J. Phys. Chem. Ref. Data 31, 387–535. https://doi.org/10.1063/1.1461829

Weinaug, Charles F., and Katz, D.L., 1943. Surface tensions of methane-propane mixtures. Ind. Eng. Chem. 35, 239–246.

Wiegand, G., Franck, E.U., 1994. Interfacial tension between water and non-polar fluids up to 473 K and 2800 bar. Berichte der Bunsengesellschaft für Phys. Chemie 98, 809–817. https://doi.org/10.1002/bbpc.19940980608

Yan, W., Zhao, G.-Y., Chen, G.-J., Guo, T.-M., 2001. Interfacial Tension of (Methane + Nitrogen) + Water and (Carbon Dioxide + Nitrogen) + Water Systems. J. Chem. Eng. Data 46, 1544–1548. https://doi.org/10.1021/je0101505

Yi-Ling, T., Yan-Fan, X., Hong-Xu, Z., Xi-Jing, D., Xiao-Wen, R., Feng-Cai, Z., 1997. Interfacial Tensions between Water and Non-polar Fluids at High Pressures and High Temperatures. Acta Physico-Chimica Sin. https://doi.org/10.3866/pku.whxb19970120

Yiling, T., Yanfan, X., Hongxu, Z., Xi-Jing, D., Xiao-Wen, R., & Feng-Cai, Z., 1997. Interfacial tensions between water and non-polar fluids at high pressures and high temperatures. Acta Physico-Chimica Sin. 13, 89–95.

Conclusions and future work

Conclusions

This thesis is a contribution to the development of biorefineries using supercritical water technology. This contribution was made on one side through the valorization of high lignin content biomass such as defatted grape seed and on the other side through a better understanding of lignin repolymerisation reaction in order to improve the production of aromatics from lignin. This thesis also presents the data of interfacial tension of water in two systems: water/water system and water/nitrogen system. The presented results for water interfacial tension in water/water were not previously reported using pendant drop measurements in the range of pressure and temperature investigated here. The pendant drop technique is an adequate methodology for interfacial tension measurements under high pressure and temperature and this work also provide detailed experimental procedure and solution to the possible problems during the measurement.

As already discussed through this thesis lignin contributes significantly to biomass recalcitrance and thus to the difficulties of biomass valorization. The first chapter of this thesis proves the ability of supercritical water to fractionate and hydrolyze defatted grape seed biomass, as an example of high lignin content biomass. The main conclusions could be summarized as:

After processing biomass in supercritical water, a sample with liquid and solid phases is obtained.

1. The maximum yield of sugars recovered in the liquid phase reaches 61 % after 0.27 s. However, the yield of sugars in the liquid phase reminds high (56 %) even after the longest reaction time of 1s, which is unexpected compared to the hydrolysis

results of biomasses with low content of insoluble lignin as are sugar beet pulp and wheat bran where the yield of sugars rapidly decreases after reaching maximum point. This can be explained by the high amount of lignin and other polyphenols as lignin could act as a barrier for supercritical water to access carbohydrate fraction, leading to their slower consumption.

2. The solid part of the sample is enriched in polyaromatic after the supercritical water process. The total extraction of carbohydrates from solid could not be obtained as after 1s still 10 % of carbohydrates remind in a solid product. Detailed 2D-NMR analysis shows that this product consists of a complex mixture that partly belongs to lignin, with a certain amount of chemically bonded carbohydrates, residual lipophilic extract and flavonoids.

3. Comparison of dioxane extract obtained from the solid residue after supercritical water process with milled wood lignin isolated from grape seeds indicates very subtle cleavage of main native lignin moieties, such as β-O-4. The analysis also shows that the guaiacyl unit is the main lignin unit in grape seeds, with a minor amount of *p*- hydroxyphenyl unit, while syringyl unit is absent. Preservation of the main lignin linkages can be very beneficial in the further valorization of this lignin residue.

The main conclusions of the study on the better understanding of lignin repolymerization reactions could be summarised as:

4. Lignin model compounds tend to react among each other in supercritical water, as shown by their high conversion rate. Conversion rate changes when sulfonated kraft lignin is presented in the reactor indicating the reaction of monomers with lignin fragments.

5. Another indicator of the tendency of model compounds to react with sulfonated kraft lignin is the higher amount of total solid in the reaction of sulfonated kraft lignin and model compounds mixture compared to the reaction of just sulfonated kraft lignin in supercritical water. GPC analysis confirmed that samples obtained in the reaction of sulfonated kraft lignin and model compounds mixture have peaks at longer reaction time compared to sample obtained just with sulfonated kraft lignin or just with model compounds.

6. The 2D-NMR analysis confirms the presence of diarylmethanes structures in the solid residue of each sample, indicating that those structures could be responsible for the repolymerisation reaction. In the solid residue of sulfonated kraft lignin formation of o-o´ and o-p´ diarylmethane structures are found, while o-p´ and p-p´ diarylmethane structures are found in the solid sample of model compounds. In the case of the solid residue obtained with the mixture of sulfonated kraft lignin and model compounds, all three diarylmethane structures are present. This indicates that the formation of these structures contributes to the repolymerisation reaction but the mechanism of their formation is different for sulfonated kraft lignin and model compounds.

6. The main reaction that happened on the structure of sulfonated kraft lignin during the supercritical water process in de-sulphonation.

7. No big changes are determined in the structure of Indulin lignin in its solid residue after the supercritical water process, indicating that the main reaction happens in the fraction of low molecular products.

The absence of an available detailed explanation on the measurements of interfacial tension of water under high pressure and temperature conditions is the

primary reason for measurements performed in Chapter 3 of the thesis. Interfacial tension of the water was measured in the liquid water and its saturated vapor (water/water system) and liquid water in pressurized nitrogen atmosphere (water/nitrogen system). Available data in the literature under high pressure and temperature conditions for measurements of water/water system are obtained using the capillary rise method, while this work is the first to report measurements using the pendant drop method. Also, in some works that report water interfacial tension more than water is used in the measurement, i.e. nitrogen or some other inert gas is used in addition. For this reason, measurements of the interfacial tension are performed in a nitrogen atmosphere as well. The main conclusions could be summarised as:

8. The result of the water/water system shows good agreement with literature data with a maximum absolute deviation of 7. 40 %. For the case of the water/nitrogen system, good agreement with reported experimental data in the literature is also obtained with a maximum absolute deviation of 2.07 %.

9. The experimental data obtained in our study are further correlated using the Macleod-Sugden equation for pure components in the case of water/water system and for mixture in the case of water/nitrogen system. The equation is in good agreement with measurements results, as AAD of 4.97 % and 3.02 % was calculated for water/nitrogen and water/water system respectively.

10. The increase of the nitrogen pressure and temperature decrease the interfacial tension of water, as could be expected.

11. Values of interfacial tension of water obtained in the water/water system are in good agreement with values obtained in the water/nitrogen system under 18 MPa and up to 200 °C. A significant deviation of interfacial tension of water in those

two systems is observed as the temperature rises above 200 °C; due to the change of nitrogen solubility.

Future work

Analysis of the solid residues obtained during the processing of defatted grape seeds in supercritical water shows that lignin presented in defatted grape seeds is mainly guaiacyl type lignin but also that main native lignin moieties with ether bonds are mainly preserved during supercritical water treatment. One of the main factors that influence the potential of lignin to be depolymerized to aromatics is the amount of C-O bonds and level of condensation. As the nature of lignin is well preserved during the supercritical water process this indicates that solid obtained after hydrolysis of defatted grape seeds could be a potentially good candidate for depolymerization to aromatics, such as vanillin. In future work hydrolysis of the solid residue obtained after processing of defatted grape seeds in supercritical water is planned in order to prove its potential as a possible source for vanillin.

The result obtained in Chapter 2 shows that the main reaction happened mainly in the oil fraction of the product. Detailed analysis of the solid residue shows the presence of diarylethene structures as responsible for repolymerization reaction. However, to have a complete and better understanding of the repolymerization process future work is planned on detailed analysis of the oil fraction of the products and kinetical study of model compounds.

Knowledge of the surface properties of polymers is of great importance for determining their potential application. The future work is planted on the

measurement of the contact angle of commercial lignin polymers and lignin polymer obtained after the supercritical water process. This information could be furtherly used to improve the knowledge of lignin composites produced, and their compatibility for addition to other polymers to enhance their mechanical properties.

Resumen

Valorización de lignina mediante tecnologías en agua supercrítica

Resumen

Valorización de lignina mediante tecnologías en agua supercrítica

Los recursos limitados de los combustibles fósiles y las preocupaciones medioambientales derivadas de su uso exhaustivo nos obligan a buscar un enfoque sostenible para la producción y el uso de la energía. El desarrollo de biorrefinerías que utilicen la biomasa para la producción de combustibles y productos químicos es una alternativa sostenible a las refinerías de petróleo. En las que basamos nuestro desarrollo. La biomasa lignocelulósica es la más abundante y fácil de cultivar. Esta biomasa, compuesta por tres componentes principales, celulosa, hemicelulosa y lignina, podría ser una buena fuente de combustible y de una amplia gama de productos químicos. Sin embargo, para utilizar esta biomasa de forma eficaz y hacer que la biorrefinería sea viable y competitiva es necesario afrontar diferentes retos. Una de las tecnologías que puede hacer frente a estos retos es la que utiliza agua supercrítica (SCW) como disolvente y medio de reacción.

Uno de los retos que debemos resolver es la dificultad de fraccionar la biomasa en sus compuestos mayoritarios debido a su estructura compleja y rígida. La lignina aporta una limitación importante a la transferencia del disolvente y de los productos del fraccionamiento, aumentando con el contenido de lignina de la biomasa. En el primer capítulo de la tesis se estudia el fraccionamiento de la semilla de uva desengrasada en agua supercrítica a 380 °C, 26,0 MPa y tiempos de reacción entre 0,18 s a 1 s, biomasa con alto contenido en lignina. El estudio se orienta en la recuperación de azúcares y la caracterización detallada de la fase sólida restante enriquecida en poliaromáticos. Con un tiempo de reacción de 1 s, se hidrolizaron los

carbohidratos de la alimentación, recuperándose como productos de su hidrolisis en el efluente liquido el 56 %, y el 10 % de permaneció en la fase sólida. Se han caracterizado la lignina de madera molida, la extraída de la biomasa, y el extracto obtenido de la fase solida con dioxano para entender los principales cambios estructurales durante el proceso de reacción en SCW. La extracción con dioxano (80 %) de la fracción sólida obtenida produce una mezcla compleja de extractos lipofílicos, flavonoides y lignina con una cierta cantidad de carbohidratos químicamente ligados. El análisis con RMN 2D del extracto de dioxano muestra cambios sutiles en las cantidades de las principales moléculas de lignina (β-O-4', β-β' (resinol) y β-5 (fenilcumarano)). Este ligero cambio de las principales estructuras de la lignina es una característica importante de este subproducto libre de sulfuro.

Como la lignina es un subproducto de los procesos de biorrefinería, su valorización es una importante contribución para la implementación de biorrefinerias sostenibles. La despolimerización de la lignina es un reto para la obtención sostenible de aromáticos. Actualmente, no hay una solución técnica viable debido a la repolimerización que se produce con las tecnologías hidrotermales, o con otros disolventes que hidrolizan la lignina. En el capítulo 2 de la tesis, se estudia las reacciones de repolimerización, siguiendo la reactividad de los productos de despolimerización de la lignina entre sí y con la lignina. Se utilizó lignina kraft sulfonada (SKL), mientras que como productos de la despolimerización de la lignina se utilizaron cuatro compuestos modelo: vainillina, ácido vainillinico, alcohol vainillinicco y acetovainillona. Como referencia para entender la repolimerización de la SKL en SCW se utilizó indulina como lignina kraft con estructura conocida. Los espectros HSQC mostraron que la formación de estructuras de diarilmetano podría ser

responsable de la repolimerización y de la disminución del rendimiento de los productos monoméricos con el tiempo de reacción. Los fragmentos liberados de lignina con estructuras β-O-4 fenólicas libres y el producto monomérico alcohol vainíllinico están implicados en la formación de estructuras de o-o' y o-p' diarilmetano. Además, los resultados cuantitativos de HSQC indican que las reacciones de repolimerización se producen a través de polimerización cross-linked. Entender el proceso de repolimerización es crucial para el desarrollo de estrategias que permitan minimizarlo, y desarrollar un proceso sostenible para la producción de aromáticos.

Las propiedades del agua varían significativamente en un amplio rango de temperaturas y presiones. Por encima del punto crítico, la densidad de la fase liquida disminuye por efecto del aumento de la temperatura, mientras que la densidad de la fase vapor aumenta por efecto del aumento de la presión, y con el aumento simultaneo de la presión y temperatura se llega a una única fase denominada fase supercrítica o fluido supercrítico, en la que no existe ningún límite entre esta fase y la fase liquida o entre esta fase y la fase vapor. El capítulo 3 de la tesis sigue los comportamientos de las fases liquida/vapor cuando se llega a esta única fase.

La tensión interfacial del agua se midió en dos sistemas: agua líquida/vapor y agua/nitrógeno. Las mediciones se realizaron mediante el método de la gota colgante. En el sistema agua/agua las mediciones siguen la línea de saturación del agua hasta la temperatura de 350 °C, mientras que en el sistema agua/nitrógeno las mediciones se realizaron bajo la presión de 10 MPa, 15 MPa y 18 MPa, y la temperatura hasta 325 °C. Los datos experimentales se correlacionaron utilizando la ecuación de Macleod-Sugden. Se encontró una buena concordancia entre los resultados calculados y los

datos experimentales, mostrando un AAS del 4,97% para el sistema agua-nitrógeno y del 3,02% para el sistema agua-agua. La tensión interfacial del agua es menor en una atmósfera presurizada de nitrógeno en comparación con el agua líquida. También disminuyo al aumentar la presión aplicada en el sistema agua/nitrógeno.

Objetivos y estructura de la tesis

Este trabajo se enmarca en el proyecto "Contribuciones al desarrollo de una biorrefinería sostenible. Disolución / hidrólisis y despolimerización de lignina en agua sub/supercrítica en reactores ultrarrápidos". Financiado por el Ministerio de Ciencia e Innovación con referencia CTQ 2016-79777, y con fondos FEDER de la EU para el desarrollo regional.

El objetivo principal es seguir la despolimerización de la lignina en SCW utilizando el análisis Raman in situ. Sin embargo, debido a las limitaciones que se justifican con detalle en la tesis, no se pudo hacer el seguimiento online y se reorientó la tesis, para hacer el seguimiento mediante reacciones de despolimerización ultra-rápidas, y la caracterización de los efluentes por análisis externos. Los nuevos objetivos se establecieron como sigue:

La hidrólisis de diferentes materias primas de biomasa, como la pulpa de remolacha azucarera (SBP) y el salvado de trigo (WB) se había realizado previamente en nuestro grupo de investigación (Demonstration of a selective process to transform biomass into sugars by ultrafast hydrolysis in supercritical wáter. Martínez-Fajardo Tesis Universidad de Valladolid) demostrando la viabilidad del hidrólisis en SCW para convertir estas materias primas en azúcares reductores. Sin embargo, tanto el

SBP como el WB son materias primas con alto contenido en carbohidratos y muy bajo contenido en lignina insoluble (2 % w/w y 4 % w/w, respectivamente).

En el proceso de obtención de aceite de semilla de uva se obtiene como residuo la semilla desengrasada, que contiene una concentración de lignina klason del 36%. El fraccionamiento de esta biomasa va a estar limitado por un aumento significativo a la transferencia del disolvente para que aceda a los carbohidratos y los hidrolice.

El primer objetivo de esta tesis propone estudiar la viabilidad del proceso de fraccionamiento, a biomasas con alto contenido en lignina, aplicándolo a la semilla de uva desengrasada procedente del proceso de obtención de aceite. Se estudiará la hidrólisis de los carbohidratos a través de la composición del efluente líquido, y la caracterización del residuo sólido donde se concentrará la fracción de lignina. Prestando especial atención a los cambios que se producen en la estructura de la lignina durante el proceso de hidrólisis. Este objetivo se desarrolla en el capítulo 1.

La lignina es un polímero de base aromática que se prevé como fuente principal de aromáticos. La despolimerización de la lignina para obtener aromáticos es un reto para el que no se dispone, a corto o medio plazo, de una solución sostenible. El principal reto de la reacción de despolimerización es la tendencia de los productos de la despolimerización a seguir reaccionando mediante las reacciones de repolimerización. En una tesis anterior (Lignin depolymerizatión by supercritical water ultrafast reactions by Nerea Abad-Fernández) se ha demostrado que el SCW podría ser un buen medio de despolimerización, y la repolimerización podría reducirse mediante la reducción del tiempo de reacción.

Así, el segundo objetivo de la tesis es entender la repolimerización de la lignina en agua supercrítica, para proporcionar tecnología y condiciones de operación que minimicen el impacto de la repolimerización.

La hipótesis con la que se plantea este objetivo es que en las reacciones de repolimerización, los compuestos monoméricos liberados reaccionan con los fragmentos de lignina, dando lugar a moléculas con mayor peso molecular. La reacción de repolimerización se va a seguir utilizando compuestos modelo obtenidos en la despolimerización de la lignina, con SKL. El objetivo es entender los cambios que se producen en la estructura de la lignina tras la reacción en SCW. Esta hipótesis se investiga en el capítulo 2. Una mejor comprensión de las no deseadas reacciones de repolimerización, ayudaran a encontrar la vía para suprimirlas y proporcionar una mejor despolimerización de la lignina en compuestos aromáticos.

El objetivo 3 de esta tesis es contribuir a una mejor comprensión del comportamiento del agua en condiciones próximas al punto crítico. Poniendo a punto un procedimiento para medir la tensión interfacial a altas presiones y temperaturas, para determinar el comportamiento de las fases liquida y vapor en las proximidades del punto crítico.

Debido a las condiciones de operación a alta presión y temperatura, se elige el método de la gota colgada. Se va a aportar un procedimiento de operación detallado, a la vez que se resuelven problemas de operación, como evitar la condensación del agua en la pared exterior de la mirilla. Aunque se dispone de datos experimentales de tensión superficial del agua solo y con otros compuestos, sólo unos pocos sistemas aportan datos experimentales de la tensión interfacial en condiciones de alta presión y temperatura.

Las mediciones de la tensión interfacial del agua se va a llevar a cabo en dos sistemas: agua líquida/vapor y agua/nitrógeno. Se van a comparar los datos obtenidos con los aportados en la bibliografía, y a investigar la influencia del nitrógeno en la tensión interfacial del agua. Los datos se van a correlacionar con la ecuación de Macleod – Sugden.

Capítulo 1 Valorización de semillas de uva desgrasadas como biomasa de alto contenido en lignina mediante tratamiento con agua supercrítica

En este trabajo se analiza la hidrólisis de semilla de uva desengrasada en agua supercrítica (SCW) a 380 °C y 260 bar desde 0,18 s hasta 1 s, siguiendo la recuperación de azúcares en la fase líquida del producto y la caracterización detallada de la fase sólida enriquecida en poliaromáticos (por ejemplo, lignina, flavonoides, etc.). La hidrólisis permitió recuperar el 56 % de los carbohidratos en la fase líquida con el mayor tiempo de reacción estudiado de 1s. El alto contenido de lignina insoluble en la biomasa (36 %), limita la transferencia de masa y presenta una característica importante en el proceso de hidrólisis, ralentizando la conversión de la fracción de carbohidratos, ya que después del tiempo máximo de 1s, el 10 % de los carbohidratos todavía permanecían en la fase sólida. La lignina de la madera molida, extraída de la biomasa y el extracto de dioxano de la fase sólida fueron caracterizados para entender los principales cambios estructurales durante el proceso de hidrólisis de SCW. La extracción con dioxano (80 %) de los sólidos produce una mezcla muy compleja de extractos lipofílicos, flavonoides y lignina con una cierta cantidad de carbohidratos químicamente ligados. El análisis de RMN 2D del extracto de dioxano

muestra cambios notablemente sutiles en las cantidades de las principales moléculas de lignina (β-O-4', β-β' (resinol) y β-5 (fenilcumarano)).

Como resultado relevante de este trabajo se presenta en la figura el rendimiento de azucares de la fase liquida en función del tiempo de reacción.

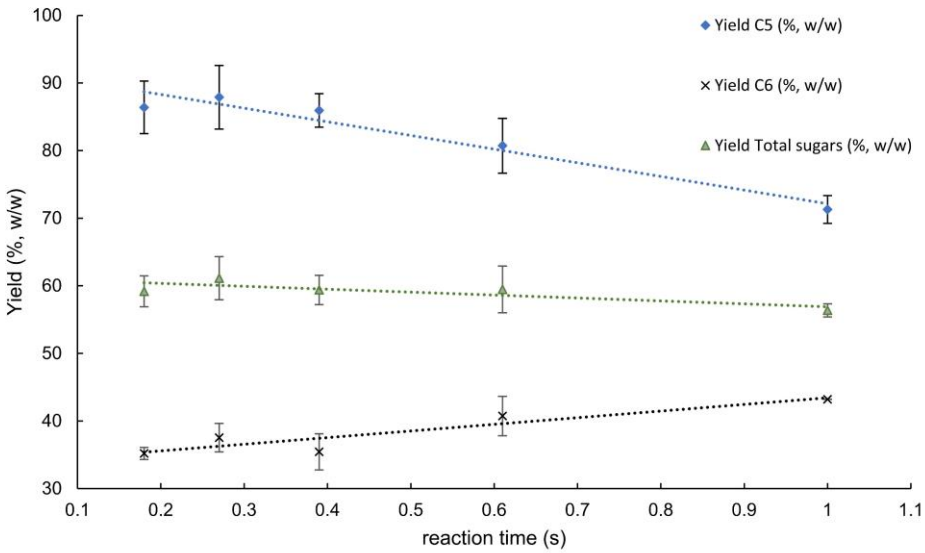

Capítulo 2 Repolimerización de lignina kraft sulfonada en medio de agua supercrítica

En este capitulo se investiga la reactividad de los monómeros obtenidos de la despolimerización de la lignina y su contribución a la repolimerización en SCW. En este estudio se utilizó lignina kraft sulfonada (SKL) junto con cuatro monómeros: vainillina, ácido vanílico, alcohol vanílico y acetovanillona. También se empleó como referencia la lignina kraft indulina para entender la repolimerización de SKL en SCW. Se detectó la formación de estructuras de diarilmetano en los espectros HSQC del

residuo sólido tras el proceso de SCW. Los fragmentos liberados de lignina con estructuras β-O-4 fenólicas libres, así como el alcohol vanílico, están implicados en la formación de estructuras de o-o' y o-p' diarilmetano. La estructura química de la lignina kraft y de su producto polimérico tras el proceso SCW fue muy similar, tal y como muestra la HSQC, lo que indica que las reacciones de repolimerización se producen a través de polimerización cross linked de las fracciones de productos de bajo peso molecular. En la figura se presenta el mecanismo propuesto para la formación de estructuras de diarilmetano en el proceso SCW: de MC (a); de SKL (b)

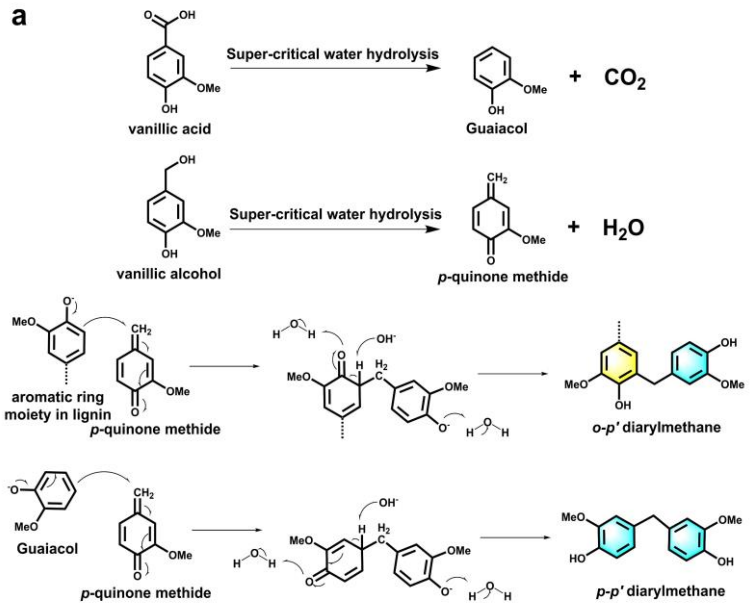

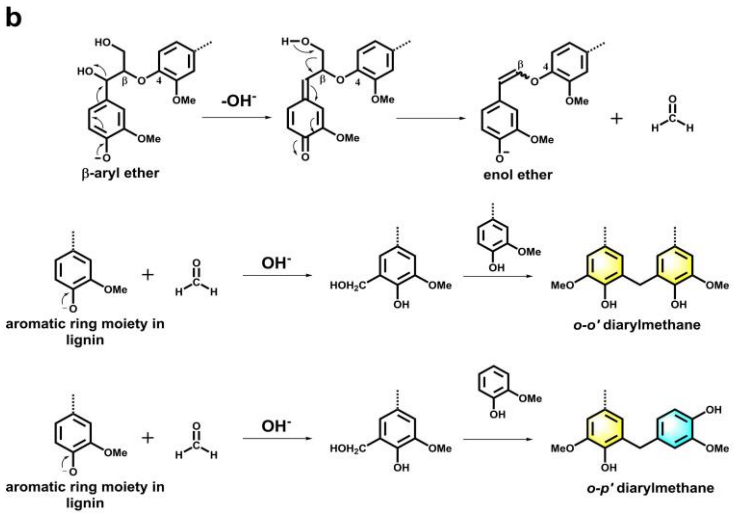

Capítulo 3 Tensión interfacial del agua líquida en atmósfera de nitrógeno presurizada y del agua líquida en su vapor saturado - medida a temperaturas de hasta 350 °C.

La tensión interfacial del agua se midió en dos sistemas: agua líquida/vapor (más adelante en el texto como sistema agua/agua) siguiendo la línea de saturación y líquido en atmósfera presurizada de nitrógeno (sistema agua/nitrógeno). La técnica de medición aplicada fue el método de la gota colgante como método adecuado para las mediciones de la tensión interfacial a temperatura y presión elevadas. La tensión interfacial del sistema agua/nitrógeno se investigó a 10, 15 y 18 MPa y hasta temperaturas de 325 °C. En el caso del sistema agua/agua, la temperatura fue de hasta 350 °C, cercana a la temperatura crítica del agua. Se utilizó la ecuación de Macleod-Sugden para describir las tensiones interfaciales medidas del sistema agua/nitrógeno, así como del sistema agua/agua. La ecuación concuerda bien con los resultados de las

mediciones, mostrando una DAA del 4,97 % para el sistema agua/nitrógeno y del 3, 02 % para el sistema agua/agua. Los resultados experimentales obtenidos están en buena concordancia con los datos de la literatura. En la figura se presenta la comparación de valores experimentales obtenidos en este trabajo para sistema agua/agua y agua/nitrógeno

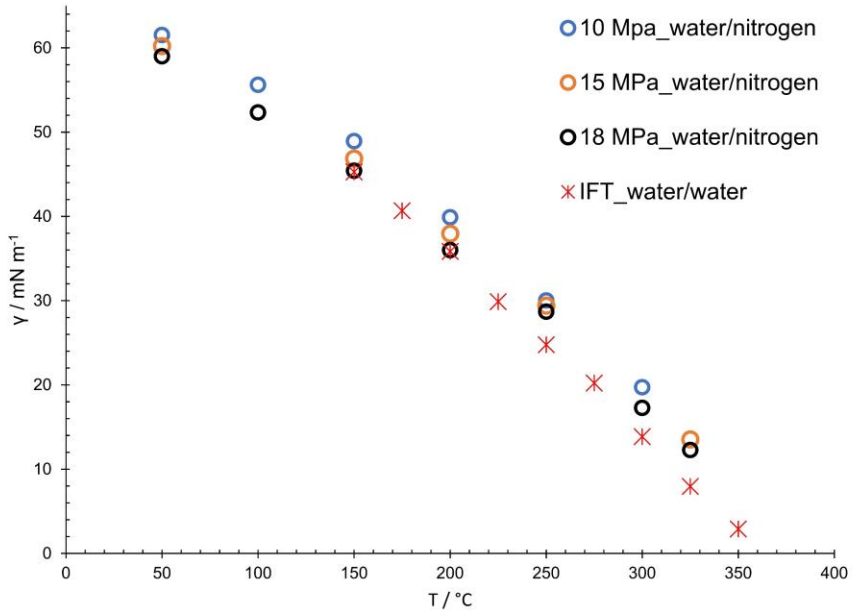

Conclusiones

Esta tesis es una contribución al desarrollo de biorrefinerías sostenibles utilizando la tecnología del agua supercrítica. Esta contribución se ha realizado, por un lado, a través de la valorización de la biomasa con alto contenido en lignina, como la semilla de uva desengrasada, y, por otro lado, a través de una mejor comprensión de la reacción de repolimerización de la lignina, para mejorar la producción de

aromáticos a partir de la misma. Esta tesis también presenta los datos de la tensión interfacial del agua en dos sistemas: sistema agua/agua y sistema agua/nitrógeno. Los resultados presentados para la tensión interfacial del agua en el sistema agua/agua no se habían publicado previamente utilizando el método de gotas colgadas en el rango de presión y temperatura que se ha investigado.

Como ya se ha discutido a lo largo de esta tesis, la lignina limita significativamente la trasferencia del disolvente para hidrolizar los carbohidratos, por lo que dificulta fraccionamiento. El primer capítulo de esta tesis demuestra la capacidad del agua supercrítica para fraccionar e hidrolizar la biomasa de semillas de uva, como ejemplo de biomasa con alto contenido en lignina. Las principales conclusiones de este capítulo, se concretan en

1. El rendimiento máximo de azúcares recuperados en la fase líquida alcanza el 61% después de 0,27 s. Sin embargo, el rendimiento de azúcares en la fase líquida sigue siendo alto (56%) incluso después del tiempo de reacción de 1s, el tiempo más alto utilizado. Tiempos mucho más altos que los obtenidos en la hidrólisis de biomasas con bajo contenido de lignina klason como son la pulpa de remolacha y el salvado de trigo, donde eran del orden de milisegundos. Esto puede explicarse por la alta cantidad de lignina y otros polifenoles, ya que la lignina actúa como una barrera para que el SCW acceda a la fracción de carbohidratos, lo que lleva a una hidrólisis más lenta.

2. La parte sólida de la muestra estaba enriquecida en poliaromáticos. La extracción total de los carbohidratos del sólido no pudo obtenerse ya que después de 1s todavía el 10% de los carbohidratos se encuentran retenidos en la fracción sólida. El análisis detallado del solido mediante 2D-NMR muestra que este producto consiste

en una mezcla compleja una parte lignina con una cierta cantidad de carbohidratos químicamente enlazados, un extracto lipofílico residual y flavonoides.

3. La comparación del efluente sólido obtenido en el proceso con SCW, con la lignina aislada de las semillas de uva indica un cambio muy débil en las principales unidades características de lignina nativa, como la β-O-4. El análisis también muestra que la unidad de guayacol es la principal unidad de lignina en las semillas de uva, con una cantidad menor de unidad de p-hidroxifenilo, mientras que la unidad de siringilo está ausente. La conservación de los enlaces principales de la lignina puede ser muy beneficiosa para la posterior valorización de este residuo de lignina.

Las principales conclusiones del estudio realizado para entender las reacciones de repolimerización de la lignina que reducen la obtención de los monómeros aromáticos, se concretan en:

4. Los monómeros de la lignina tienen tendencia a reaccionar entre sí en la repolimerizacion de la SKL, como demuestra su elevada tasa de conversión. La tasa de conversión también aumenta con la presencia de SKL en el reactor, lo que indica la reacción de los monómeros con los fragmentos de lignina.

5. Otro indicador de la tendencia de los monómeros a reaccionar con el SKL es la mayor cantidad de sólidos totales en la reacción de la lignina y los monómeros añadidos en comparación con la reacción de la repolimerización de la lignina en el SCW. El análisis GPC confirmó que las muestras obtenidas en la reacción de la mezcla de SKL y monómeros tienen picos a mayor tiempo de reacción en comparación con la muestra obtenida sólo con SKL o sólo con compuestos modelo.

6. El análisis 2D-NMR confirmó la presencia de estructuras de diarilmetanos en el residuo sólido de cada muestra, indicando que dichas estructuras podrían ser

responsables de la reacción de repolimerización. En el residuo sólido de SKL se encontraron estructuras de o-o' y o-p' diarilmetano, mientras que en la muestra sólida de los compuestos modelo se encontraron estructuras de o-p' y p-p' diarilmetano. En el caso del residuo sólido obtenido con la mezcla de SKL y compuestos modelo, están presentes las tres estructuras de diarilmetano. Esto indica que la formación de estas estructuras contribuye a la reacción de repolimerización, pero el mecanismo de su formación es diferente para el SKL y los compuestos modelo. La principal reacción que se produce en la estructura de SKL durante el proceso de SCW en la des-sulfonación.

7. No se encuentran cambios significativos en la estructura de la lignina de Indulina en su residuo sólido después del proceso SCW, lo que indica que la reacción principal ocurre en la fracción de productos de bajo peso molecular.

La ausencia de una discusión detallada sobre las mediciones de la tensión interfacial del agua en condiciones de alta presión y temperatura fue la razón principal de las mediciones realizadas en el capítulo 3 de la tesis. La tensión interfacial del agua se midió en el sistema agua/agua y agua/nitrógeno. Los datos disponibles en la literatura en condiciones de alta presión y temperatura para las mediciones del sistema agua/agua se obtienen utilizando el método de ascenso capilar, mientras que este trabajo es el primero que informa de las mediciones utilizando el método de la gota colgante, más adecuado para operar a elevada presión y temperatura. Además, resulta de interés disponer de más datos de tensión interfacial de sistemas agua con nitrógeno o algún otro gas inerte. Por esta razón, las mediciones de la tensión interfacial se realizan también en una atmósfera de nitrógeno. Las principales conclusiones podrían resumirse como:

8. El resultado del sistema agua/agua muestra una buena concordancia con los datos de la bibliografia, con una desviación absoluta máxima del 7. 40 %. Para el caso del sistema agua/nitrógeno, también se obtiene una buena concordancia con los datos experimentales reportados en la literatura con una desviación absoluta máxima del 2,07 %.

9. Los datos experimentales obtenidos en nuestro estudio se correlacionan además utilizando la ecuación de Macleod-Sugden para los componentes puros en el caso del sistema agua/agua y para la mezcla en el caso del sistema agua/nitrógeno. Los resultados calculados con la ecuación concuerdan con los resultados de las mediciones, con una DAA de 4,97 % y 3,02 % para el sistema agua/nitrógeno y agua/agua respectivamente.

10. Los valores de la tensión interfacial del agua obtenidos en el sistema agua/agua están en buena concordancia con los valores obtenidos en el sistema agua/nitrógeno por debajo de 18 MPa y hasta 200 °C. Se observa una desviación significativa de la tensión interfacial del agua en estos dos sistemas a medida que la temperatura se eleva por encima de los 200 °C; debido al cambio de solubilidad del nitrógeno.

Trabajo futuro

El análisis de los residuos sólidos obtenidos durante el procesado de las semillas de uva desgrasadas en SCW muestra que la lignina que se encuentra en las semillas de uva es principalmente lignina de tipo G, pero también que las principales moléculas de lignina nativa con enlaces éteres se conservan principalmente durante el

tratamiento con SCW. Uno de los principales factores que influyen en el potencial de la lignina para ser despolimerizada a aromáticos es la cantidad de enlaces C-O y el nivel de condensación. Como la naturaleza de la lignina se conserva bien durante el proceso de SCW, esto indica que el sólido obtenido tras la hidrólisis de las semillas de uva desgrasadas podría ser un potencial buen candidato para la despolimerización a aromáticos, como la vainillina, ya que esta lignina es del tipo G. En futuros trabajos está prevista la hidrólisis del residuo sólido obtenido tras el procesado de las semillas de uva desgrasadas en SCW para demostrar su potencial como posible fuente de vainillina.

El resultado obtenido en el capítulo 2 muestra que la reacción principal se produjo principalmente en la fracción oleosa del producto. Sin embargo, el análisis detallado del residuo sólido muestra la presencia de estructuras de diareleno como responsables de la reacción de repolimerización. Con el fin de tener una completa y mejor comprensión del proceso de repolimerización se platea en el trabajo futuro realizar un análisis detallado de la fracción de aceite de los productos y el estudio cinético de los compuestos modelo.

El conocimiento de las propiedades superficiales de los polímeros es de gran importancia para determinar su potencial aplicación. El trabajo futuro se centra en la medición del ángulo de contacto de los polímeros de lignina comerciales y del polímero de lignina obtenido tras el tratamiento con SCW. Esta información podría utilizarse para ampliar el conocimiento de las propiedades de la lignina como polímero, y su compatibilidad para adicionarla a otros polímeros para reforzar sus propiedades mecánicas.

Acknowledgement

En primer lugar, me gustaría agradecer a la prof. Maria Jose Cocero por la oportunidad de trabajar en Press Tech Group. Le agradezco todo el apoyo, la confianza, el aliento, los conocimientos que compartió conmigo y el tiempo que me dedicó en los últimos años. Fue un verdadero honor trabajar con ella.

I would like to thank prof. Mikhail Balakshin for his support, shared knowledge and the time he dedicated to our collaboration.

I would like to thank my husband Michael for his love, help, unlimited support and for being my inexhaustible source of motivation and strength. I also want to thank him for being the first 'unofficial' reviewer of this document and for all his time taken for that.

Неизмерно хвала мојој породици у Србији, посебно мојим родитељима Нади и Небојши за сву њихову љубав и подршку током мог школовања. Хвала им за сав њихов напор и труд и за све могућности које су ми отворили. Велико хвала и мојим бакама Милени и Мирјани, мојим сестрама Ивани, Невени, Трњини и Цвети, мојим зетовима Милану и Ненаду и мојим најмилијим сестричинама и сестрићу Ангели, Круни и Александру за сву њихову љубав, подршку и неисцрпну мотивацију коју ми пружају. Желим такође да захвалим мом ујаку Блажу и тетки Ради за сву подршку и љубав коју сам одувек имала од њих.

Muchas gracias a mi amiga Isa por ser un gran apoyo para mí en todos los momentos difíciles. También le agradezco a ella y su familia por todos los maravillosos momentos que compartieron conmigo que me hicieron sentir como en casa muchas veces. Le agradezco este precioso tiempo que siempre será uno de mis mejores recuerdos de España.

Many thanks to my friend Sergio for all the great time we had together and all his support and help in Spain.

Gracias a mi amigo Reinal por todo su apoyo y ayuda. Agradecerle por ser mi guía por Valladolid y la cultura española y por tener la paciencia de hablarme en español conmigo. Le agradezco el gran tiempo que pasamos juntos que tuve muchos momentos preciosos.

Хвала пуно мојим пријатељима Ани, Ињигу, Луни, Весни и Ксенији за сву подршку и помоћ. Хвала им за драгоцено време проведено заједно које је много значило.

Big thanks to my friend Celia who was the first one to introduce me to the thematics of Supercritical water and lab work on the plants. I thank her for all the knowledge she shared with me and all her attention and time.

Many thanks to all my friends and colleagues from the lab for the great time that we shared during this period. Thank Rafaela, Vito, Maria, Laura, Chari, Eloisa, Elaine, Marta and all others that I did not mention here.

About the author

Tijana Adamović (Prijepolje – Serbia, 1992) started her studies of Chemical Engineering at the University of Belgrade (Serbia) in 2011 and graduated in 2015. The same year she joined the master program at the same University and obtained a master degree in 2016. During her master thesis, she worked at the Institute of Nuclear Science in Belgrade as a trainee. 2016 she joined the doctorate program of Fluid thermodynamics at the University of Valladolid. In 2018 she did her internship at ITUN Institute in Freiberg, Germany in the group of Prof. Dr Andreas S. Braeuer. Her thesis is focused on the valorisation of biomass and especially the lignin fraction of biomass to contribute to the development of biorefineries. Her thesis is supervised by Prof. Dr Maria Jose Cocero.

List of publications:

Adamovic, T., Tarasov, D., Demirkaya, E., Balakshin, M., Cocero, M.J., 2021. A feasibility study on green biorefinery of high lignin content agro-food industry waste through supercritical water treatment. J. Clean. Prod. 323, 129110. https://doi.org/10.1016/j.jclepro.2021.129110

Cocero, M.J., Cabeza, Á., Abad, N., **Adamovic, T**., Vaquerizo, L., Martínez, C.M., Pazo-Cepeda, M.V., 2018. Understanding biomass fractionation in subcritical & supercritical water. J. Supercrit. Fluids 133, 550–565. https://doi.org/10.1016/j.supflu.2017.08.012

Martínez, C.M., **Adamovic, T.,** Cantero, D.A., Cocero, M.J., 2019a. Scaling up the production of sugars from agricultural biomass by ultrafast hydrolysis in supercritical water. J. Supercrit. Fluids 143, 242–250. https://doi.org/10.1016/j.supflu.2018.08.017

Martínez, C.M., **Adamovic, T.**, Cantero, D.A., Cocero, M.J., 2019b. Ultrafast hydrolysis of inulin in supercritical water: Fructooligosaccharides reaction pathway and Jerusalem artichoke valorization. Ind. Crops Prod. 133, 72–78. https://doi.org/10.1016/j.indcrop.2019.03.016

Milovanovic, S., **Adamovic, T.**, Aksentijevic, K., Misic, D., Ivanovic, J., Zizovic, I., 2017. Cellulose Acetate Based Material with Antibacterial Properties Created by Supercritical Solvent Impregnation. Int. J. Polym. Sci. 2017, 1–9. https://doi.org/10.1155/2017/8762649

Zizovic, I., Senerovic, L., Moric, I., **Adamovic, T.**, Jovanovic, M., Krusic, M.K., Misic, D., Stojanovic, D., Milovanovic, S., 2018. Utilization of supercritical carbon dioxide in fabrication of cellulose acetate films with anti-biofilm effects against Pseudomonas aeruginosa and Staphylococcus aureus. J. Supercrit. Fluids 140, 11–20. https://doi.org/10.1016/j.supflu.2018.05.025

Conference contribution

Oral presentations:

Adamovic T., Demirkaya E., Perez Velilla E., Cocero, M. J. Aromatic compounds from lignin by supercritical water ultrafast reactions. *18th European Meeting on Supercritical Fluids (EMSF)*, Bordeaux (France) April 2021

Adamovic, T., Martinez, M C., Cocero, M. J. Valorisation of high lignin content biomass using supercritical water technology. *The 12th European Congress of Chemical Engineering and 5th European Congress of Applied Biotechnology*, Florence (Italy), September 2019

Adamovic, T., Demirkaya, E., Perez Velilla, E., Cocero, M. J. Following lignin repolymerization in the presence of model compounds in supercritical water.

The 20th International Symposium on Wood, Fiber and Pulping Chemistry, Tokyo (Japan), September 2019

Cocero Alonso, M. J., Martinez, M C., Vaquerizo, L., **Adamovic, T.** Lignocellulosic biomass refinery by Subcritical/Subcritical water ultra-fast hydrolysis, *4th Iberoamerican Congress on Biorefineries*, Jaen (Spain), October 2018

Cocero Alonso, M. J., **Adamovic, T.,** Fernandez, N., Perez, E. Engineering lignocellulose biomass fractionization by Subcritical water: *Production of aromatics and lignin composites. 5th Iberoamerican Conference on Supercritical Fluids*, Campinas (Brazil), September 2019

Poster presentations:

Adamovic, T., Martinez, M C., Vaquerizo, L., Cocero, M. J. Fractionation of high lignin content biomass by supercritical water technology. *International Symposium on Supercritical Fluids 2018*, Antibes-Juan-les-Pins (France), April 2018

Adamovic, T., Demirkaya, E., Cocero, M.J. Sustainable valorization of wine industry sub product by sub/supercritical water fractionation. *9th Nordic Wood Biorefinery Conference*, Stockholm (Sweden), Oktober 2020

Cocero, M.J., **Adamovic, T.**, Demirkaya, K., Leontijevic, V. Biomass fractionation by ultrafast supercritical water hydrolysis (SCHW): Sustainability analysis. *1st Greening Internacional Conference*, Costa de Caparica (Portugal), February 2021